Diabetes Exacerbates Atherosclerosis via Inflammasome- and APOC3-Dependent Pathways

Cheng-Chieh Hsu

A dissertation

submitted in partial fulfillment of the

requirements for the degree of

Doctor of Philosophy

University of Washington

2023

Reading Committee:

Karin Bornfeldt, Chair

David Dichek

Jessica Hamerman

Program Authorized to Offer Degree:

Molecular Engineering and Sciences

University of Washington

Abstract

Diabetes Exacerbates Atherosclerosis via Inflammasome- and APOC3-Dependent Pathways

Cheng-Chieh Hsu

Chair of the Supervisory Committee:

Karin Bornfeldt

Department of Medicine

Individuals with diabetes suffer from increased cardiovascular disease (CVD) death regardless of statin treatment. The persistently elevated CVD risk among individuals with diabetes suggests the presence of diabetes-associated CVD risks beyond LDL-cholesterol. Multiple risk factors, including glucose, inflammation, and abnormal metabolism of triglyceride-rich lipoproteins (TRLs) and their remnants, have been proposed as contributors to diabetes-associated CVD risk. This work focuses on testing whether increased circulating apolipoprotein C3 (APOC3), inflammasome activation in immune cells, and abnormal TRL metabolism contribute to diabetes-associated atherosclerosis. We have shown that blocking hematopoietic inflammasome activation leads to suppressed atherogenesis in diabetic mice. Our findings further highlight the unique role of hematopoietic inflammasome activation in inducing atherosclerotic lesions but not necrotic core progression in diabetes. Lesion necrotic core progression in diabetes could be dependent on

the lesional accumulation of APOC3. Large lesion necrotic cores can lead to CVD events. Previous studies demonstrated that elevated serum APOC3 levels predict incident CVD in humans and promote necrotic core progression in a mouse model of type 1 diabetes, but the underlying APOC3-associated mechanism remains elusive. We showed that delipidated, but not lipidated, APOC3 can induce inflammasome activation. Given the association between lesional APOC3 accumulation and necrotic core progression, we propose that lesional APOC3 and TRL accumulation could be responsible for necrotic core expansion in diabetes. Together, our work demonstrates that diabetes exacerbates atherosclerosis via inflammasome- and APOC3-dependent pathways. These findings suggest that inhibiting both pathways may provide novel therapeutics for reducing CVD risk in individuals with diabetes.

List of Abbreviations

Abbreviation	Definition
AIM2	absent in melanoma 2
ADVANCE	Action in Diabetes and Vascular Disease: Preterax and Diamicron Modified Release Controlled Evaluation
ACCORD-Lipid	Action to Control Cardiovascular Risk in Diabetes Lipid trial
APOB	apolipoprotein B
APOC3	apolipoprotein C3
CANTOS	Canakinumab Anti-inflammatory Thrombosis Outcome Study
CVD	cardiovascular disease
CD68	cluster of differentiation 68
CD45	cluster of differentiation 45
DCCT/EDIC	Diabetes Control and Complications Trial/Epidemiology of Diabetes Interventions and Complications
GSDMD	gasdermin D
HbA1c	glycated hemoglobin
HDL	high-density lipoprotein
IL-1β	interleukin 1β
IL-18	interleukin 18
LPL	lipoprotein lipase
LDL	low-density lipoprotein
NLRP3	NOD, LRR and pyrin domain–containing protein 3

PROMINENT	Pemafibrate to Reduce cardiovascular OutcoMes by reducing triglycerides IN diabetic patiENTs
RLP	remnant lipoprotein
SUV	small unilamellar vesicle
TLR2	toll-like receptor 2
TLR4	toll-like receptor 4
TRL	triglyceride-rich lipoprotein
T1D	type 1 diabetes
T2D	type 2 diabetes
VLDL	very low-density lipoprotein

Table of Contents

List of Figures

List of Tables

Acknowledgments

This work would not have been possible without the guidance and support of my mentors, friends, and family.

I would like to first thank my advisor, Dr. Karin Bornfeldt. I am thankful that she took me as a student and introduced me to the field of vascular complications in diabetes. Karin is a great scientist and mentor. She always provides great suggestions and comments for my writing and research plans. Having the opportunity to chat with her about the project when she was in the office and hallways also helped shape this project tremendously. Furthermore, she is open to new ideas and cares about my scientific and career development. I am fortunate to have her as my advisor and her mentoring style allows me to grow as a scientist and prepares me for independent scientific endeavors.

Besides great scientific advice, this work would not be possible without the support from my colleagues/friends in the Bornfeldt Lab. I joined the lab with limited wet lab experience and thank you all for having the patience to show me how to perform each procedure. In particular, I would like to thank Dr. Jenny Kanter and Farah Kramer for helping with the animal work and tissue collection. Without their help, it would have been impossible for me to finish the project. I would also like to thank Dr. Vishal Kothari, Dr. Masami Shimizu-Albergine, Dr. Jingjing Tang, and Luz Wigzell for their hard work and support. I enjoyed my time and experience in the lab and am sad to leave.

I would like to thank my committee members – Dr. David Dichek, Dr. Jessica Hamerman, and Dr. Brad Cookson – for providing valuable scientific, career, and life advice. Without their feedback, the projects would not be as completed and published in great journals. Their advice also trained me to tackle questions from multiple angles and allowed me to grow as a scientist.

In the end, I would like to thank my family and friends who provided tremendous support during my graduate study. Thank you all for celebrating the ups and supporting the downs in my life. I would not have made it here without them.

Chapter 1 : Introduction

1.1 Association between cardiovascular disease and diabetes

Cardiovascular disease (CVD) is the leading cause of death in the United States and atherosclerosis, characterized by chronic arterial inflammation (1), is the underlying pathology of most CVD events (2). Monocytes and macrophages play important roles in all stages of atherosclerotic lesion development (3). The retention of apolipoprotein B (APOB)-containing lipoproteins in the subendothelial space, via ionic interactions between the extracellular matrix and APOB lipoproteins (4) leads to monocyte entry and initiation of atherosclerotic lesions (3). The accumulation of monocytes and their subsequent differentiation into macrophages, in response to lipoprotein accumulation, exacerbate chronic arterial inflammation (5). Macrophages can undergo programmed cell death after taking up lipids and form a lipid-rich, acellular necrotic core that contributes to the progression of the advanced lesion (3; 5). Defective clearance of dead cells or efferocytosis by macrophages has been suggested to be one of the contributors to necrotic core expansion (6; 7).

Compared with individuals without diabetes, those with diabetes suffer from an elevated risk of CVD events and mortality (2; 8; 9). With the introduction of statins, effective drugs in treating and preventing CVD (2), individuals with and without diabetes have reduced events and mortality over the years (9; 10). However, despite the administration of statins, individuals with diabetes still present with increased CVD risk and mortality (9; 11; 12). The discrepancy in CVD risk and mortality between individuals with and without diabetes suggests the presence of CVD risk factors attributable to diabetes (11; 13). Hyperglycemia (14), abnormal metabolism of TRLs (13), elevated levels of APOC3 (15), and increased inflammation (16; 17) have been considered likely mediators of vascular complications among individuals with diabetes but the underlying mechanism remains elusive.

1.2 Diabetes and its potential culprits for accelerating atherosclerosis progression

1.2.1 Hyperglycemia

Diabetes is characterized by hyperglycemia, which is defined by having fasting plasma glucose greater than or equal to 7 mmol/L or glycated hemoglobin (HbA1c) greater than or equal to 6.5% (18). Hyperglycemia develops as a result of underlying insulin deficiency and/or insulin resistance. The lack of insulin actions can also lead to dyslipidemia in individuals with T2D or uncontrolled T1D due to insulin's lipid regulatory effects (19; 20). Hyperglycemia has long been considered the main culprit for increased cardiovascular events in patients with diabetes (14), however, the cardioprotective benefit of glycemic control in diabetic subjects is inconclusive (21).

Even though the Diabetes Control and Complications Trial/Epidemiology of Diabetes Interventions and Complications (DCCT/EDIC) study demonstrated that reduced HbA1c is associated with reduced CVD events and mortality in participants with T1D (22; 23), the association between glycemic control and CVD was confounded by the therapy used. The DCCT/EDIC study recruited 1441 subjects with T1D and administered intensive insulin or conventional treatments for 6.5 years (DCCT) and conducted a series of observational follow-ups (EDIC) on most subjects. The DCCT/EDIC study demonstrates the cardioprotective benefit of improved glycemic control, but intensive insulin therapy was accompanied by multiple improvements in other CVD risk factors (24), which blurred the contribution of glycemic control on CVD outcomes. Furthermore, individuals who received intensive insulin therapy still have an HbA1C level above 6.5%, which challenged whether the effects observed were solely dependent on improved glycemic control (22).

The Action in Diabetes and Vascular Disease: Preterax and Diamicron Modified Release Controlled Evaluation (ADVANCE) study also challenges the causal relationship between

hyperglycemia and CVD outcomes in participants with T2D (25). The ADVANCE study enrolled 11,140 subjects with T2D to study the contributions of blood pressure lowering and glycemic control to CVD outcomes. The sulfonylurea-based glucose-lowering therapy was employed to remove the confounding effects of insulin administration. The intensive glycemic control group, aiming to achieve an HbA1c level of less than 6.5%, failed to reduce macrovascular events and mortality when compared to the control group (26). This finding suggests the presence of non-glucose mediators that drive CVD outcomes in individuals with diabetes. Together, these clinical studies provided evidence suggesting the presence of risk factors, other than hyperglycemia, that contribute to the development and progression of advanced atherosclerotic lesions under diabetic conditions.

1.2.2 Abnormal metabolism of triglyceride-rich lipoproteins and their remnants

T2D and poorly controlled T1D are often accompanied by hypertriglyceridemia, a condition in which circulating levels of triglycerides are elevated. Hypertriglyceridemia is diagnosed when the triglyceride level of an individual is above 150 mg/dl and this condition has been associated with increased risk of CVD (27). Although population studies have demonstrated a strong association between triglyceride-lowering *LPL* variants and reduced CVD risk (28), clinical trials involving triglyceride-lowering therapies have been largely negative (21). The Action to Control Cardiovascular Risk in Diabetes Lipid trial (ACCORD-Lipid) suggested that triglyceride-lowering by combination therapy with a statin plus a fibrate has no additional cardioprotective benefits for individuals with T2D beyond statin therapy (29). The ACCORD-Lipid enrolled 5518 subjects with T2D to study the contribution of triglyceride-lowering, by treatment with fibrate, to CVD outcomes beyond LDL-cholesterol lowering. All study participants received statin, but some received fibrate to lower plasma triglyceride levels. Plasma triglyceride

levels were significantly reduced with fibrate therapy, but CVD events and mortality were similar between the two groups. Despite the overall neutral findings of ACCORD-Lipid, an extended post-trial follow-up study demonstrated cardioprotective effects of triglyceride-lowering in diabetic individuals with increased triglycerides (>200 mg/dL) and reduced HDL-cholesterol (<34 mg/dL) (30). The cardioprotective effect of triglyceride-lowering in this subgroup was addressed by the Pemafibrate to Reduce cardiovascular OutcoMes by reducing triglycerides IN diabetic patiENTs (PROMINENT) trial (31).

The PROMINENT trial recruited 10,497 type 2 diabetic subjects with median baseline fasting triglycerides at 271 mg/dL and HDL-cholesterol at 33 mg/dL (31). Although pemafibrate therapy significantly lowered plasma triglyceride levels, subjects who received pemafibrate showed no cardioprotective benefit when compared to subjects who received a placebo. The pemafibrate therapy also increased plasma LDL-cholesterol levels, suggesting that the cardioprotective benefit of triglyceride-lowering could be masked by increased LDL-cholesterol levels. As remnant lipoproteins (RLPs) can be effectively converted to LDL (32), the trial suggests that pemafibrate improves the clearance of TRLs but not of their remnants (31). Since both RLPs and LDL-cholesterol have been associated with CVD risk (13; 32), the trial suggests clearing both LDL-cholesterol and RLPs are needed for reducing CVD events in diabetic individuals (31).

1.2.3 Elevated apolipoprotein C3 (APOC3) levels

Recently, APOC3 has been considered a likely mediator of vascular complications in three cohorts of individuals with T1D (15; 33; 34) and free APOC3 has been demonstrated to activate the NLRP3 inflammasome in human monocytes (35). Together, these findings suggest that APOC3 could contribute to diabetes-accelerated atherosclerosis via inflammasome activation. Although the mechanisms remained unknown, the association between APOC3 and CVD events is

consistent with the findings that individuals with *APOC3* loss-of-function mutations have reduced levels of plasma triglycerides and an apparent protection against CVD (36).

APOC3 is an apolipoprotein that can cause an elevation of plasma triglyceride levels by reducing lipolysis and the hepatic clearance of TRLs and RLPs. This interpretation is consistent with the finding that mice expressing a human APOC3 transgene have hypertriglyceridemia and reduced VLDL clearance (37). The mechanism behind APOC3-mediated inhibition of triglyceride lipolysis is proposed to involve inhibition of LPL activity when LPL is bound to glycosylphosphatidylinositol-anchored HDL-binding protein 1 on endothelial cells(38), perhaps by blocking the access of LPL to TRL triglycerides. When APOC3 levels are very high, it might also work by displacing APOC2 from the surface of the TRLs (39).

Furthermore, APOC3 inhibits the hepatic clearance of TRLs and RLPs through LDLR and LRP1(40), by a mechanism believed to be due to interference with APOE binding to those receptors. The relative contribution of these mechanisms differs in different conditions. In humans with a loss-of-function mutation in APOC3, a 50% reduction in plasma APOC3 levels results in increased fractional clearance rates of VLDL triglycerides and APOB and a higher conversion rate of VLDL remnants to LDL, suggesting increased LPL activity (41). The fractional clearance rates of both APOC3 and APOC2 were also higher in these subjects. On the other hand, suppression of plasma APOC3 leads to reduced plasma triglycerides in individuals with familial chylomicronemia syndrome and genetic deficiency of LPL, demonstrating that APOC3 also acts through an LPL-independent pathway (42). This finding, together with the finding that APOC3 can displace APOE from small VLDL (43) supports the conclusion that APOC3 can increase plasma triglycerides and cholesterol independently of LPL, by inhibiting hepatic clearance of TRLs and RLPs.

Although the pro-atherogenic effects of APOC3 could be likely associated with abnormal metabolism of TRLs and RLPs, individuals with T1D are often free of dyslipidemia but still have increased CVD incidents. It is possible that APOC3 might have direct effects on atherosclerosis progression via inflammatory activation. Overall, there is strong evidence that APOC3 is a biomarker and mediator of CVD and atherosclerosis in the setting of T1D. Further studies are needed to understand the underlying mechanisms and address whether similar relationships are present in T2D.

1.2.4 Inflammation

Although the major culprit that is responsible for diabetes-associated CVD risks in individuals with diabetes has yet to be identified, macrophages have been identified as a major contributor to accelerated atherosclerosis progression in diabetic subjects. Individuals with diabetes have an increased accumulation of $CD68^+$ cells and necrotic core area (44), suggesting macrophages and necrotic core expansion play roles in accelerating atherosclerotic lesion progression in diabetic subjects. Macrophages from individuals with diabetes also have an elevated propensity to secrete pro-inflammatory cytokines, such as IL-1β and IL-18, when stimulated *in vitro* (45; 46) Together, these findings support the hypothesis that macrophages accelerate atherosclerotic lesion progression and necrotic core expansion under diabetic conditions.

Increased inflammation, as measured by high-sensitivity C-reactive protein (hs-CRP), has been associated with increased CVD risk (47). Individuals with diabetes not only have elevated levels of hs-CRP (48; 49) but also have a heightened risk of CVD events and mortality when their hs-CRP levels are elevated (50). However, the causal relationship between increased inflammation and CVD outcomes has been debatable. A recent meta-analysis conducted on the role of hs-CRP in CVD outcomes suggests targeting hs-CRP does not offer additional cardiovascular benefits over

targeting LDL with traditional statin therapy (51). The cardiovascular inflammation reduction trial (CIRT) also provides evidence for challenging the role of inflammation in CVD outcomes (52). The study employed low-dose methotrexate, an effective treatment for inflammatory conditions, as a method for lowering inflammation in participants. When compared to individuals who received a placebo, those who received low-dose methotrexate had similar incidents of CVD and mortality. However, it is possible that inflammation plays a more significant role only when an individual has increased inflammation. Increased inflammation was not part of the recruitment requirement of the CIRT and the pro-inflammatory status, as measured by IL-1β and hs-CRP, was not reduced by the low-dose methotrexate therapy (52).

Increased inflammation might be an important CVD risk factor. The recent Canakinumab Anti-inflammatory Thrombosis Outcome Study (CANTOS) highlighted the involvement of IL-1β in atherosclerotic CVD events in individuals with increased inflammation but without LDL lowering (53). However, the study showed no additional CVD benefits for subjects with diabetes (54). Regardless of diabetes status, subjects who achieved hs-CRP levels less than 2 mg/L after the monoclonal antibody treatment demonstrated greater cardiovascular benefits than those who did not (55). Besides CANTOS, the Low-dose Colchicine 2 (LoDoCo2) trial also supported the role of inflammation in CVD events (56). Consistent with CANTOS (54), the LoDoCo2 trial shows no additional CVD benefits for subjects with diabetes (57). The lack of additional benefits for diabetic subjects in the two studies could be due to heightened inflammatory status in nondiabetic subjects, which may mask the diabetes effect. Together, these studies indicate that inflammation plays a role in CVD outcomes when an individual has heightened inflammation. It is also possible that inflammation, especially the IL-1β-associated pathway, could play a partial role in accelerating

atherosclerosis progression under diabetic conditions, especially when diabetes results in heightened inflammation.

IL-1β and IL-18 are pro-inflammatory cytokines that are released upon the activation of inflammasome pathways (58). The NLRP3 inflammasome has been demonstrated to be activated under diabetes conditions and may be a potential mediator for vascular complications under diabetic conditions (45; 59). When compared to healthy individuals, some studies show that those with T2D have elevated levels of plasma IL-1β and IL-18 (45). The monocytes from individuals with diabetes also demonstrated elevated levels of pro-inflammatory cytokines released *in vitro* (45; 46). Moreover, when compared to monocytes isolated from healthy individuals, those from individuals with acute myocardial infarction also demonstrated elevated levels of NLRP3 inflammasome-related markers (60). Together, these results suggest that inflammasome activation could participate in diabetes-accelerated atherosclerosis.

The contribution of inflammasome activation in atherosclerosis progression under diabetic conditions has been highlighted by a recent study demonstrating an atheroprotective effect of an NLRP3 inflammasome inhibitor (16). In a streptozotocin-induced insulin-deficient T1D apolipoprotein E-knockout mouse model, inhibition of NLRP3 inflammasome activation reduced atherosclerosis lesion size and IL-1β accumulation under diabetes conditions (16). Previous studies indicated the importance of hematopoietic cells for these effects in that hematopoietic NLRP3-deficiency (61) or caspase-1/11-deficiency (62)reduced atherosclerosis lesion progression in *Ldlr*$^{-/-}$ mice. However, whether the same pathway exists under diabetes conditions remains unclear. Multiple factors can stimulate the NLRP3 inflammasome under diabetic conditions, including, but not limited to, cholesterol crystals (61; 63), oxidized LDL (64; 65), and APOC3(35).

1.3 Thesis Objectives and Overview of Chapters

The work presented in this dissertation aims to provide insights into the underlying mechanisms that exacerbate atherosclerosis progression under diabetes conditions. This work will provide insights on how diabetes exacerbates atherosclerosis via inflammasome- and APOC3-dependent pathways. The association among inflammasomes, APOC3, and diabetes-accelerated atherosclerosis is introduced and demonstrated in Chapter 2 by using a mouse model of T1D. The work in Chapter 2 also provides evidence demonstrating that inflammasome-related pro-inflammatory cytokines can be released from non-hematopoietic cells and suggesting the role of hematopoietic inflammasomes in diabetes-associated atherosclerosis might be independent of plasma IL-18 and IL-1β. Although APOC3 has been shown to contribute to diabetes-associated atherosclerosis and diabetes is associated with elevated plasma APOC3 and inflammasome activation, the association between APOC3 and inflammasome activation under diabetes conditions remained elusive. The work in Chapter 3 demonstrates that the ability of APOC3 to induce inflammasome activation is dependent on the lipidation state of the protein. This finding at the molecular level is further investigated with multiple mouse models and human genetic data in Chapter 3, which demonstrates that endogenous APOC3 does not lead to inflammasome activation under diabetes conditions. Although circulating levels of de-lipidated APOC3 are not high enough to induce inflammasome activation in circulation, de-lipidated APOC3 may still exist in tissue and induce inflammasome activation locally. Together, the work presented in this dissertation highlights the role of inflammasome- and APOC3-dependent pathways in accelerated atherosclerosis progression in mouse models of T1D. These findings suggest that inhibiting both pathways may provide novel therapeutics for reducing CVD risk in individuals with diabetes.

Chapter 2 : Hematopoietic NLRP3, AIM2 Inflammasomes, and Pyroptosis Promote Lesion Progression but not Necrotic Core Expansion under Diabetes Condition

Portions of this chapter were published as a manuscript in *Diabetes* (66).

2.1 Background

Despite the success of statins in reducing cardiovascular disease (CVD) events (67), CVD remains the leading cause of death in the US (67). Numerous efforts have been made to reduce CVD mortality but the trend has stalled, in part due to the rising prevalence of diabetes (67; 68). Individuals with type 1 or type 2 diabetes suffer from an increased risk of atherosclerotic CVD (67; 68). The persistently elevated CVD risk among individuals with diabetes, despite LDL-lowering, suggests the presence of diabetes-associated risks. Multiple risk factors—including glucose (14), inflammation (16; 17), and abnormal metabolism of triglyceride-rich lipoproteins (TRLs) and their remnants (13; 69; 70) —have been proposed as contributors to diabetes-associated increases in CVD.

Monocytes and macrophages play important roles in all stages of atherosclerotic lesion development (3; 17). The accumulation of monocytes in response to lipoprotein accumulation in the artery wall and their subsequent differentiation into macrophages exacerbate arterial inflammation (5). Macrophages can undergo programmed cell death after taking up lipoproteins, contributing to the lipid-rich, acellular necrotic cores that characterize the progression of the advanced lesion (3; 5). Individuals with diabetes have increased lesional macrophage content (based on $CD68^+$ immunoreactivity) and necrotic cores that could contribute to the acceleration of atherosclerosis (44) as well as CVD events (71). With the Canakinumab Anti-inflammatory Thrombosis Outcome Study (CANTOS) highlighting the causal involvement of IL-1β in atherosclerotic cardiovascular events in individuals with and without diabetes (53), the roles of macrophages and inflammation—especially the inflammasome pathway responsible for the secretion of mature IL-1β and IL-18—in diabetes-associated atherosclerosis have gained intense interest.

Apolipoprotein C3 (APOC3) has been reported to predict future CVD events in individuals with type 1 diabetes from three different cohorts (15; 33; 34). Although APOC3 likely exacerbates diabetes-associated atherosclerosis primarily via inhibiting the clearance of TRLs and their remnants (70) lipid-free APOC3 has been shown to activate an alternative inflammasome pathway in human and mouse monocytes (35; 72).

The findings above, together with a report demonstrating that individuals with type 2 diabetes have elevated serum levels of IL-1β and IL-18 (45), make it tempting to speculate that inflammasome pathways could contribute to atherosclerosis and clinical events in individuals with both T1 and T2DM and that inflammasome inhibition might be beneficial in diabetes. Furthermore, statins can increase the incidence of type 2 diabetes through a mechanism that may involve inflammasome activation (73; 74). Hematopoietic deficiencies in essential inflammasome components—such as NLRP3 (75-77), AIM2 (78), apoptosis-associated speck-like protein containing a CARD (ASC) (77), or caspase-1/11 (75) —have been reported to be atheroprotective in mice with diseases that promote inflammasome activation. Moreover, a recent study demonstrated that systemic inhibition of the NLRP3 pathway using the small-molecule NLRP3 inhibitor MCC950 is atheroprotective in diabetic apolipoprotein E-deficient (*Apoe*$^{-/-}$) mice (16). However, whether inflammasome components contribute to diabetes-associated atherosclerosis via the hematopoietic compartment remains unexplored.

Upon activation of NLRP3 or AIM2 inflammasomes, activated caspase-1 cleaves IL-1β and IL-18 into their mature forms, which are secreted upon caspase-1 activation of the pore-forming protein gasdermin D (GSDMD) (79). GSDMD activation also promotes pro-inflammatory cell death called pyroptosis (79). Consistent with the studies demonstrating that inflammasome pathways contribute to atherosclerosis, global GSDMD-deficiency has been reported to be

atheroprotective in some (80) but not other studies (78) in *Ldlr*$^{-/-}$ mice. It is not known if similar mechanisms contribute to diabetes-accelerated atherosclerosis.

To address whether hematopoietic inflammasome activation and pyroptosis contribute to diabetes-associated atherosclerosis, we investigated the role of hematopoietic GSDMD, AIM2, and NLRP3. We demonstrate that diabetes is associated with inflammasome activation and elevated plasma IL-1β and IL-18. Furthermore, while both hematopoietic NLRP3 and AIM2 inflammasomes and GSDMD contributed to lesion area progression in diabetic mice, the necrotic core expansion could not be explained by macrophage pyroptosis, as hematopoietic GSDMD-deficiency failed to provide protection.

2.2 Materials and Methods

2.2.1 Mouse models

All animal studies were approved by the Institutional Animal Care and Use Committees of the University of Washington and Columbia University.

Virus-induced mouse model of type 1 diabetes-accelerated atherosclerosis: As described previously (81), *Ldlr*$^{-/-}$ mice expressing the lymphocytic choriomeningitis virus (LCMV) glycoprotein transgene (*Gp*^{Tg}) under control of the rat insulin promoter, allowing reliable induction of CD8^{+} T-cell-mediated β-cell destruction upon LCMV injection (Armstrong 53b; 1.3x10^{4} pfu/mouse), were used as one of the mouse models of type 1 diabetes-accelerated atherosclerosis. Littermates without the glycoprotein transgene (*Gp*^{0}) were used for evaluating the possible effects of LCMV independent of diabetes. Female mice were used in this study because the NLRP3 inflammasome pathway has been reported to play a more important role in atherosclerosis in female mice than in male mice (82).

For the study on plasma analytes, 8- to 12-week-old female *Ldlr*$^{-/-}$;*Gp*^{Tg} and *Ldlr*$^{-/-}$;*Gp*^{0} mice on a C57BL/6J background were injected with LCMV (Armstrong 53b; 1.3x10^4 pfu/mouse) to serve as the diabetic group and virus control group. Non-diabetic littermates received saline. After the onset of diabetes, defined by blood glucose greater than 13.9 mmol/L, animals received insulin pellets (LinShin Canada Inc.) to provide baseline insulin and liquid insulin injections (Lantus) as needed to prevent ketonuria and severe weight loss. The mice were maintained on a low-fat diet (LFD) described previously (81) for 4 weeks before the termination of the study.

For the atherosclerosis studies, 6- to 10-week-old female *Ldlr*$^{-/-}$;*Gp*^{Tg} mice on a C57BL/6J background were maintained on a semipurified high-fat-diet (HFD) for 12 weeks to allow the formation of pre-existing atherosclerosis lesions and to allow us to study the effect of diabetes and GSDMD on advanced lesions without confounding effects on lesion initiation. The HFD contains 40% fat and 1.25% added cholesterol (81). After 12 weeks of HFD, the mice were switched to chow diet to normalize plasma lipid levels before being irradiated with 10 Gy from a cesium gamma source and receiving 5x10^6 bone marrow cells/recipient harvested from mice with and without GSDMD-deficiency. The donor mice with CRISPR-edited GSDMD-deficiency (83), were generously provided by Genentech. The mice recovered for 5 weeks on a chow diet before induction of diabetes with LCMV. After the onset of diabetes, animals were maintained on a LFD for 4 weeks before the termination of the study, according to a published study design (84).

Mouse model of acute inflammasome activation: 8- to 12-week-old female and male *Gsdmd*$^{-/-}$, *Gsdmd*$^{+/+}$, *Ldlr*$^{-/-}$;*Gp*^{Tg}, and C57BL/6J mice received an i.p. injection of 5 mg ultrapure LPS (List Labs) or saline. Four hours after the first injection, animals received an i.p. injection of 5 mM ATP or PBS. The experiment was terminated 1 hour after the second injection. To investigate the role of hematopoietic GSDMD in IL-18 and IL-1b release following inflammasome activation, 8- to

12-week-old male *Ldlr*$^{-/-}$ mice received bone marrow harvested from mice with and without GSDMD-deficiency. After a 5-week recovery on a chow diet, the mice received ultrapure LPS and ATP injections. Solutions were sterile-filtered before the injections.

Streptozotocin (STZ)-induced type 1 diabetes mouse model: 8- to 10-week-old female *Ldlr*$^{-/-}$ mice on a C57BL/6J background were irradiated with 10.5 Gy from a cesium gamma source and receiving 4x10^6 bone marrow cells/recipient harvested from female *Nlrp3*$^{-/-}$ (Jackson 021302), *Aim2*$^{-/-}$ (Jackson 013144), *Nlrp3*$^{-/-}$*Aim2*$^{-/-}$ (DKOs), or control wildtype bone marrow. Mice recovered for four weeks on a chow diet before STZ injection (i.p., 50 mg/kg, 5 consecutive days) and were then switched to a Western diet (ENVIGO TD.88137) for 8 weeks before the termination of the experiment.

Atherosclerosis study in whole-body GSDMD-deficient mouse model: Eight to 12-week-old male mice with whole-body gasdermin D-deficiency and wildtype littermate controls on a C57BL/6 background were maintained on a high-fat high-sucrose diet with added cholesterol (HFHS), as described previously (85), for 16 weeks before the termination of the experiment. While the mice were maintained on the HFHS diet, they received weekly i.p. injections of a GalNAc-conjugated LDLR antisense oligonucleotide (ASO, 5 mg/kg, Ionis Pharmaceuticals).

2.2.2 Genotyping

Genotyping for *Ldlr*, *Nlrp3* and *Aim2* was conducted by following the manufacturer's protocols (The Jackson Laboratory). *Gsdmd* genotyping was performed with blood or peritoneal cavity lavage. Leukocytes were enriched from the samples by removing erythrocytes with an ammonium-chloride-potassium buffer. After removing erythrocytes, samples were purified for DNA following the manufacturer's instructions (QIAGEN). DNA samples were quantified for *Gsdmd* wildtype and knockout mutant gene (one base pair thymidine insertion) expression with the real-time PCR

method. DNA samples were incubated with Taqman gene expression master mix (Thermo Fisher Scientific), *Gsdmd* forward primer (5'-GTCGATGGGAACATTCAG-3'), *Gsdmd* reverse primer (5'-TGAGTCACACGCAGTATA-3'), *Gsdmd* wildtype probe (5'-/56FAM/CCT+GA+C+A+AA+CA+TCA/3IABkFQ/-3'), and *Gsdmd* mutant probe (5'-/5HEX/CCT+GA+C+A+A+CA+TCA/3IABkFQ/-3; all from Integrated DNA Technologies). Initial denaturation at 95°C, 10 minutes, cycling denaturation at 95°C, 10 seconds, cycling annealing at 60°C, 30 seconds, cycling extension at 72°C, 10 seconds, 40 cycles.

Analysis of blood glucose and plasma analytes

Blood glucose levels were measured with a glucometer (OneTouch Ultra; LifeScan). Any values above 33.3 mmol/L were reported as 33.3 mmol/L as they reached the maximum detection limit of the device. Plasma analytes were measured with respective assays or kits described in **Table 1.**

2.2.3 Quantification of atherosclerosis

The aortae were dissected after perfusion with PBS and fixed with 10% phosphate-buffered formalin. The aortae were opened longitudinally and stained with Sudan IV as described (15; 81). The aortic sinuses were fixed with 10% phosphate-buffered formalin, paraffin-embedded, then serially sectioned for histological analysis. The sinus sections were stained with Movat's pentachrome stain or hematoxylin and eosin to visualize lesion morphology. The sinuses were analyzed at three different sites, beginning at the appearance of all 3 aortic valve leaflets , using ImageJ. Lesional Mac-2, a-SMA, APOC3, apolipoprotein B (APOB), and apolipoprotein E (APOE) immunoreactivity was determined by immunofluorescence. Stained samples were coverslipped with DAPI-containing mounting medium (Vector Laboratories) before imaging and quantifying with a fluorescence microscope (Keyence, BZ-X800). Lesion severity was analyzed according to the scoring system described by Stary et al. (86): 0, no lesion; 1, intimal change only (matrix); 2,

fatty streak without dramatic matrix expansion; 3, fatty streaks with cholesterol clefts (extracellular lipids); 4, lesions with necrotic cores; 5, lesions with necrotic cores and abundant matrix; 6, ruptured lesions. The scores were summarized for each mouse. Investigators were blinded to the treatment groups during the processing and analysis of the samples. Co-stained areas were quantified before the single-stained areas. Details on the antibodies and negative controls are available in **Table 2 and Fig. 1-2**.

Flow cytometry analysis of blood leukocytes

Blood leukocyte populations were analyzed by flow cytometry and a gating strategy was determined using single-stained and unstained controls (**Fig. 3** and **Table 3**). Details on the antibodies are available in **Table 4**.

2.2.4 Immunoblotting

Peritoneal cavity cells were harvested immediately with cold EDTA-containing PBS after experiment termination. A protease and phosphatase inhibitor cocktail (Thermo Fisher Scientific) was added immediately after sample collection. The samples were centrifuged at 400xg for 5 minutes at 4°C to isolate peritoneal cavity cells and fluid. Peritoneal cavity cells were purified with an F4/80-positive-selection kit (Thermo Fisher Scientific) to enrich the macrophage population, following the manufacturer's instructions. Enriched $F4/80^+$ peritoneal cavity cells were lysed with RIPA buffer (Thermo Fisher Scientific) containing a protease and phosphatase inhibitor cocktail. Samples were separated on SDS-PAGE gels and transferred to nitrocellulose membranes. Membranes were probed with primary and secondary antibodies before imaging (LICOR). Antibody information is available in **Table 5**.

2.2.5 Statistical analysis

Power calculations were used to determine the number of animals per group. Investigators were blinded to the treatment groups during sample processing and data analysis. Statistical analyses were performed using GraphPad Prism 9.4.0 (GraphPad Software). Normality tests were performed by the D'Agostino & Pearson test. Data are displayed as mean ± SEM. Based on the normality of the data, they were analyzed with two-sided Mann-Whitney test, Kruskal-Wallis test and Dunn's multiple comparisons tests, or two-way ANOVA followed by Tukey multiple comparisons test. A p-value of less than 0.05 was considered statistically significant. Statistical outliers were identified by Grubb's test with alpha = 0.01. All removed statistical outliers are described in the figure legends.

2.2.6 Data and Resource Availability

The datasets generated during and/or analyzed during the current study are available from the corresponding author upon reasonable request. No applicable resources were generated or analyzed during the current study.

2.3 Results

2.3.1 Diabetes Elevates Plasma Triglycerides, APOC3, and Inflammasome Signatures

To investigate whether diabetes activates inflammasome pathways, *Ldlr*$^{-/-}$ *Gp*^{Tg} mice were injected with saline or LCMV and maintained on LFD for 4 weeks (**Fig**. **4A**). The *Gp*^{Tg} animals had elevated levels of blood glucose after LCMV injection, as compared with those that received saline injections (**Fig. 4B**). Animals with blood glucose above 13.9 mmol/L were considered diabetic. To verify that the effects of LCMV were due to diabetes and not to the LCMV per se, a virus control group (*Ldlr*$^{-/-}$*;Gp*^{0}) was included (**Fig. 4A**). Due to the lack of the GP transgene in b-cells, animals from the virus control group did not develop diabetes upon LCMV injection (**Fig. 4B**). Compared with non-diabetic animals, diabetic animals demonstrated elevated levels of plasma triglycerides,

IL-18, IL-1b, and APOC3 (**Fig. 4C-G**). Consistent with the previous study by Zewinger and colleagues (35), elevated plasma APOC3 was accompanied by elevated plasma IL-18 and IL-1b, suggesting that activation of an inflammasome pathway in diabetic mice could be related to elevated levels of APOC3. Moreover, cleaved caspase-1 and the ratio of cleaved caspase-1 over full-length caspase-1 were elevated in the peritoneal cavity fluid from diabetic animals (**Fig. 4H-J**), further indicating inflammasome activation. Monocytosis and increased numbers of $Ly6C^{high}$ monocytes, which have been suggested to contribute to atherosclerosis progression (87; 88), were not observed in this mouse model of type 1 diabetes (**Table 3**). The animals in the virus control group did not have these analytes elevated when compared to the non-diabetic animals. The phenotypes of diabetic mice are therefore unlikely to be confounded by LCMV injections.

2.3.2 Hematopoietic gasdermin D reduces lesion area but does not affect atherosclerosis lesion phenotypes in diabetic mice

To investigate whether diabetes accelerates the progression of pre-existing atherosclerotic lesions via a hematopoietic GSDMD-dependent pathway, female *Ldlr*$^{-/-}$*;Gp*^{Tg} mice with pre-existing lesions received bone marrow transplants from animals with or without GSDMD-deficiency before being rendered diabetic for 4 weeks (**Fig. 5A**). A subset of animals was euthanized before diabetes induction to evaluate the effects of genotypes on bone marrow reconstitution efficiency and lesion morphologies. Bone marrow GSDMD-deficient chimeras exhibited a 98-95% reconstitution in the blood, spleen, or peritoneal cavity (**Fig. 6A**). Concurrently, hematopoietic deletion of GSDMD did not affect lesion morphologies at baseline, prior to induction of diabetes (**Fig. 6B-I**). After 4 weeks of LFD, compared with non-diabetic animals, diabetic animals demonstrated elevated levels of blood glucose, plasma triglycerides, cholesterol, IL-18, IL-1b, and APOC3 (**Fig. 5B-G**), consistent with the short-term study (**Fig. 4**). However, hematopoietic GSDMD-deficiency did not alter these

levels. Current literature predicts that myeloid cells are the major source of IL-1b and IL-18 released upon inflammasome and GSDMD activation (79). However, our findings suggested that plasma IL-1b and IL-18 are secreted by hematopoietic cells independently of GSDMD or is secreted by non-hematopoietic cells.

Although plasma IL-18 and IL-1b were not suppressed by hematopoietic GSDMD-deficiency in mice with diabetes, we reasoned that GSDMD-mediated pyroptosis could contribute to atherosclerosis progression and necrotic core expansion. Similar to a human study (44) and our previous studies (15; 84), aortic sinus necrotic core size was exacerbated by diabetes without an effect on the size of pre-existing sinus lesions (**Fig. 4H-I**) and aortic *en face* Sudan IV area (**Fig. 7A-C**). Hematopoietic GSDMD-deficiency resulted in smaller lesions in diabetic mice, but did not alter necrotic core size in these mice (**Fig. 4H-I**). The lack of effects of the hematopoietic GSDMD-deficiency on necrotic core size was not due to differences in monocytosis or accumulation of lesional macrophages (quantified by $Mac2^+$ immunoreactivity) or smooth muscle cells (quantified by a-SMA^+ immunoreactivity) (**Table 6-7** and **Fig. 8**). The lack of protective effects in this study suggests that diabetes exacerbates necrotic core expansion via mechanisms independent of hematopoietic GSDMD. We can only speculate on the reason behind the increased necrotic core area in non-diabetic mice with hematopoietic GSDMD-deficiency (**Fig. 4I**). It is possible that other cell death pathways are activated in GSDMD-deficient cells (89) or that GSDMD-deficiency results in increased inflammasome activation through a feedback loop mediated by the N-terminal GSDMD fragment (90). Such effects might be masked by the increased necrosis in diabetes.

To verify that whole-body deletion of GSDMD results in protection from atherosclerosis development, as has been reported by others (80), a control cohort of whole-body GSDMD-deficient mice and wildtype littermate controls were injected with LDLR ASO and fed an HFHS

diet to initiate and promote atherosclerosis (**Fig. 9A**). Whole-body GSDMD-deficiency resulted in reduced lesion area, consistent with a previous study (80), and reduced relative necrotic core area (**Fig. 9B-D**).

2.3.3 Non-hematopoietic gasdermin D contributes to the release of circulating IL-18 and IL-1β

To investigate whether hematopoietic GSDMD is responsible for the release of IL-1b and IL-18 to plasma in vivo, animals with and without whole-body- or hematopoietic GSDMD-deficiency were treated with ultrapure LPS and ATP for acute inflammasome activation in the peritoneal cavity (**Fig. 10A** and **10D**). Animals with whole-body GSDMD-deficiency exhibited markedly suppressed plasma IL-1b and IL-18 levels upon inflammasome activation (**Fig. 10B-C** and **Fig. 11**). There were no marked differences in plasma IL-18 responses between male and female mice, or between C57BL/6 mice and $Ldlr^{-/-};Gp^{Tg}$ mice to LPS and ATP stimulation (**Fig. 11**). These findings concur with previous studies demonstrating that GSDMD contributes to the release of IL-1b and IL-18 (79). However, hematopoietic GSDMD-deficiency failed to suppress plasma IL-1b and IL-18 levels upon inflammasome activation (**Fig. 10E-F**), consistent with the lack of plasma IL-1b and IL-18 reduction in diabetic mice with hematopoietic GSDMD-deficiency (**Fig. 5E-F**). Our findings suggest that the release of IL-18 and IL-1b to the plasma compartment might be mediated via non-hematopoietic cells in this model of acute inflammasome activation.

To further investigate whether diabetes induces inflammasome activation in macrophages through a GSDMD-dependent pathway, we analyzed inflammasome activation in $F4/80^+$ peritoneal macrophages. These studies confirmed the successful deletion of GSDMD in $F4/80^+$ peritoneal cavity macrophages. We were unable to detect increased levels of cleaved (active) forms of GSDMD and caspase-1in macrophage lysates from diabetic mice. However, diabetes increased levels of cleaved GSDMD and caspase-1 in the peritoneal cavity fluid through a mechanism that

was independent of hematopoietic GSDMD-deficiency (**Fig. 12**). These findings suggest that while inflammasome activation may occur in macrophages (or possibly in other cell types) in diabetic mice, the release of cleaved caspase-1 is independent of GSDMD.

2.3.4 Hematopoietic AIM2- and NLRP3-deficiencies do not alter blood glucose, serum lipids, IL-1b or IL-18 in diabetic mice, but hematopoietic NLRP3-deficiency results in reduced serum APOC3 levels

Previous studies demonstrated that hematopoietic inflammasome activation can promote lesion progression in other models (75-78), which prompted the investigation of whether hematopoietic AIM2, NLRP3, and double-deficiencies of AIM2 and NLRP3 (DKOs)—upstream of GSDMD—can prevent early atherosclerosis initiation and progression under diabetic conditions. Female *Ldlr*$^{-/-}$ mice received bone marrow transplants from donors with AIM2-deficiency, NLRP3-deficiency, or DKOs before induction of diabetes and Western diet-feeding for 8 weeks (**Fig. 13A**). Hematopoietic inflammasome-deficiencies did not significantly affect blood glucose, serum triglycerides, serum cholesterol levels, serum IL-1b or IL-18 levels (**Fig. 13B-F**), consistent with the lack of effect from hematopoietic GSDMD deficiency (**Fig. 5B-F**). However, hematopoietic NLRP3-deficiency resulted in lower serum levels of APOC3, an effect observed both in diabetic mice with NLRP3-deficiency and in NLRP3- AIM2-double-deficiency (**Fig. 13G**).

2.3.5 Hematopoietic AIM2- and NLRP3-deficiencies suppress the aortic sinus lesion area but not the relative necrotic core area in diabetic mice

Diabetic mice with hematopoietic deletions of NLRP3 and/or AIM2 had reduced sinus lesion size (**Fig. 13H**), which is consistent with previous studies (75-78). However, the hematopoietic deletions of NLRP3 and AIM2 failed to reduce the relative necrotic core area (**Fig. 13I**). Neither NLRP3- nor AIM2-deficiency resulted in changes in lesion MAC2^{+} area or α-SMA^{+} area (**Fig.**

14). Thus, hematopoietic NLRP3 and AIM2 inflammasome activation contributes to lesion development (lesion area) but not to a relative expansion of the necrotic core area or marked changes in cell type composition in diabetic mice at an 8-week time-point of atherosclerosis. Importantly, although the STZ-diabetic mice in this experiment were less severely diabetic than the LCMV-diabetic mice (as shown by their lower blood glucose levels) and had higher serum cholesterol than the LCMV model because of the Western-style diet, there were no significant differences between the STZ model and the LCMV model of type 1 diabetes in triglycerides, IL-18, IL-1b, sinus lesion area, relative necrotic core area, or overall lesion severity (**Table 8**).

2.3.6 Diabetes increases APOC3 and APOE accumulation in the aortic sinus through a GSDMD-independent mechanism

To further investigate the potential culprit responsible for necrotic core expansion in diabetes-accelerated advanced atherosclerosis, aortic sinuses harvested from animals with and without diabetes and/or hematopoietic GSDMD-deficiency were immunostained for APOC3, APOB, and APOE, apolipoproteins present on TRLs. Our data show that diabetes not only elevates plasma APOC3 levels (**Fig. 4G** and **5G**) but also increases lesional APOC3 accumulation, as measured by $APOC3^+$ immunoreactivity (**Fig. 15A** and **15F**). Lesional $APOE^+$ immunoreactivity and lesion area positive for both $APOB^+APOE^+$ were also increased under diabetes conditions (**Fig. 15B-E**), consistent with the known APOC3 effect in inhibiting the clearance of TRLs and their remnants (13; 69; 70). There was no effect of hematopoietic GSDMD-deficiency. Likewise, diabetic mice with hematopoietic NLRP3/AIM2 double-deficiency showed no significant differences in either lesional $APOC3^+$ or $APOB^+APOE^+$ immunoreactivities (**Fig. 14**). Together, these findings suggest that APOC3, through abnormal metabolism of TRLs and their remnants, might be indirectly

responsible for accelerating necrotic core progression under diabetes conditions, consistent with our previous studies (15; 84).

2.4 Discussion

Atherosclerosis is a chronic inflammatory disease that can involve hematopoietic inflammasome activation. Previous studies have demonstrated that hematopoietic deletion of essential inflammasome components confers atheroprotection under conditions associated with increased inflammasome activation (75-78). With the clinical effectiveness of IL-1β inhibition in preventing CVD events in individuals with and without diabetes (53), the presence of a similar pathological mechanism in diabetes-associated atherosclerosis becomes a plausible hypothesis. The involvement of inflammasome pathways in diabetes-associated atherosclerosis is further supported by studies demonstrating that APOC3 predicts future CVD events in individuals with type 1 diabetes (15; 33; 34) and that de-lipidated APOC3 can induce alternative NLRP3 inflammasome activation in human monocytes (35; 72). Moreover, systemic inhibition of the NLRP3 inflammasome pathway using a small-molecule inhibitor prevented atherosclerosis in diabetic mice (16). We now show that mice with type 1 diabetes indeed exhibit increased inflammasome activation, measured as elevated plasma IL-18 and IL-1b and increased levels of cleaved caspase-1 in the peritoneal cavity interstitial fluid. Furthermore, our study provides strong evidence that hematopoietic NLRP3 and AIM2, as well as GSDMD, contribute to lesion size but not to a relative increase in necrotic core expansion, a feature associated with clinical events in humans (71), in diabetic mice. Deletion of the cholesterol exporters ABCA1 and ABCG1 in myeloid cells is known to activate the NLRP3 inflammasome (75). Reduced expression of these transporters in macrophages in the setting of diabetes (91; 92) might therefore contribute to NLRP3 activation. The AIM2 inflammasome, which is potentially activated by cytosolic double-stranded

DNA from phagocytosed dead cells or damaged nuclei or mitochondria (93), has not previously been shown to contribute to atherosclerosis in diabetes. Although the mechanism whereby diabetes activates the AIM2 inflammasome needs further investigation, an interesting possibility is that mitochondrial dysfunction in macrophages from diabetic mice (94) could contribute to the activation of the AIM2 inflammasome. Oxidative DNA damage has been implicated in AIM2 activation and accelerated atherosclerosis associated with clonal hematopoiesis (78).

Despite the increased inflammasome activation in diabetic mice, our results indicate that hematopoietic GSDMD deletion does not reduce the release of IL-1b and IL-18 to plasma. The lack of reduction in plasma IL-1b and IL-18 levels in animals with hematopoietic GSDMD-deficiency suggests that IL-1b and IL-18 that reach the plasma pool are secreted from hematopoietic cells via pathways independent of GSDMD, such as through gasdermin E (79), or potentially from non-hematopoietic cells. However, measurements of plasma levels of IL-1b and IL-18 might not capture local effects in tissues or on lesion development, especially since IL-18 is expressed by nearly all epithelial cells and keratinocytes, in addition to myeloid cells (95).

The inability of hematopoietic GSDMD-deficiency to suppress plasma IL-1b and IL-18 levels provided an opportunity to study the effects of the GSDMD pyroptotic pathway on diabetes-associated atherosclerosis independent of pro-inflammatory cytokine suppression. Macrophage cell death is considered a major contributor to lesional necrotic core formation (79), however, whether pyroptosis contributes to necrotic core formation under diabetes conditions remained unexplored. Pyroptosis is defined as cell death mediated by GSDMD (96). Because there are many other types of cell death, pyroptosis can currently only be selectively measured in vivo as cell death prevented by GSDMD-deficiency (79). Consistent with previous studies (15; 84), diabetes accelerated aortic sinus necrotic core expansion without increasing the lesion area of pre-existing

lesions in our study. However, targeting hematopoietic GSDMD did not affect the relative necrotic core area, suggesting that this aspect of diabetes-accelerated atherosclerosis is governed by mechanisms independent of hematopoietic GSDMD-mediated pyroptosis.

Together, our study provides evidence demonstrating that while hematopoietic NLRP3, AIM2 and GSDMD do not play critical roles in necrotic core expansion, NLRP3, AIM2, and GSDMD contribute to overall lesion size in diabetic mice. The reasons for the different results on the role of hematopoietic NLRP3, AIM2 and GSDMD on atherosclerosis in different mouse models (61; 62; 75-78) are uncertain, but could be related to female-specific effects (82) or the presence of different factors that lead to increased inflammasome activation. Together, these studies suggest a greater effect of hematopoietic inflammasome activation in mice or humans with additional conditions or mutations that promote inflammasome activation, such as diabetes or clonal hematopoiesis associated with the $JAK2^{V617F}$ variant (78).

Our results suggest that the relative necrotic core expansion in lesions of diabetic mice involves a mechanism independent of inflammasome activation and pyroptosis. There are multiple risk factors associated with increased CVD risk in individuals with diabetes (21), one of which could be abnormal metabolism of TRLs (13; 69; 70). We have previously shown that silencing of APOC3 prevents lesion initiation, necrotic core expansion and accumulation of lesion APOC3 immunoreactivity in diabetic mice (15). Consistently, human studies show a correlation between plasma APOC3 and necrotic core volume (97). The current study demonstrates that diabetes increases the accumulation of immunoreactive APOC3 and APOE, as well as co-localization of APOE and APOB in the aortic sinus. TRLs and their remnants are APOB lipoproteins that carry APOC3 and APOE (13). It is therefore tempting to speculate that the increased necrotic core size in diabetic mice could be due to accumulation of TRLs or TRL remnants, which are readily taken

up by macrophages (98) and endothelial cells (99). However, some of the APOE is derived from cells in the lesion rather than from circulation. The exact mechanism whereby increased APOC3 in diabetes promotes lesion necrotic core expansion needs further investigation, but could involve indirect effects mediated by TRL remnants in endothelial cells, smooth muscle cells, or lesion immune cell populations. It is possible that other forms of cell death, such as ferroptosis or necroptosis (79), could contribute to APOC3-mediated necrotic core expansion in the setting of diabetes.

Our study sheds further light on the links between NLRP3 and APOC3. APOC3 can activate an alternative NLRP3 inflammasome pathway in both human and mouse monocytes, but only in its delipidated form (35; 72). When APOC3 is bound to lipid particles, which it is in the circulation, this effect is lost (72). Moreover, silencing of APOC3 did not lower plasma IL-18 levels in our mouse model of type 1 diabetes (72). It is therefore unlikely that APOC3 acts upstream of NLRP3 inflammasome activation. However, there is an association between an *NLRP3* variant that results in increased NLRP3 activation and plasma APOC3 levels (100). Our finding that serum APOC3 levels are lower in diabetic mice with hematopoietic NLRP3-deficiency raises the possibility that NLRP3 might act upstream of APOC3 rather than downstream of APOC3 in vivo. It is, for example, possible that NLRP3 activation in hepatic leukocytes results in increased APOC3 production or reduced APOC3 clearance. Furthermore, since the decrease in APOC3 levels (from 740 to 420 mg/mL) that attended NLRP3 deficiency did not lead to a decrease in necrotic core area, this suggests that a more extensive reduction in APOC3 is required to prevent necrotic core expansion or that the association between plasma APOC3 and necrotic core area does not indicate direct causation.

Our study has several limitations. Although the two different type 1 diabetes models exhibited similar levels of plasma IL-1b and IL-18 and similar lesion sizes and severity, direct quantitative comparisons are not possible. For example, in the STZ-diabetes experiment hematopoietic NLRP3 and AIM2 deficiencies were present during both lesion initiation and progression whereas the GSDMD experiment was designed to investigate effects on pre-existing lesions. Moreover, non-diabetic controls might have been informative in the STZ experiment, as would inclusions of male mice in all experiments. Also, it is likely that IL-1b and IL-18 act locally within the lesion. Direct measurements of inflammasome activation and release of mature IL-1b and IL-18 in lesions of atherosclerosis are hampered by the lack of antibodies able to distinguish mature and pro-forms of these cytokines.

Despite these limitations, our findings demonstrate that hematopoietic NLRP3, AIM2, and GSDMD promote lesion development in the setting of diabetes, but that increased necrotic core expansion is independent of hematopoietic GSDMD or pyroptosis. Further studies are needed to clarify the relative importance of inflammasome activation and APOC3-containing TRL remnants in cardiovascular complications of diabetes.

Table 1: Information on assays or kits used for measuring plasma analytes.

Assay/kit	Manufacturer	Catalog number
Mouse IL-1β ELISA kit	Thermo Fisher Scientific	88-7013-88
Mouse IL-18 ELISA kit	Thermo Fisher Scientific	88-50618-88
Mouse APOC3 ELISA kit	Abcam	ab217777
Cholesterol E Assay	Wako Diagnostics	999-02601
Triglyceride Liquicolor	Stanbio Laboratory	2100-430
Cholesterol Liquicolor	Stanbio Laboratory	1010-430
Mouse Enhanced Sensitivity Master Buffer Kit	BD Biosciences	562246
Mouse IL-1β Enhanced Sensitivity Flex Set	BD Biosciences	562278

Table 2: Information on antibodies and reagents used for immunofluorescence.

Antibody/reagents	Catalog number	Manufacturer	Concentration/dilution
Mac-2	CL8942AP	Cedarlane	2 μg/mL
α-Smooth muscle actin	AB5694	Abcam	0.4 μg/mL
APOC3	-	Ionis Pharmaceuticals	1:1000
APOB-biotinylated	BAF3556	Novus Biologicals	4 μg/mL
APOE	AB183597	Abcam	0.35 μg/mL
Biotinylated Goat IgG control	BAF108	Novus Biologicals	See APOB
Rabbit IgG control	02-6102	Thermo Fisher Scientific	See APOE, α-SMA
Rat IgG control	553927	BD Biosciences	See Mac-2
Anti-rabbit IgG, AlexaFluor647	A21245	Thermo Fisher Scientific	1:500
Anti-rat IgG, AlexaFluor555	405420	BioLegend	1:500
Tyramide-AlexaFluor488	B40953	Thermo Fisher Scientific	Per manufacturer's instructions
HRP-conjugated Streptavidin	016-030-084	Jackson ImmunoResearch Labs	1:5000
Mounting Medium with DAPI	H-2000	Vector Laboratories	Per manufacturer's instructions
Avidin/Biotin Blocking Kit	SP-2001	Vector Laboratories	Per manufacturer's instructions

Table 3: Circulating leukocyte counts from a 4-week type 1 diabetes mouse model.

(k/μL)	Non-diabetes	Diabetes	Virus control
Total leukocytes	5.98 ± 0.314	4.78 ± 0.596	7.21 ± 0.483†
Monocytes	0.355±0.031	0.143±0.018***	0.351±0.04††
GR1^{high} (Ly6C^{high}) Monocytes	0.215±0.020	0.101±0.017***	0.207±0.021†
GR1^{low} (Ly6C^{low}) Monocytes	0.102±0.013	0.032±0.004***	0.127±0.02†††
Neutrophils	0.968±0.062	2.01±0.327*	0.357±0.040†††‡‡

Female low-density lipoprotein receptor-deficient mice with a virus glycoprotein transgene (*Ldlr*$^{-/-}$*;Gp*^{Tg}) were rendered diabetic with lymphocytic choriomeningitis virus (LCMV). Saline was used as a control. *Ldlr*$^{-/-}$ mice without the glycoprotein (*Ldlr*$^{-/-}$*;Gp*^{0}) transgene were injected with LCMV as a virus control. At the onset of diabetes, the animals were switched to a low-fat, semipurified diet with no added cholesterol (LFD) and maintained for 4 weeks. Mice were bled retro-orbitally under isoflurane sudation after 4 weeks of diabetes. The total leukocyte count was determined by a hematology analyzer (Drew Scientific). Erythrocytes were lysed and removed with an ammonium-chloride-potassium buffer before staining. The leukocytes were stained for viability, CD45, CD115, and GR1. The single cell, live, CD45+, CD115+ population was identified as monocytes. The monocyte population was divided into GR1^{high} (Ly6C^{high}) and GR1^{low} (Ly6C^{low}) subpopulations. The single cell, live, CD45+, CD115-, and GR1^{high} population was identified as neutrophils. The single cell, live, CD45+ population was identified as leukocytes and normalized to the total leukocyte count. Flow analysis was conducted on a FACSCanto RUO Flow cytometer (BD Biosciences). Data show means ± SEM (n=21, 19, 7 mice/group). Statistical analyses were performed by Kruskal-Wallis test and Dunn's multiple comparisons tests. Normality test was performed by D'Agostino & Pearson test. *Significant between non-diabetes and diabetes groups. †Significant between diabetes and virus control groups. ‡Significant between non-diabetes and virus control groups. P<0.05 (*, †, ‡), <0.01 (**, ††, ‡‡), and < 0.001 (***, †††, ‡‡‡) are considered statistically significant. Outliers were removed based on Grubbs' test with alpha = 0.01. (0,1,0) data points were removed for monocytes; (0,1,0) data points were removed for GR1^{high} (Ly6C^{high}) monocytes; no other data points were removed.

Table 4: Information on antibodies used for flow cytometric analysis.

Antibody	Clone/catalog number	Manufacturer
CD45-FITC	30-F11	eBioscience
CD115-APC	AFS98	eBioscience
GR1-PE-Cy7	RB6-8C5	eBioscience
Viability dye e450	65-0863-14	eBioscience

Table 5: Information on antibodies and reagents used for immunoblotting and genotyping.

Antibody/reagent	Catalog number	Manufacturer	Concentration/dilution
Gasdermin D	-	Genentech	1 μg/mL
Caspase-1	14-9832-37	Thermo Fisher Scientific	1:50
Anti-rat HRP	A9037	Sigma-Aldrich	1:1000
Mouse F4/80 positive selection kit	8802-6863-74	Thermo Fisher Scientific	Per manufacturer's instructions
Ultrapure mouse CD11B microbeads	130-126-725	Miltenyi Biotec	Per manufacturer's instructions
DNA isolation and purification kit	158043	QIAGEN	Per manufacturer's instructions
RIPA lysis and extraction buffer	89900	Thermo Fisher Scientific	Per manufacturer's instructions
Protease and phosphatase inhibitor cocktail	78440	Thermo Fisher Scientific	Per manufacturer's instructions

Table 6: Circulating leukocyte counts from a 4-week diabetes mouse model with and without hematopoietic GSDMD-deficiency.

(k/μL)	No diabetes (*Gsdmd*$^{+/+}$)	No diabetes (*Gsdmd*$^{-/-}$)	Diabetes (*Gsdmd*$^{+/+}$)	Diabetes (*Gsdmd*$^{-/-}$)
Total leukocytes	10.7±0.79	9.94±0.79	7.72±1.15*	7.59±0.794
Monocytes	0.786±0.06	0.714±0.05	0.346±0.05***	0.327±0.04‡‡‡
GR1^{high}(Ly6C^{high}) Monocytes	0.576±0.06	0.466±0.03	0.227±0.04***	0.222±0.03‡‡‡
GR1^{low} (Ly6C^{low}) Monocytes	0.206±0.02	0.199±0.02	0.083±0.01***	0.074±0.01‡‡‡
Neutrophils	1.85±0.22	1.69±0.17	1.56±0.21	1.75±0.19

Female *Ldlr*$^{-/-}$*;Gp*^{Tg} mice were maintained on a high-fat diet (HFD) for 12 weeks to allow the formation of pre-existing lesions. Mice were lethally irradiated and received bone-marrow cells from animals with and without gasdermin D-deficiency. The animals were maintained on a chow diet and recovered for 5 weeks. Mice were rendered diabetic (D) with lymphocytic choriomeningitis virus (LCMV). Saline was used as a control (non-diabetic, ND). At the onset of diabetes, the animals were switched to a low-fat, semipurified diet with no added cholesterol (LFD) and were maintained for 4 weeks. Total leukocytes were measured with a hematology analyzer and the cell types were identified by flow cytometry as described in Table 3. Data show means ± SEM (n=22, 25, 24, 22 mice/group). Statistical analyses were performed by Kruskal-Wallis test and Dunn's multiple comparisons tests. Normality test was performed by D'Agostino & Pearson test. *Significant between non-diabetes (WT) and diabetes (WT) groups. †Significant between non-diabetes (WT) and non-diabetes (KO) groups. ‡Significant between non-diabetes (KO) and diabetes (KO) groups. P<0.05 (*, †, ‡), <0.01 (**, ††, ‡‡), and < 0.001 (***, †††, ‡‡‡) are considered statistically significant. Outliers were removed based on Grubbs' test with alpha = 0.01. (1,0,0,0) data points were removed for total leukocytes; (1,0,0,0) data points were removed for monocytes; (1,1,1,1) data points were removed for GR1^{low} (Ly6C^{low}) monocytes; (1,0,0,0) data points were removed for neutrophils; no other data points were removed.

Table 7: Lesion immunoreactivity area from a 4-week diabetes mouse model with and without hematopoietic GSDMD-deficiency.

x1000 µm²	No diabetes (*Gsdmd*$^{+/+}$)	No diabetes (*Gsdmd*$^{-/-}$)	Diabetes (*Gsdmd*$^{+/+}$)	Diabetes (*Gsdmd*$^{-/-}$)	Diabetes Effect p-value	Genotype Effect p-value
APOB$^+$ area	74.5±9.3	73.6±6.7	92.9±8.4	66.8±5.7	0.451	0.0824
APOE$^+$ area	146.6±13.1	132.3±10.6	184.8±10.4	142.2±6.8§	0.026	0.0087
APOB$^+$ APOE$^+$ area	57.0±6.8	53.1±4.9	77.9±5.8*	53.0±4.0§§	0.04	0.0097
MAC2$^+$ area	48.5±6.3	42.3±3.9	52.9±3.9	37.9±4.0	0.996	0.0245
αSMA$^+$ area	22.5±4.0	25.7±4.7	25.9±5.2	21.0±3.5	0.8845	0.8453
APOC3$^+$ area	18.2±3.5	13.4±3.3	27.4±6.0	27.9±7.1	0.026	0.69

Female *Ldlr*$^{-/-}$*;Gp*^{Tg} mice were maintained on a high-fat diet (HFD) for 12 weeks to allow the formation of pre-existing lesions. Mice were lethally irradiated and received bone-marrow cells from animals with and without gasdermin D-deficiency. The animals were maintained on a chow diet and recovered for 5 weeks. Mice were rendered diabetic (D) with lymphocytic choriomeningitis virus (LCMV). Saline was used as a control (non-diabetic, ND). At the onset of diabetes, the animals were switched to a low-fat, semipurified diet with no added cholesterol (LFD) and were maintained for 4 weeks. Aortic sinus immunoreactivity of APOB$^+$, APOE$^+$, APOB$^+$APOE$^+$, MAC2$^+$, αSMA$^+$, and APOC3$^+$ area was stained and measured. Immunofluorescence staining was conducted at 0 µm. Data show means ± SEM (n=19, 20, 21, 19 mice/group). Statistical analyses were performed by two-way ANOVA followed by Tukey's multiple comparisons test. Normality test was performed by D'Agostino & Pearson test. *Significant between non-diabetes (WT) and diabetes (WT) groups. †Significant between non-diabetes (WT) and non-diabetes (KO) groups. ‡Significant between non-diabetes (KO) and diabetes (KO) groups. §Significant between diabetes (WT) and diabetes (KO). P<0.05 (*, †, ‡, §), <0.01 (**, ††, ‡‡, §§), and < 0.001 (***, †††, ‡‡‡, §§§) are considered statistically significant. p-values between two groups were calculated by multiple comparisons test and the overall group effects (p-values) as calculated by two-way ANOVA. Outliers were removed based on Grubbs' test with alpha = 0.01. (0,0,1,0) data points were removed for APOB$^+$APOE$^+$ area; (0,0,1,0) data points were removed for MAC2$^+$ area; (0,0,0,1) data points were removed for APOE$^+$ area; no other data points were removed.

Table 8: Comparison of phenotypes in the LCMV and STZ models of type 1 diabetes.

Mean ± SEM (n=7-25 mice/group); statistical analysis by two-tailed unpaired t-test (for normally distributed data) or Kruskal-Wallis (for non-parametric data). Note that the LCMV and STZ *Ldlr*$^{-/-}$ models of diabetes were studied to address different questions and that the studies were not performed side-by-side. The data should therefore be interpreted with caution.

	Diabetic LCMV	**Diabetic STZ**	**p-value**
Blood glucose (mmol/L)	28.2±1.1	21.6±2.6	0.01
Plasma cholesterol (mmol/L)	7.9±0.7	30.6±5.2	<0.0001
Plasma triglycerides (mmol/L)	2.9±0.2	3.0±0.2	0.747
Plasma APOC3 (μg/mL)	229.5±29.2	742.8±209.3	0.0009
Plasma IL-1β (fg/mL)	580.5±235.1	92.0±32.9	0.173
Plasma IL-18 (pg/mL)	397.5±55.3	523.7±150.7	0.337
Sinus lesion area (μm^{2}x1000)	350.7±27.0	319.6±58.0	0.219
Necrotic core area (%)	19.0±1.6	14.9±3.9	0.278
Mac2$^+$ lesion area (%)	16.5±1.7	17.3±4.6	0.847
α-SMA$^+$ lesion area (%)	9.8±2.0	2.3±0.5	0.055
APOB$^+$ lesion area (%)	26.5±1.7	21.8±2.1	0.128
APOE$^+$ lesion area (%)	55.5±3.7	19.6±3.8	<0.0001
APOC3$^+$ lesion area (%)	8.8±1.1	31.7±1.6	<0.0001
Lesion severity score	9.0±0.3	9.7±0.9	0.504

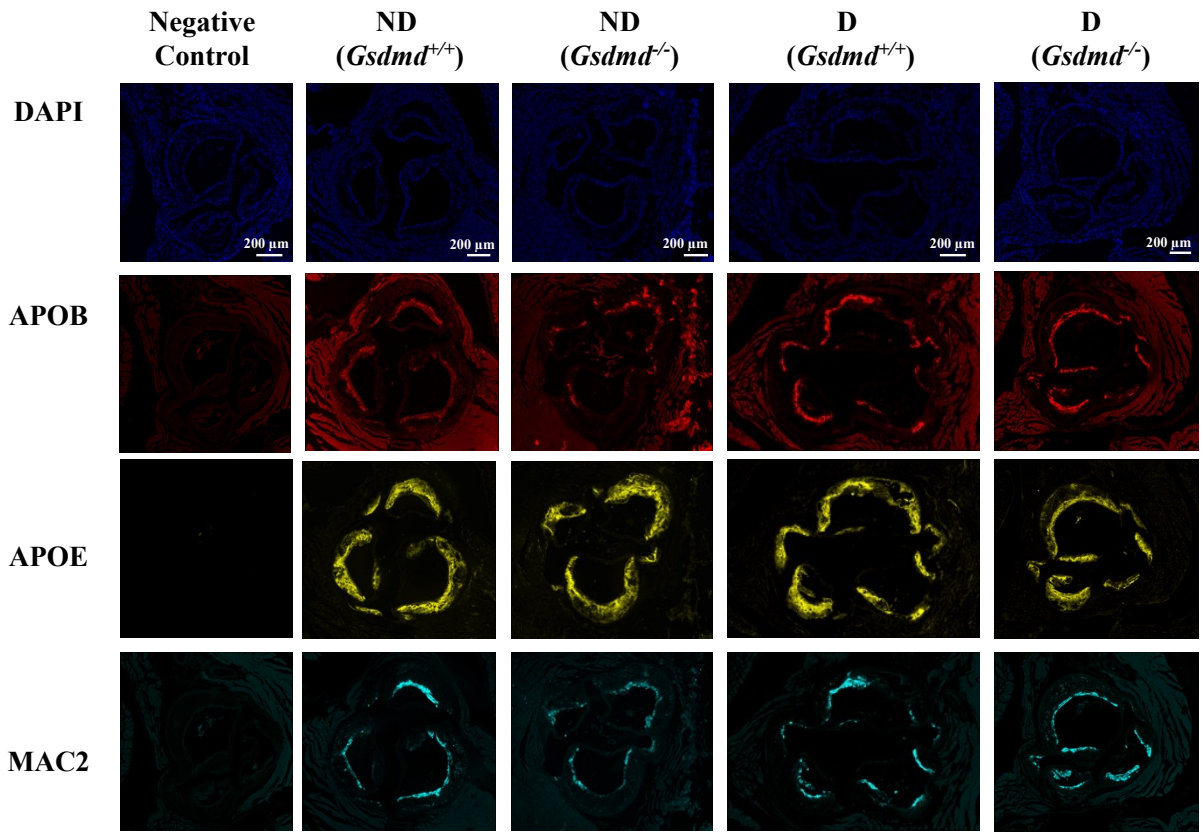

Figure 1: Representative aortic sinus images from the type 1 diabetes-accelerated atherosclerosis mouse model with and without hematopoietic gasdermin D-deficiency stained for nuclei (DAPI), APOB, APOE, or MAC2.

Female *Ldlr*$^{-/-}$*;Gp*^{Tg} mice were maintained on a high-fat diet (HFD) for 12 weeks to allow the formation of pre-existing lesions. Mice were lethally irradiated and received bone-marrow cells from animals with and without gasdermin D-deficiency. The animals were maintained on a chow diet and recovered for 5 weeks. Mice were rendered diabetic (D) with lymphocytic choriomeningitis virus (LCMV). Saline was used as a control (non-diabetic, ND). At the onset of diabetes, the animals were switched to a low-fat, semipurified diet with no added cholesterol (LFD) and were maintained for 4 weeks. Immunohistochemistry was performed using the antibodies and negative controls listed in Table 2. Biotinylated goat IgG was used as the negative control for APOB. Rabbit IgG was used as the negative control for APOE. Rat IgG was used as the negative control for MAC2.

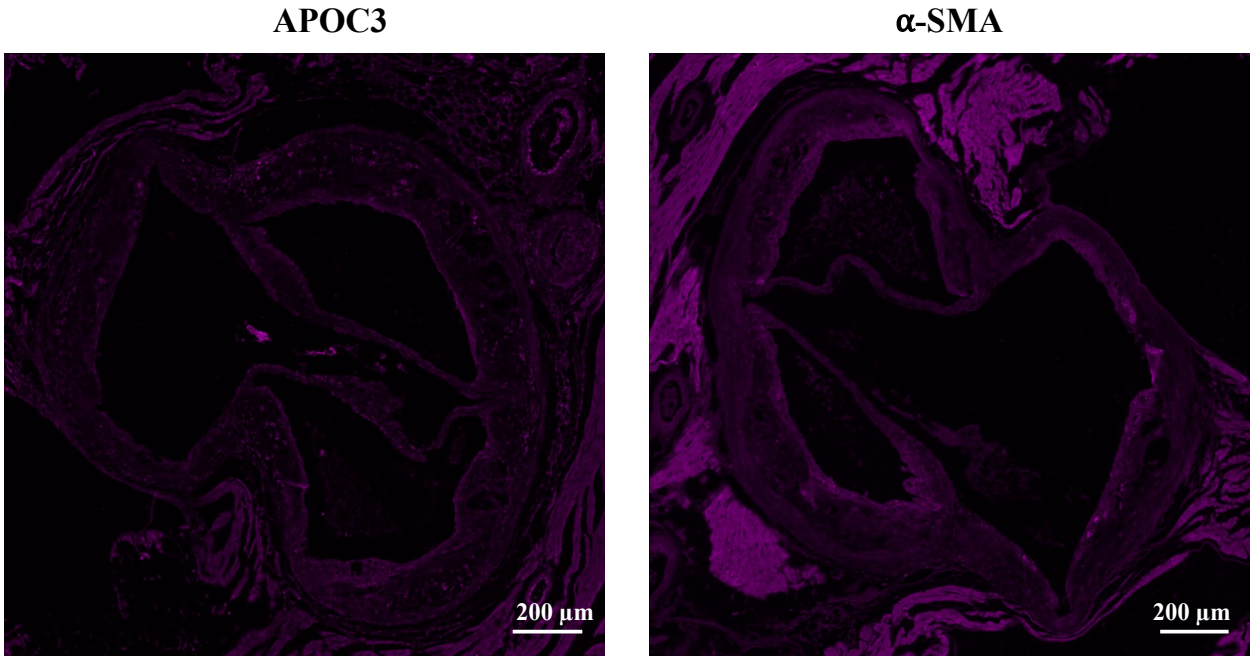

Figure 2: Representative aortic sinus negative controls for APOC3 and α-SMA immunohistochemistry.

Female *Ldlr*$^{-/-}$*;Gp*^{Tg} mice were maintained on a high-fat diet (HFD) for 12 weeks to allow the formation of pre-existing lesions. Mice were lethally irradiated and received bone-marrow cells from animals with and without gasdermin D-deficiency. The animals were maintained on a chow diet and recovered for 5 weeks. Mice were rendered diabetic (D) with lymphocytic choriomeningitis virus (LCMV). Saline was used as a control (non-diabetic, ND). At the onset of diabetes, the animals were switched to a low-fat, semipurified diet with no added cholesterol (LFD) and were maintained for 4 weeks. Immunohistochemistry was performed using the antibodies and negative controls listed in Table 2. Normal rabbit serum was used as the negative control for APOC3. Rabbit IgG was used as the negative control for α-SMA.

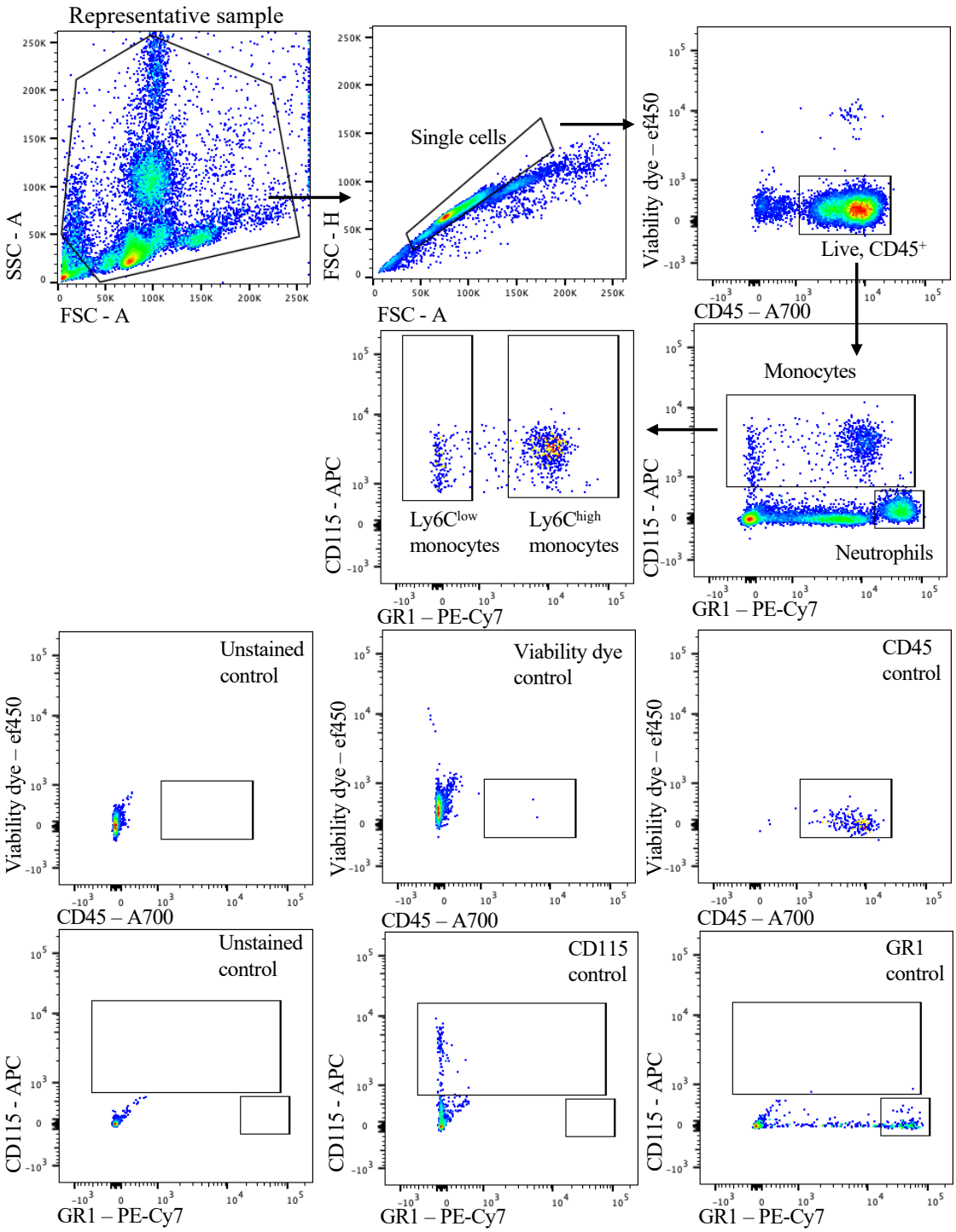

Figure 3: Flow cytometry gating of blood samples.

The gating strategy was determined with single-stained and unstained controls. Live, $CD45^+$ population ($CD45^+$, viability dye^-) was gated after gating for single cells. Monocytes ($CD115^+$) and neutrophils ($CD115^-$, $GR1^+$) were gated from the live, $CD45^+$ population. The monocyte population was further gated for $ly6C^{high}$ ($GR1^+$) and $ly6C^{low}$ ($GR1^-$) populations.

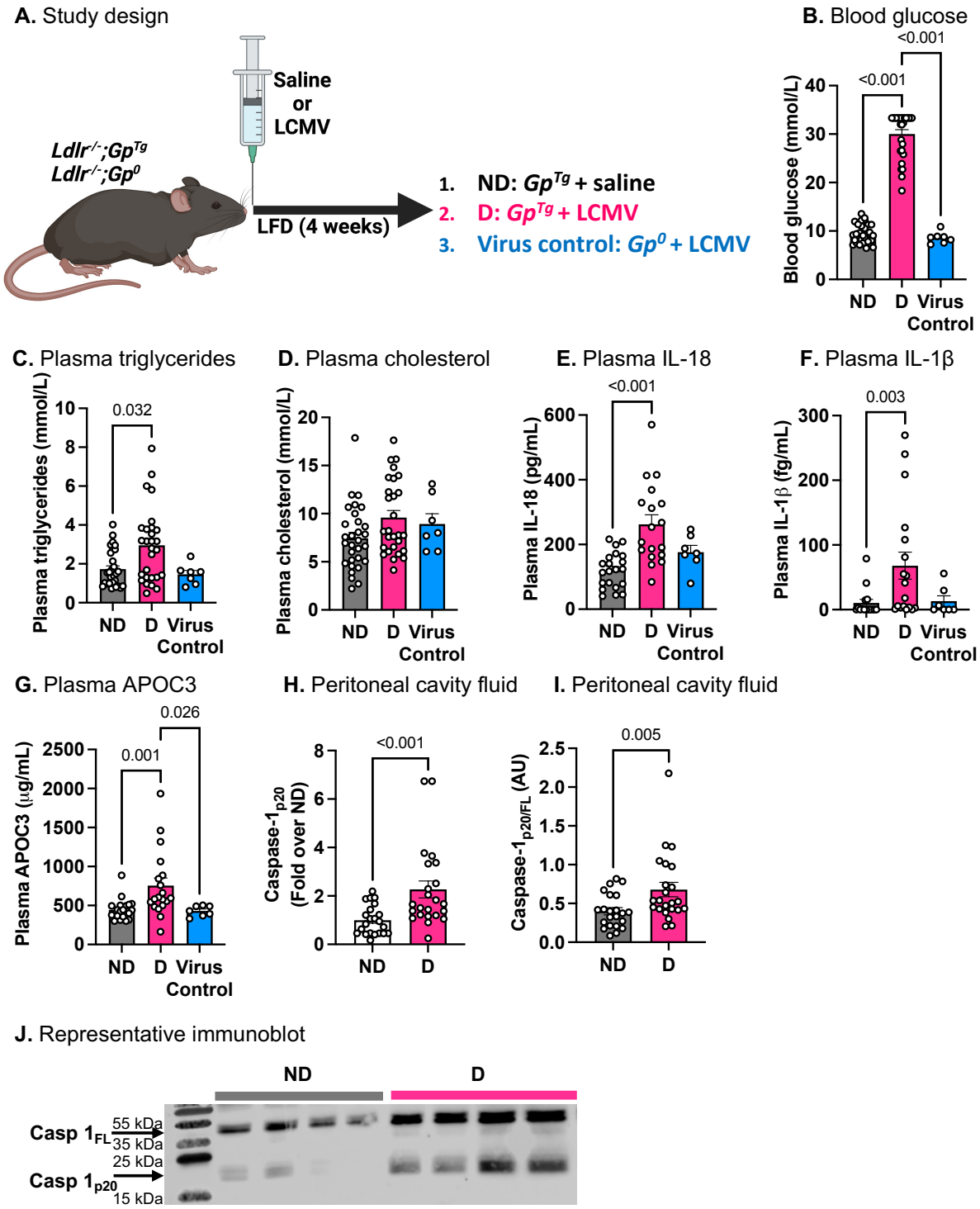

Figure 4: Diabetes leads to elevated plasma triglycerides, APOC3, and inflammasome signatures.

Female low-density lipoprotein receptor-deficient mice with a virus glycoprotein transgene (*Ldlr*$^{-/-}$;*Gp*^{Tg}) were rendered diabetic (D) with lymphocytic choriomeningitis virus (LCMV). Saline was used as a control (non-diabetic, ND). *Ldlr*$^{-/-}$ mice without the glycoprotein (*Ldlr*$^{-/-}$;*Gp*^{0})

transgene were injected with LCMV as a virus control. At the onset of diabetes, the animals were switched to a low-fat, semipurified diet with no added cholesterol (LFD) and maintained for 4 weeks. **A.** Schematic of study design. **B.** Blood glucose levels. Glucose values greater than 33.3 mmol/L are expressed as 33.3 mmol/L. **C.** Plasma triglycerides levels. **D.** Plasma cholesterol levels. **E.** Plasma IL-18. **F.** Plasma IL-1β. **G.** Plasma APOC3. **H.** Peritoneal cavity fluid was immunoblotted for cleaved caspase 1 ($casp1_{p20}$) and **I.** for cleaved caspase 1 over full-length caspase 1 ($casp1_{p20}/casp1_{FL}$). **J.** Representative immunoblot. N=7-30 individual mice per group. Normality tests were performed by the D'Agostino & Pearson test. Statistical analyses were performed by Kruskal-Wallis test and Dunn's multiple comparisons test in B-D and F-G, one-way ANOVA followed by Tukey multiple comparisons test in E, and Mann-Whitney test in H-I. Outliers were removed based on Grubbs' test with alpha = 0.01. (1,0,0) data points were removed in F; (0,1) data points were removed in H; (0,1) data points were removed in I; no data points were removed in B-E and G.

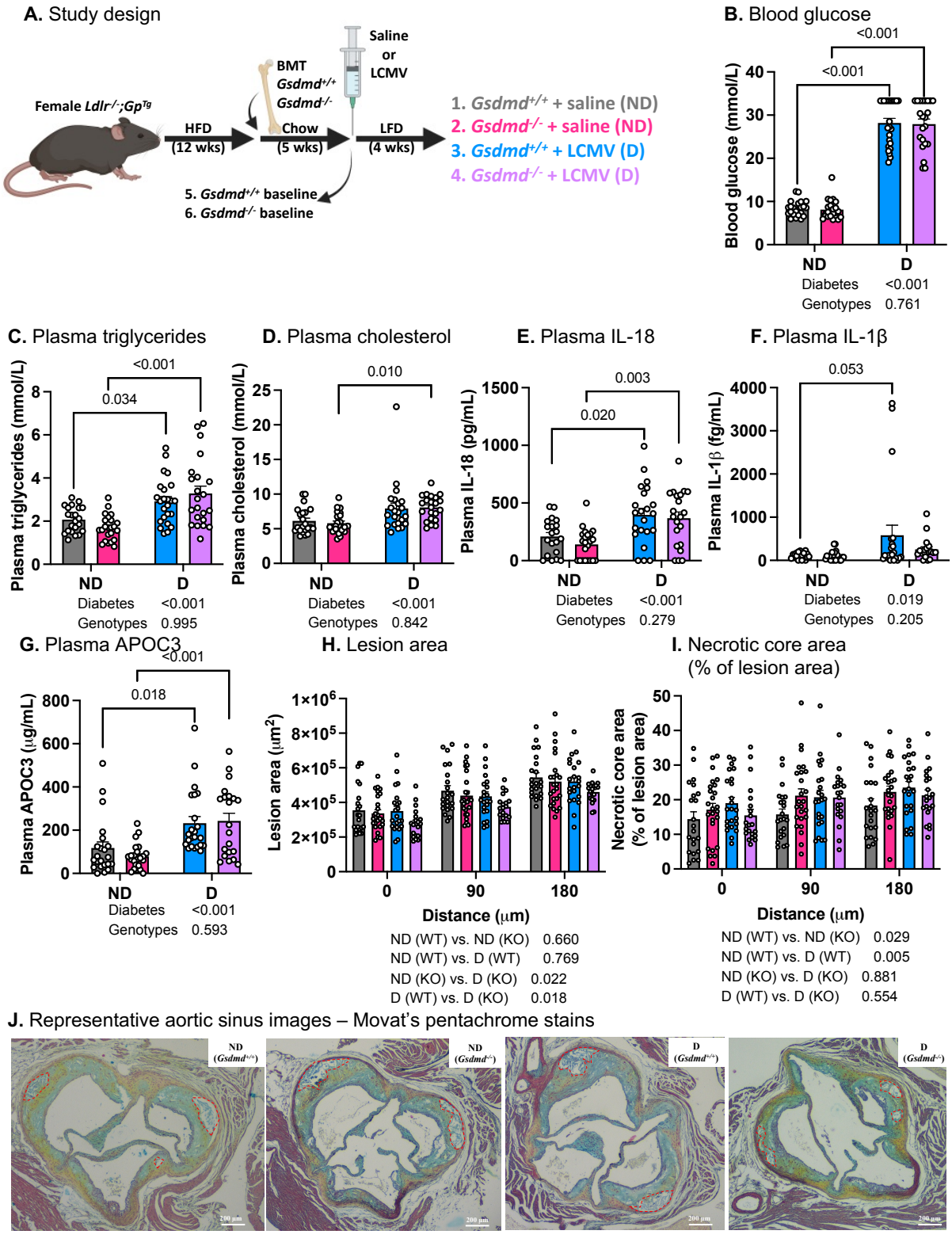

Figure 5: Hematopoietic gasdermin D-deficiency does not prevent the effect of diabetes on lesion necrotic core expansion.

Female *Ldlr*$^{-/-}$*;Gp*^{Tg} mice were maintained on a high-fat diet (HFD) for 12 weeks to allow the formation of pre-existing lesions. The mice were then lethally irradiated and received bone-marrow cells from animals with and without gasdermin D (GSDMD)-deficiency. The animals were maintained on a chow diet and recovered for 5 weeks. Mice were rendered diabetic (D) with lymphocytic choriomeningitis virus (LCMV). Saline was used as a control (non-diabetic, ND). At the onset of diabetes, the animals were switched to a low-fat, semipurified diet with no added cholesterol (LFD) and were maintained for 4 weeks. A subset of animals was euthanized after 5 weeks of recovery to evaluate lesion morphology before diabetes (baseline). **A.** Schematic of study design. **B.** Blood glucose levels. Glucose values greater than 33.3 mmol/L are expressed as 33.3 mmol/L. **C.** Plasma triglyceride levels. **D.** Plasma cholesterol levels. **E.** Plasma IL-18 levels. **F.** Plasma IL-1β levels. **G.** Aortic sinus lesion area. 0 μm represents the first appearance of the three aortic valve leaflets. **H.** Aortic sinus % necrotic core area calculated as necrotic core area/lesion area. **I.** Representative aortic sinus lesions stained with Movat's pentachrome stain. Representative necrotic core areas are circled in red. ND; non-diabetic; D, diabetic. Data show means ± SEM (n=19-25 mice/group). Statistical analyses were performed by two-way ANOVA followed by Tukey's multiple comparisons test. In B-G, lines between two groups indicate p-values calculated by multiple comparisons test and the text underneath the graphs indicates overall group effects (p-values) as calculated by two-way ANOVA. In H-I, the text underneath the graphs indicates group effects (p-values) as calculated by the multiple comparisons test. Outliers were removed based on Grubbs' test with alpha = 0.01. (0,0,1,0) data points were removed in D; (0,0,1,1) data points were removed in F; (0,0,1,0) data points were removed in G; (0,0,0,0,0,0,0,1,1,1,0,1) data points were removed in H; no data points were removed in B-C, E, and I.

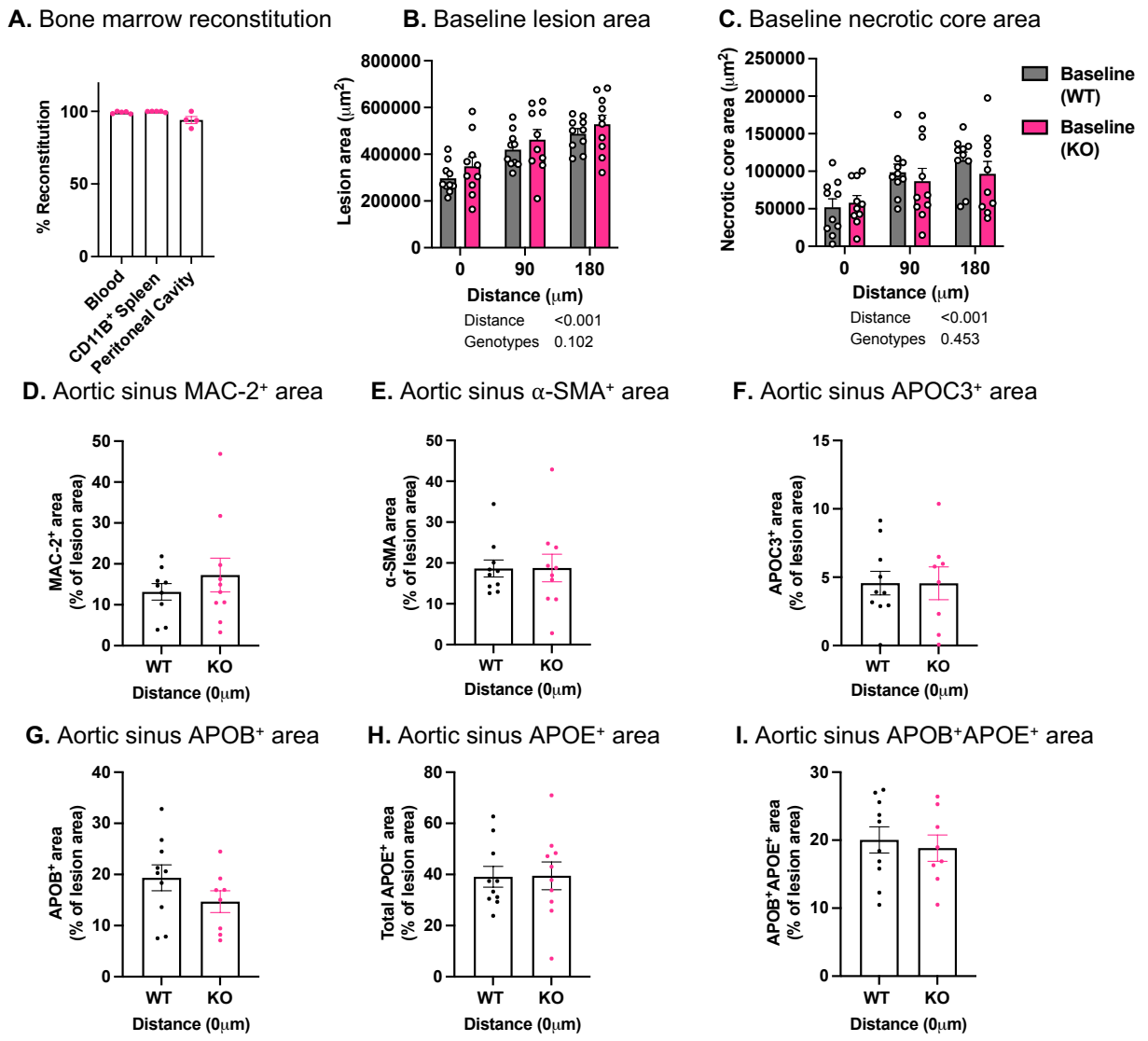

Figure 6: Despite good reconstitution efficiency, mice with hematopoietic gasdermin D-deficiency show no differences in lesion morphologies at baseline.

Female *Ldlr*$^{-/-}$*;Gp*^{Tg} mice were maintained on a high-fat diet (HFD) for 12 weeks to allow the formation of pre-existing lesions. Mice were lethally irradiated and received bone-marrow cells from animals with and without gasdermin D-deficiency. The animals were maintained on a chow diet and recovered for 5 weeks. Animals was euthanized after 5 weeks of recovery to evaluate lesion morphology before diabetes (baseline). **A.** % reconstitution of gasdermin D-deficiency donor cells in the blood, CD11B^{+} spleen, and peritoneal cavity cells harvested from the recipient mice. **B.** Aortic sinus lesion area. 0 μm represents the first appearance of the three aortic valve leaflets. **C.** Aortic sinus necrotic core area. **D.** Aortic sinus MAC2^{+} area. **E.** Aortic sinus α-SMA^{+} area. **F.** Aortic sinus APOC3^{+} area. **G.** Aortic sinus total APOB^{+} area. **H.** Aortic sinus total APOE^{+} area. **I.** Aortic sinus APOB^{+}APOE^{+} area. Immunofluorescence staining of MAC2, α-SMA, APOC3, APOB, and APOE were conducted at 0 μm. Data show means ± SEM (n=5, 5, 4

mice/group in A; n=10 mice/group in B-E; n=10, 9 mice/group in F; n= 10, 8 mice/group in G-I). Statistical analyses were performed by two-way ANOVA followed by Tukey's multiple comparisons test in B-C; Mann-Whitney test in D-E and G-H; Welch's test in F and I. Normality test was performed by D'Agostino & Pearson test. Outliers were removed based on Grubbs' test with alpha = 0.01. (1,0) data points were removed in D; (0,1) data points were removed in F; no data points were removed in A-C, E, and G-I.

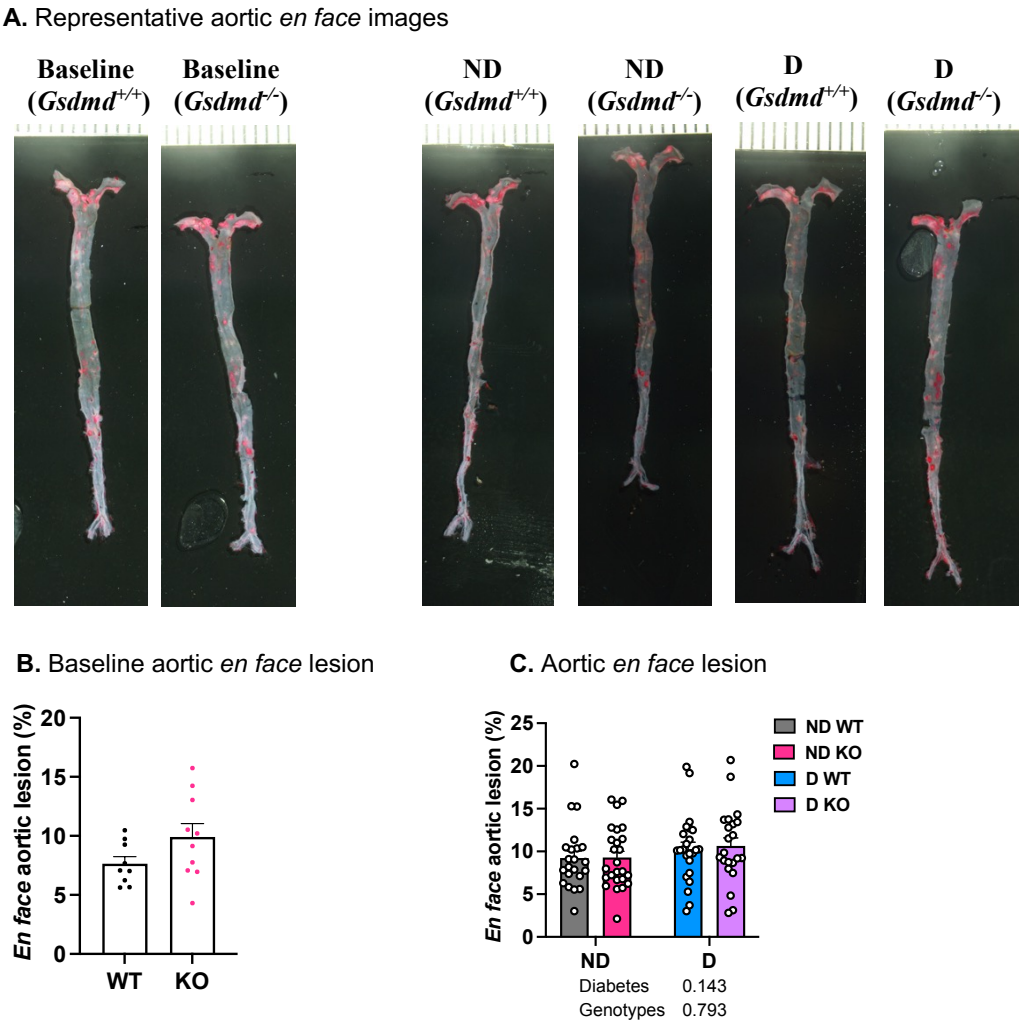

Figure 7: Neither diabetes nor gasdermin D affects aortic Sudan IV-positive *en face* area in mice with pre-existing lesions.

Female *Ldlr*$^{-/-}$*;Gp*^{Tg} mice were maintained on a high-fat diet (HFD) for 12 weeks to allow the formation of pre-existing lesions. Mice were lethally irradiated and received bone-marrow cells from animals with and without gasdermin D-deficiency. The animals were maintained on a chow diet and recovered for 5 weeks. Mice were rendered diabetic (D) with lymphocytic choriomeningitis virus (LCMV). Saline was used as a control (non-diabetic, ND). At the onset of diabetes, the animals were switched to a low-fat, semipurified diet with no added cholesterol (LFD) and were maintained for 4 weeks. A subset of animals was euthanized after 5 weeks of recovery to evaluate aortic Sudan IV-positive area before diabetes (baseline). **A.** Representative aortic *en face* lesions with Sudan IV staining. **B.** Aortic *en face* Sudan IV lesion at baseline. **C.** Aortic *en face* Sudan IV lesion. Data show means ± SEM (n=10 mice/group in B; n=22, 25, 24, 23 mice/group in C). Statistical analyses were performed by Welch's test in B; two-way ANOVA followed by Tukey's multiple comparisons test in C. Normality test was performed by D'Agostino & Pearson test. The text underneath panel C indicates group effects (p-values) as calculated by two-way ANOVA. Outliers were removed based on Grubbs' test with alpha = 0.01. (1,0) data points were removed in B; no data points were removed in C.

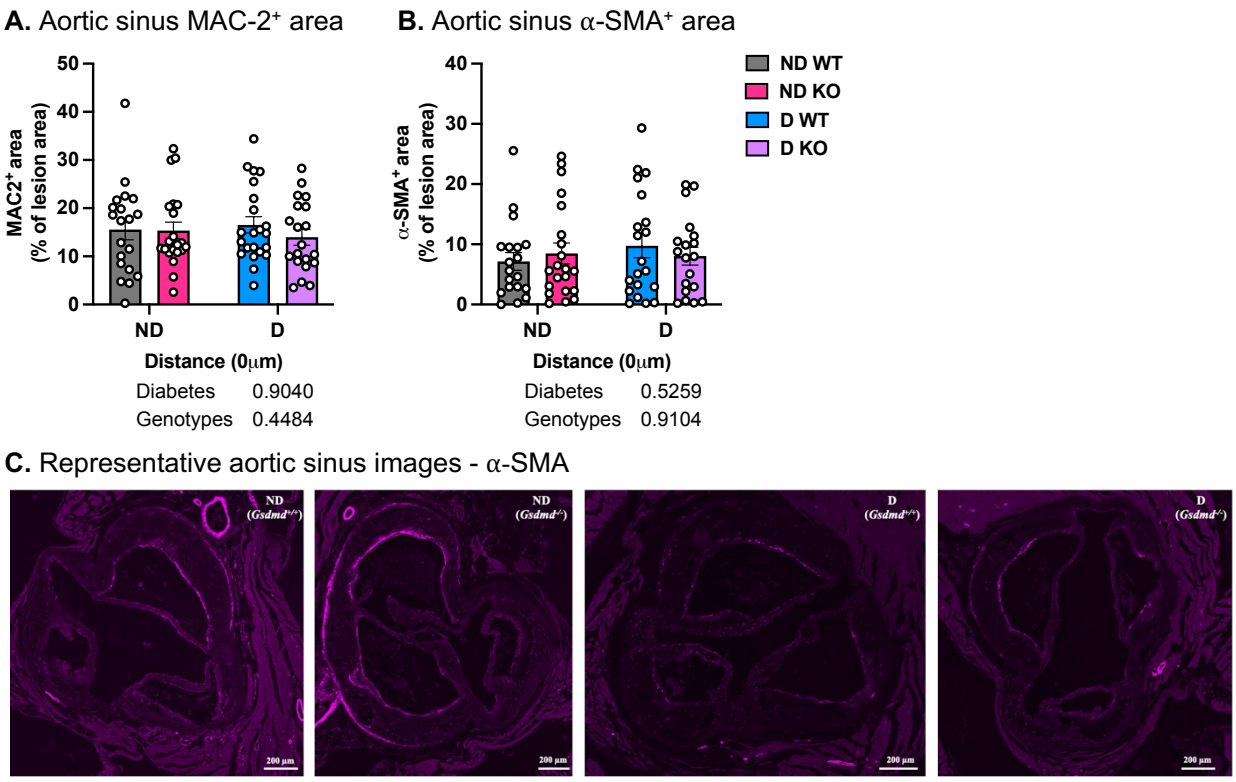

Figure 8: Neither diabetes nor hematopoietic gasdermin D-deficiency alters macrophage or smooth muscle accumulation in pre-existing lesions of atherosclerosis.

Female *Ldlr*$^{-/-}$*;Gp*^{Tg} mice were maintained on a high-fat diet (HFD) for 12 weeks to allow the formation of pre-existing lesions. Mice were lethally irradiated and received bone-marrow cells from animals with and without gasdermin D-deficiency. The animals were maintained on a chow diet and recovered for 5 weeks. Mice were rendered diabetic (D) with lymphocytic choriomeningitis virus (LCMV). Saline was used as a control (non-diabetic, ND). At the onset of diabetes, the animals were switched to a low-fat, semipurified diet with no added cholesterol (LFD) and were maintained for 4 weeks. **A.** Aortic sinus MAC2$^+$ area. **B.** Aortic sinus α-SMA$^+$ area. **C.** Representative aortic sinuses stained with an α-SMA antibody. Immunofluorescence staining of MAC2 and α-SMA were conducted at 0 μm. Data show means ± SEM (n=20, 22, 21, 20 mice/group in A; n=19, 21, 20, 19 mice/group in B). Statistical analyses were performed by two-way ANOVA (group effect p-values underneath graphs). Outliers were removed based on Grubbs' test with alpha = 0.01. No data points were removed in A-B.

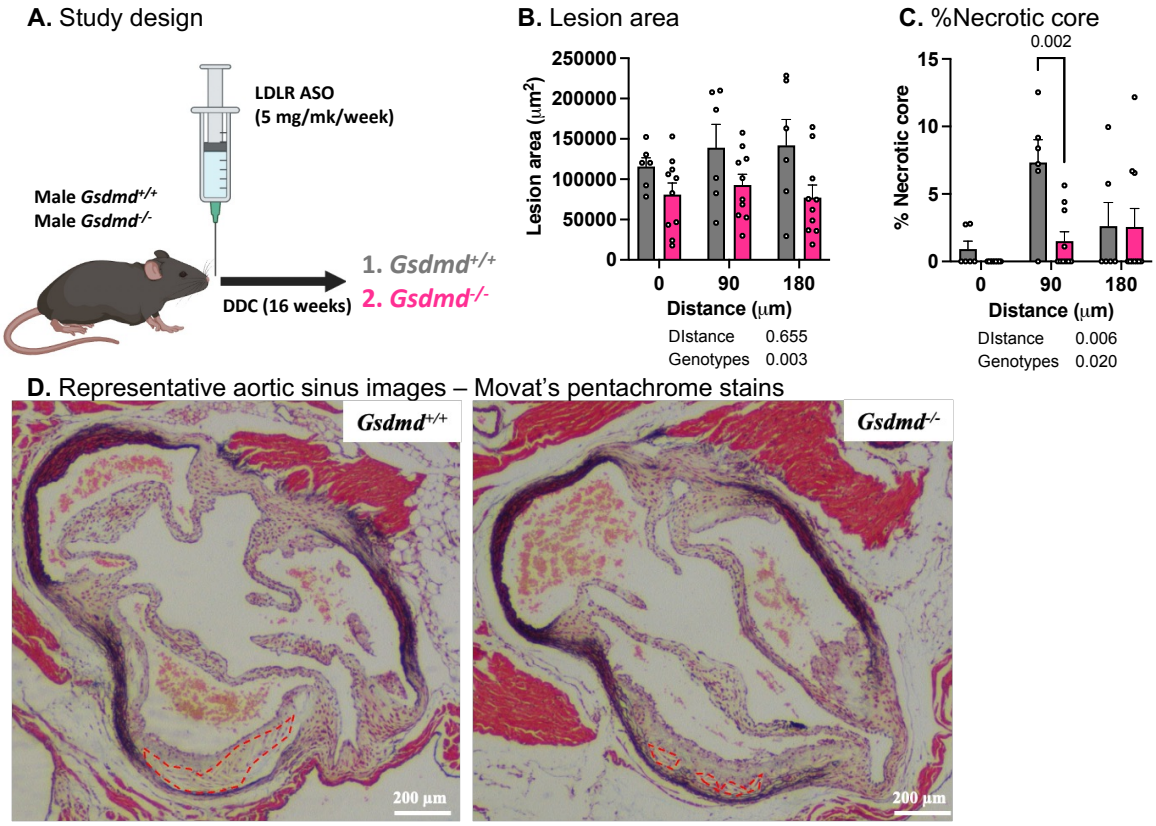

Figure 9: Mice with whole-body gasdermin D deficiency demonstrate atheroprotective effects.

Male mice with and without gasdermin D-deficiency were maintained on a high-fat high-sucrose diet for 16 weeks to allow the formation of atherosclerotic lesions Mice received weekly i.p. injection of GalNAc-conjugated LDLR ASO (5 mg/kg) throughout the study. A. Schematic of study design. B. Aortic sinus lesion area. C. Aortic sinus % necrotic core calculated as necrotic core area/lesion area. D. Representative aortic sinus lesions stained with Movat's pentachrome stain. Representative necrotic core areas are circled in red. Data show means ± SEM (n=6, 10 mice/group). Statistical analyses were performed by two-way ANOVA (group effect p-values underneath graphs) followed by Tukey's multiple comparisons test (p-values indicated above bars). Outliers were removed based on Grubbs' test with alpha = 0.01. (0,1,0,0,0,0) data points were removed in C; no data points were removed in B.

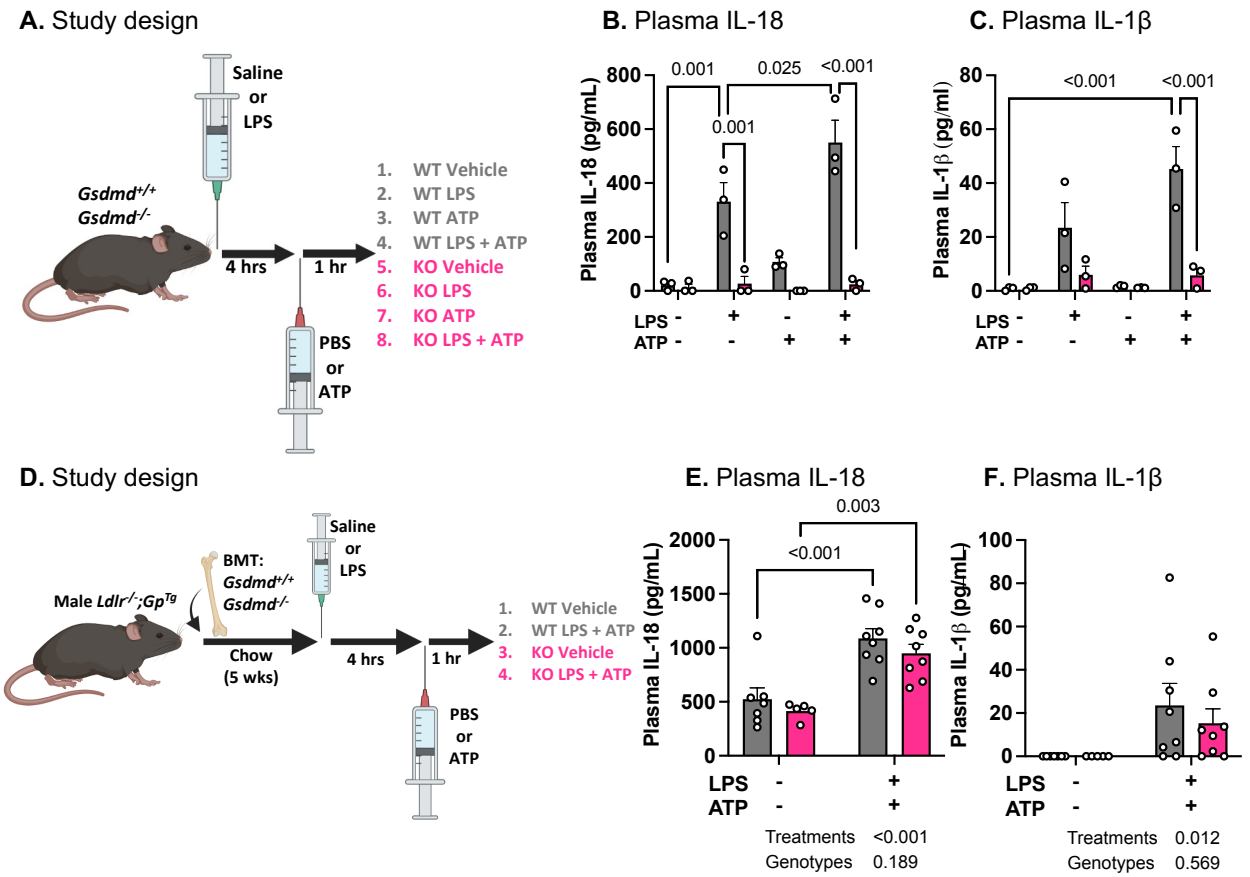

Figure 10: Full-body but not hematopoietic gasdermin D-deficiency contributes to the release of circulating IL-18 and IL-1β.

Male and female mice with and without whole-body gasdermin D (GSDMD)-deficiency received i.p. injections with and without ultrapure LPS and ATP to induce inflammasome activation. **A.** Schematic of study design. **B.** Plasma IL-1β. **C.** Plasma IL-18. Data show means ± SEM (n=3 mice/group in B-C). Statistical analyses were performed by two-way ANOVA followed by Tukey's multiple comparisons test. **D-F.** Male *Ldlr*$^{-/-}$*;Gp*^{Tg} mice were lethally irradiated and received bone-marrow cells from animals with and without gasdermin D-deficiency. The animals were maintained on a chow diet and recovered for 5 weeks. The mice were then injected with and without ultrapure LPS and ATP after 5 weeks of recovery. **D.** Schematic of study design. **E.** Plasma IL-1β. **F.** Plasma IL-18. Data show means ± SEM (n=7, 5, 8, 8 mice/group in E-F). Statistical analyses were performed by two-way ANOVA followed by Tukey's multiple comparisons test. In B-C and E-F, the lines between two groups indicate p-values between the groups as calculated by multiple comparisons test. In E-F, the text underneath the graphs indicates overall group effects (p-values) as calculated by two-way ANOVA. Outliers were removed based on Grubbs' test with alpha = 0.01. No data points were removed in B-C and E-F.

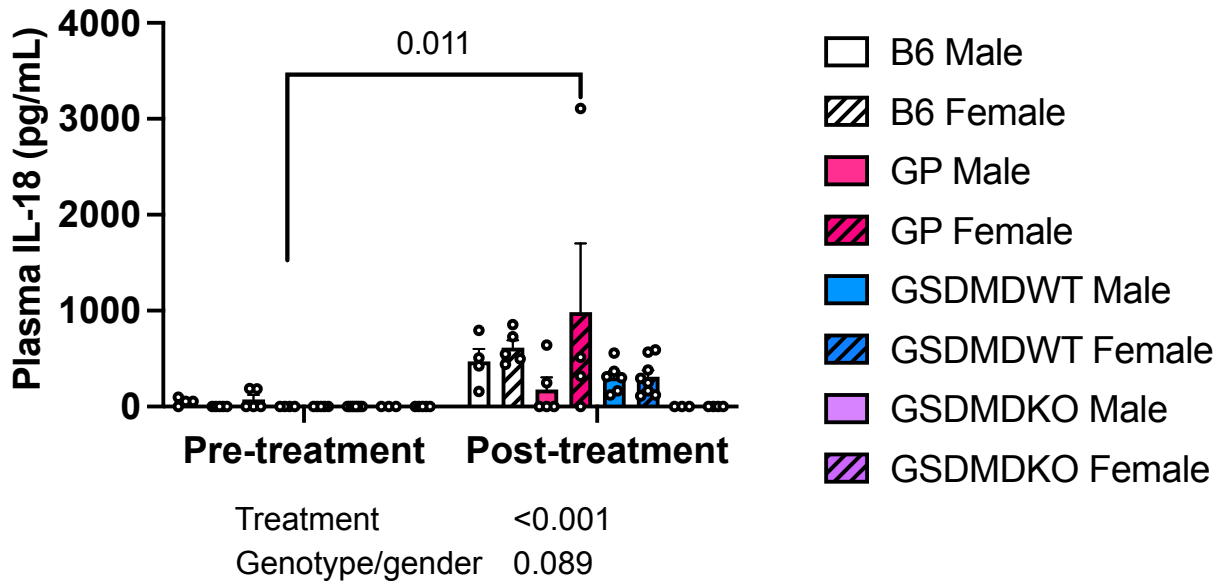

Figure 11: Neither gender nor genotype affects the release of IL-18 to plasma.

Male and female mice with and without whole-body gasdermin D (GSDMD)-deficiency and with and without transgenic glycoprotein (GP) received i.p. injections with and without ultrapure LPS and ATP to induce inflammasome activation. Data show means ± SEM (n=4-8 individual mice/group). Statistical analyses were performed by two-way ANOVA (group effect p-values underneath graphs) followed by Tukey's multiple comparisons test (p-values indicated above bars). Outliers were removed based on Grubbs' test with alpha = 0.01. (0,0,0,1,1,0,1,0; 0,0,0,1,0,0,1,1) data points were removed. B6, C57BL/6 mice; GP, *Ldlr*$^{-/-}$ *Gp*^{Tg} mice; GSDMDWT, C57BL/6 wildtype GSDMD controls; GSDMDKO, C57BL/6 whole-body GSDMD-deficient mice.

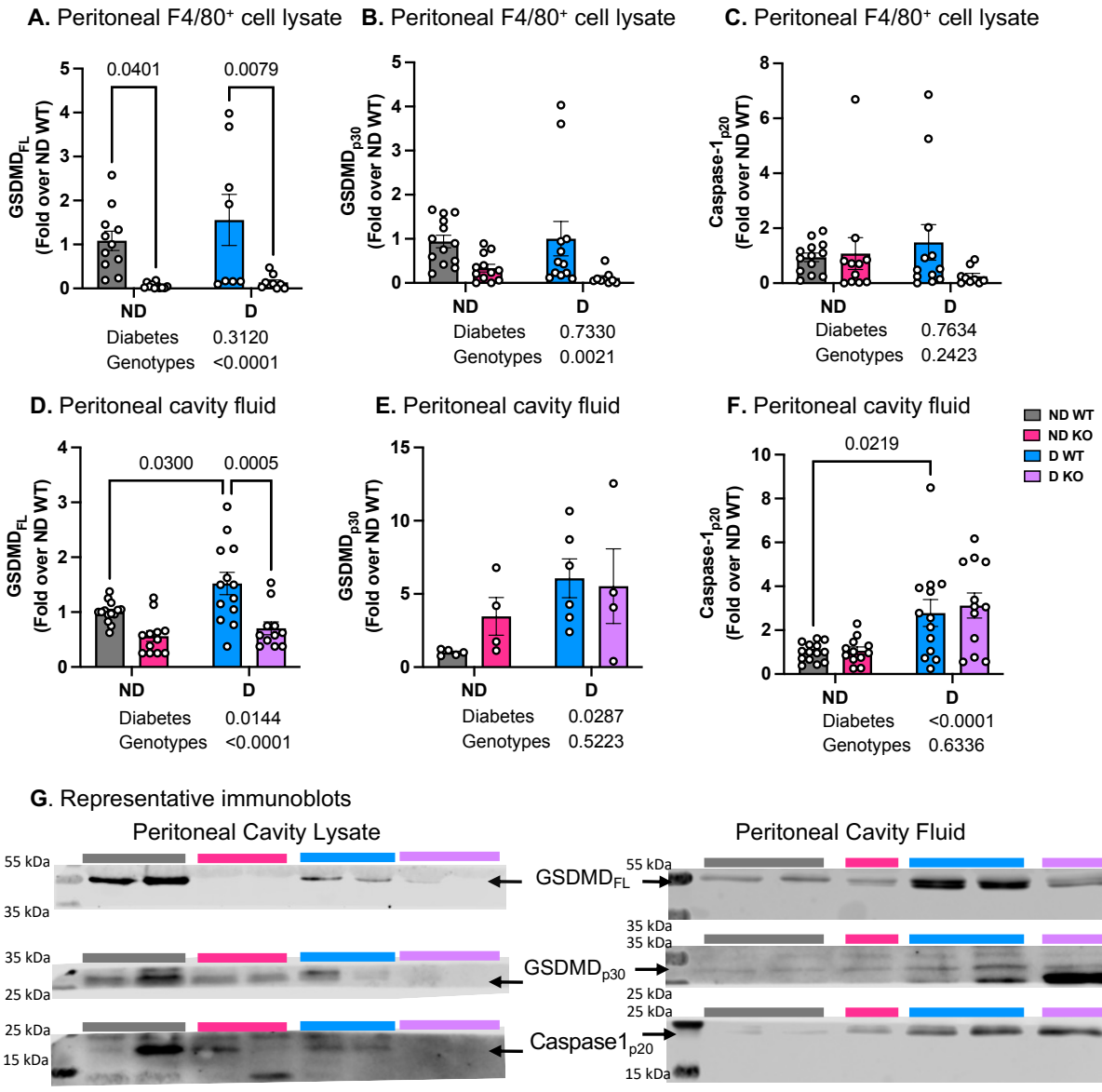

Figure 12: Diabetes induces inflammasome activation in F4/80$^-$ cells in the peritoneal cavity through a mechanism independent of hematopoietic GSDMD-deficiency

Peritoneal cavity fluid and cells were isolated from the lavage with centrifugation from the mice described in figure 2. Peritoneal cavity cells were further enriched with F4/80-positive immunoselection beads. Peritoneal cavity F4/80$^+$ cell lysate was immunoblotted for **A.** Full-length gasdermin D. **B.** Cleaved gasdermin D. **C.** Cleaved caspase1. Peritoneal cavity fluid was immunoblotted for **D.** Full-length gasdermin D. **E.** Cleaved gasdermin D. **F.** Cleaved caspase1. **G.** Representative immunoblots. Data show means ± SEM (n=11, 11, 8, 9 mice/group in A; n=13, 12, 12, 10 mice/group in B; n=13, 12, 12, 9 mice/group in C; n=14, 12, 13, 12 mice/group in D and F; n=5, 4, 6, 4 mice/group in E). Statistical analyses were performed by two-way ANOVA (group effect p-values underneath graphs) followed by Tukey's multiple comparisons test (p-values indicated above bars) in A-F. Outliers were removed based on Grubbs' test with

alpha = 0.01. (0,0,0,1) data points were removed in B; (0,1,0,0) data points were removed in C; (0,0,0,1) data points were removed in D; no data points were removed in A and E-F.

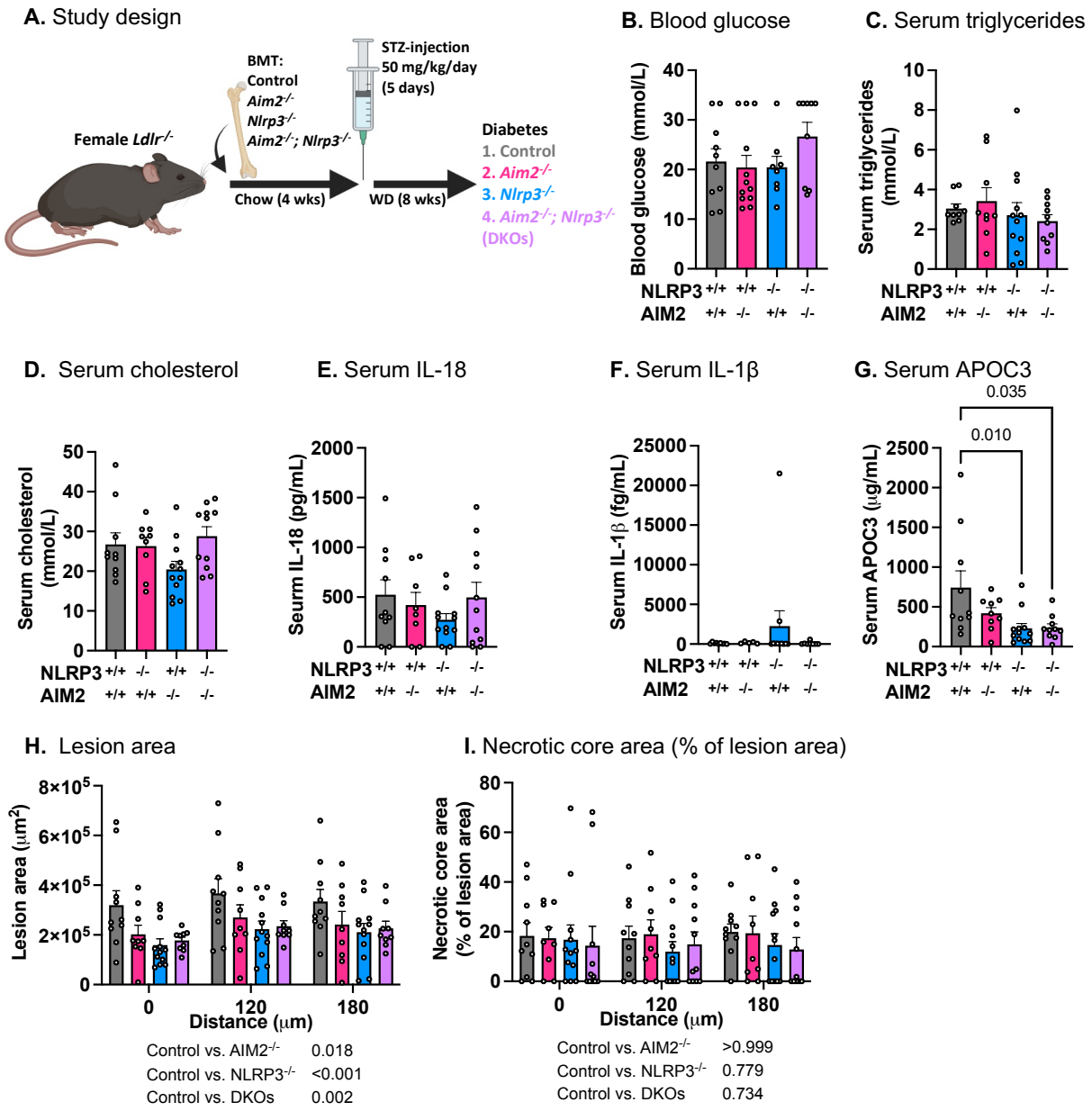

Figure 13: Hematopoietic AIM2-, NLRP3-, and AIM2/NLRP3 double-deficiencies contribute to lesion area but not necrotic core area in the setting of diabetes.

Female *Ldlr*$^{-/-}$ mice were lethally irradiated and received bone-marrow from mice with and without Nlrp3-deficiency (*Nlrp3*$^{-/-}$), Aim2-deficiency (*Aim2*$^{-/-}$), or double-deficiency of Nlrp3 and Aim2 (DKO). The animals were recovered on chow for 4 weeks before diabetes was induced with 5 days of streptozotocin (STZ) injections (50 mg/kg/day). Animals were maintained on a Western diet for 8 weeks. **A.** Schematic of study design. **B.** Blood glucose levels. Glucose values greater than 33.3 mmol/L are expressed as 33.3 mmol/L. Animals with average blood glucose less than 13.9 mmol/L were removed from the study. **C**. Serum triglyceride levels. **D.** Serum cholesterol levels. **E.** Serum IL-18 levels. **F.** Serum IL-1β levels. **G.** Serum APOC3 levels. **H.** Aortic sinus lesion area. 0 μm represents the first appearance of the three aortic valve leaflets. **I.** Aortic sinus necrotic core area calculated as % lesion area/necrotic core area. Data show means ±

SEM (n= 9-12 mice/group). Statistical analyses were performed by Kruskal-Wallis test and Dunn's multiple comparisons test in B-G and performed by two-way ANOVA followed by Tukey's multiple comparisons test in H-I. Normality test was performed by D'Agostino & Pearson test. In H-I, the text underneath the graphs indicates p-values between the groups as calculated by the multiple comparisons test. Outliers were removed based on Grubbs' test with alpha = 0.01. (1,1,1,1) data points were removed in F; no data points were removed in B-E and G-H.

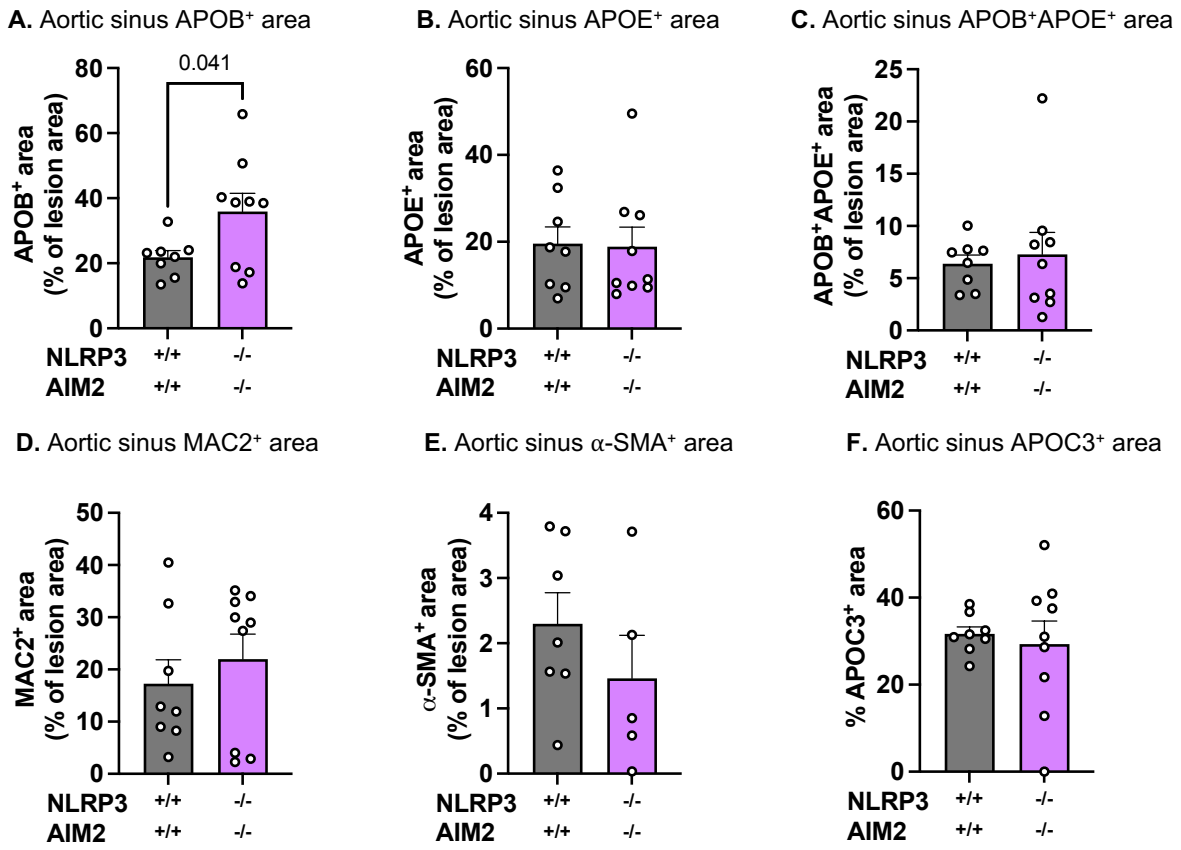

Figure 14: Hematopoietic AIM2/NLRP3 double-deficiencies alter lesional APOB accumulation in the setting of diabetes.

Female *Ldlr*$^{-/-}$ mice were lethally irradiated and received bone-marrow from mice with and without NLRP3-deficiency (*Nlrp3*$^{-/-}$), AIM2-deficiency (*Aim2*$^{-/-}$), or double-deficiency of NLRP3 and AIM2 (DKO). The animals were recovered on chow for 4 weeks before diabetes was induced with 5 days of streptozotocin (STZ) injections (50 mg/kg/day). Animals were maintained on a Western diet for 8 weeks. **A.** Aortic sinus APOB^{+} area expressed as % of lesion area (total APOB^{+} area; 68,408±12,054 v.s. 67,017±12,116 mm^2; NLRP3$^{+/+}$AIM2$^{+/+}$ v.s. NLRP3$^{-/-}$AIM2$^{-/-}$; p=0.936). **B.** Aortic sinus APOE^{+} area expressed as % of lesion area (total APOE^{+} area; 61,686±12,358 v.s. 34,583±8,040 mm^2; p=0.09). **C**. Aortic sinus APOB^{+}APOE^{+} area expressed as % of lesion area (total APOB^{+}APOE^{+} area; 21,750±4,847 v.s. 14,865±5,147 mm^2; p=0.236). **D.** Aortic sinus MAC2^{+} area expressed as % of lesion area (total MAC2^{+} area; 41,156±6,787 v.s. 40,113±8,620 mm2, p=0.926). **E.** Aortic sinus α-SMA^{+} area expressed as % of lesion area (total α-SMA^{+} area; 8,062±2,921 v.s. 3,610±1,876 mm^2; p=0.202). **F.** Aortic sinus APOC3^{+} area expressed as % of lesion area (total APOC3^{+} area; 5,187±1,080 v.s. 2,589±821 mm^2; p=0.128). Data show means ± SEM (n= 5-9 mice/group). Statistical analyses were performed by Welch's t test in A, D, and F; Mann-Whitney test in B, C, and E. Normality test was performed by D'Agostino & Pearson test. Outliers were removed based on Grubbs' test with alpha = 0.01. No data points were removed in A-F.

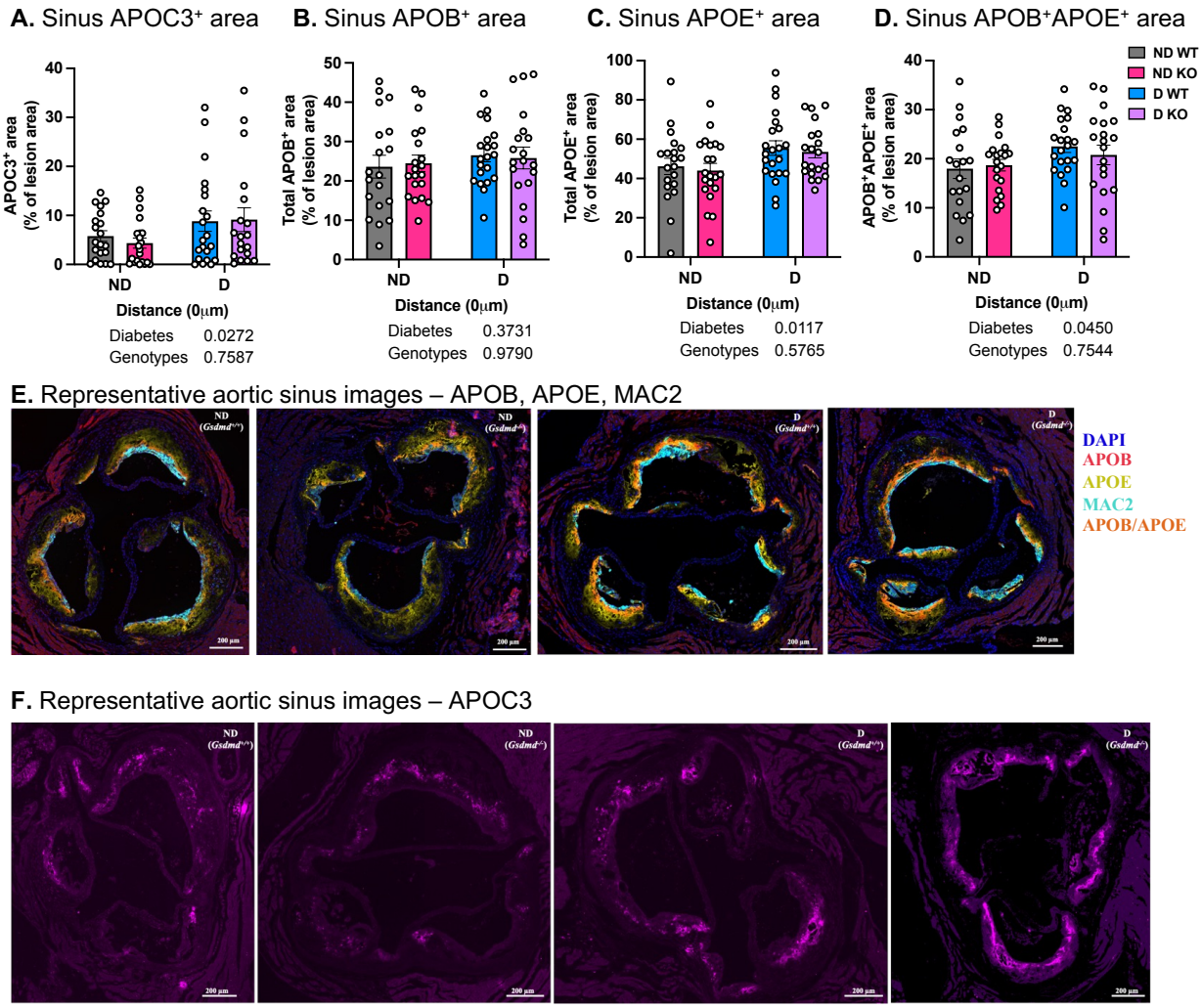

Figure 15: Diabetes increases APOC3 and APOE accumulation in aortic sinus lesions, but hematopoietic gasdermin D-deficiency has no effect.

Female *Ldlr*$^{-/-}$*;Gp*^{Tg} mice were maintained on a high-fat diet (HFD) for 12 weeks to allow the formation of pre-existing lesions. Mice were lethally irradiated and received bone-marrow cells from animals with and without gasdermin D (GSDMD)-deficiency. The animals were maintained on a chow diet and recovered for 5 weeks. Mice were rendered diabetic (D) with lymphocytic choriomeningitis virus (LCMV). Saline was used as a control (non-diabetic, ND). At the onset of diabetes, the animals were switched to a low-fat, semipurified diet with no added cholesterol (LFD) and were maintained for 4 weeks. **A.** Aortic sinus APOC3^{+} area. **B.** Aortic sinus total APOB^{+} area. **C.** Aortic sinus total APOE^{+} area. **D.** Aortic sinus APOB^{+}APOE^{+} area. **E.** Representative aortic sinuses with MAC2, APOB, and APOE staining. **F.** Representative aortic sinuses with APOC3 staining. Immunofluorescence staining of MAC2, APOC3, APOB, and APOE were conducted at 0 µm. Data show means ± SEM (n=20, 21, 21, 20 mice/group in A; n=19, 20, 21, 20 mice/group in B and D; n=20, 21, 22, 20 mice/group in C). Statistical analyses were performed by two-way ANOVA followed by Tukey's multiple comparisons test in A-D. The text underneath the graphs indicates overall group effects (p-values) as calculated by two-

way ANOVA. Outliers were removed based on Grubbs' test with alpha = 0.01. (0,0,0,1) data points were removed in A; no data points were removed in B-D.

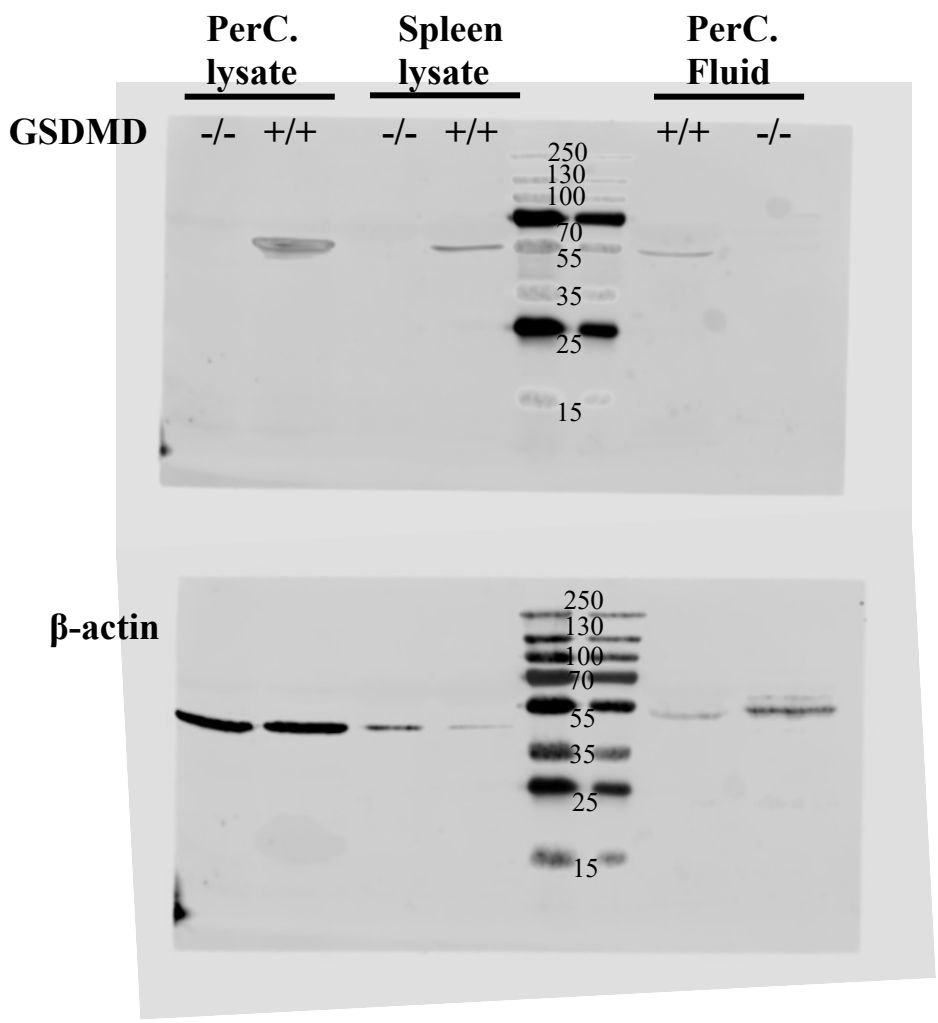

Figure 16: Immunoblotting of gasdermin D (GSDMD) and β-actin from animals with and without gasdermin D-deficiency.

Peritoneal cavity fluid, cell lysate, and spleen cell lysate were harvested from mice with and without gasdermin D-deficiency.

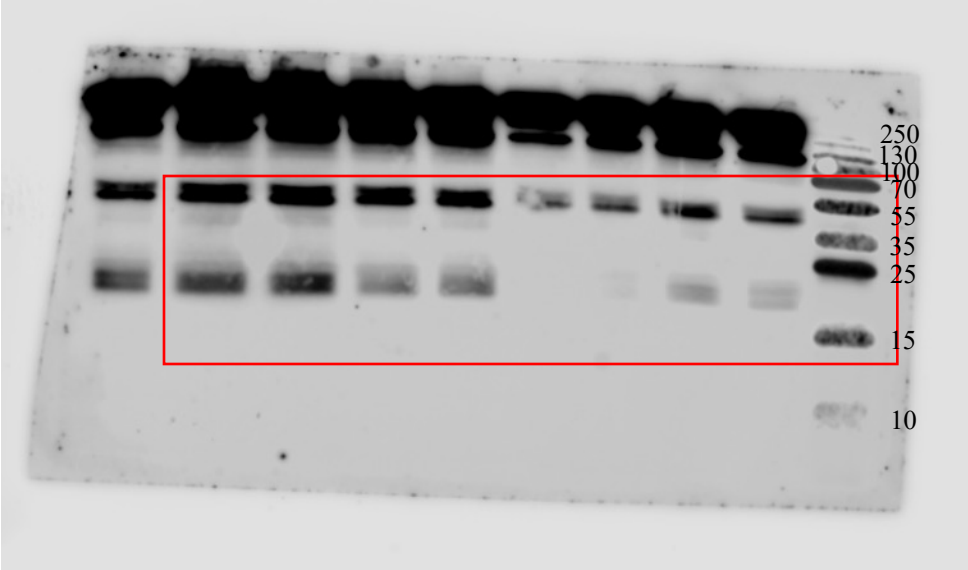

Figure 17: Immunoblot of cropped blot used in figure 4I.

The section cropped is boxed in red.

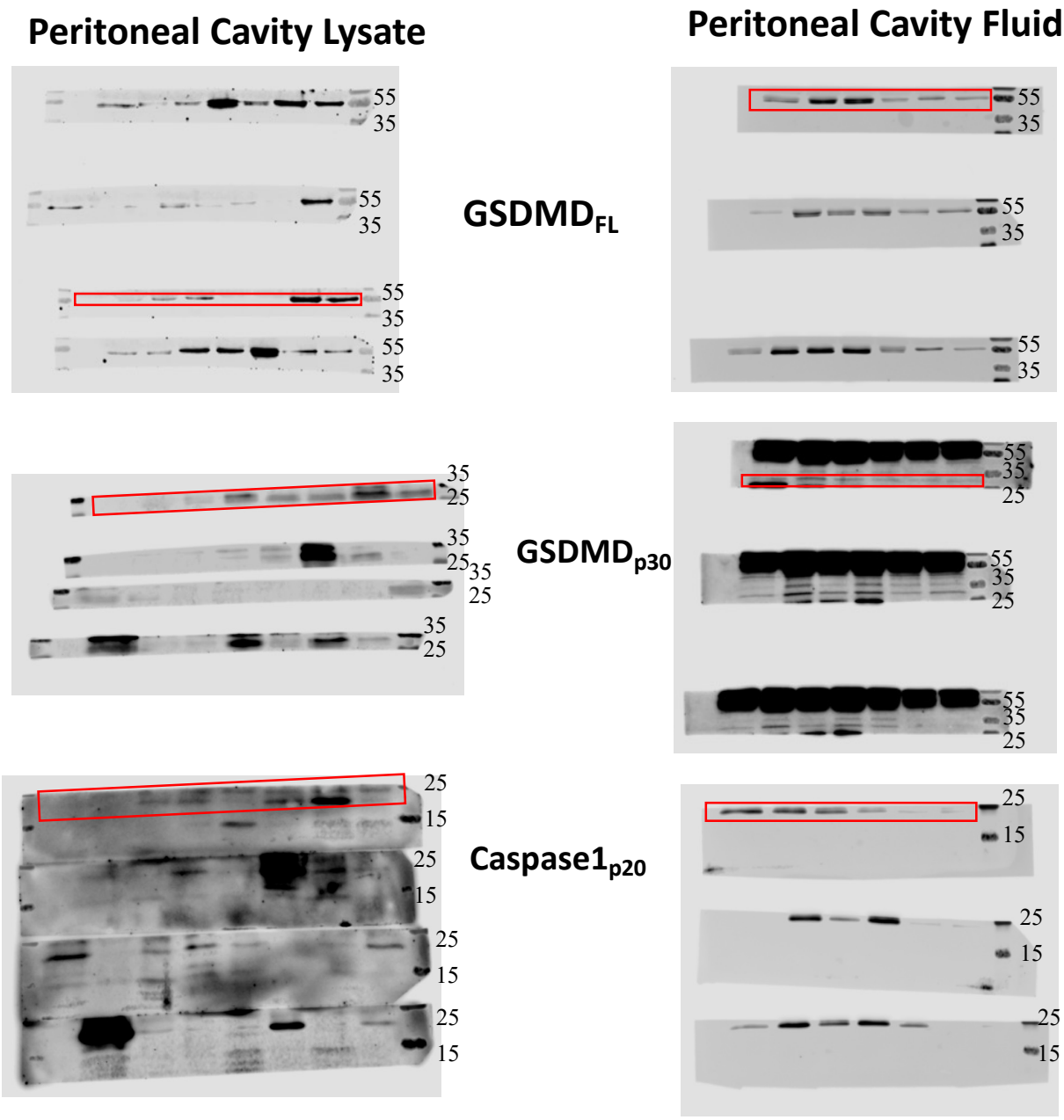

Figure 18: Immunoblots of cropped blots used in figure 12G.

The cropped sections are boxed in red.

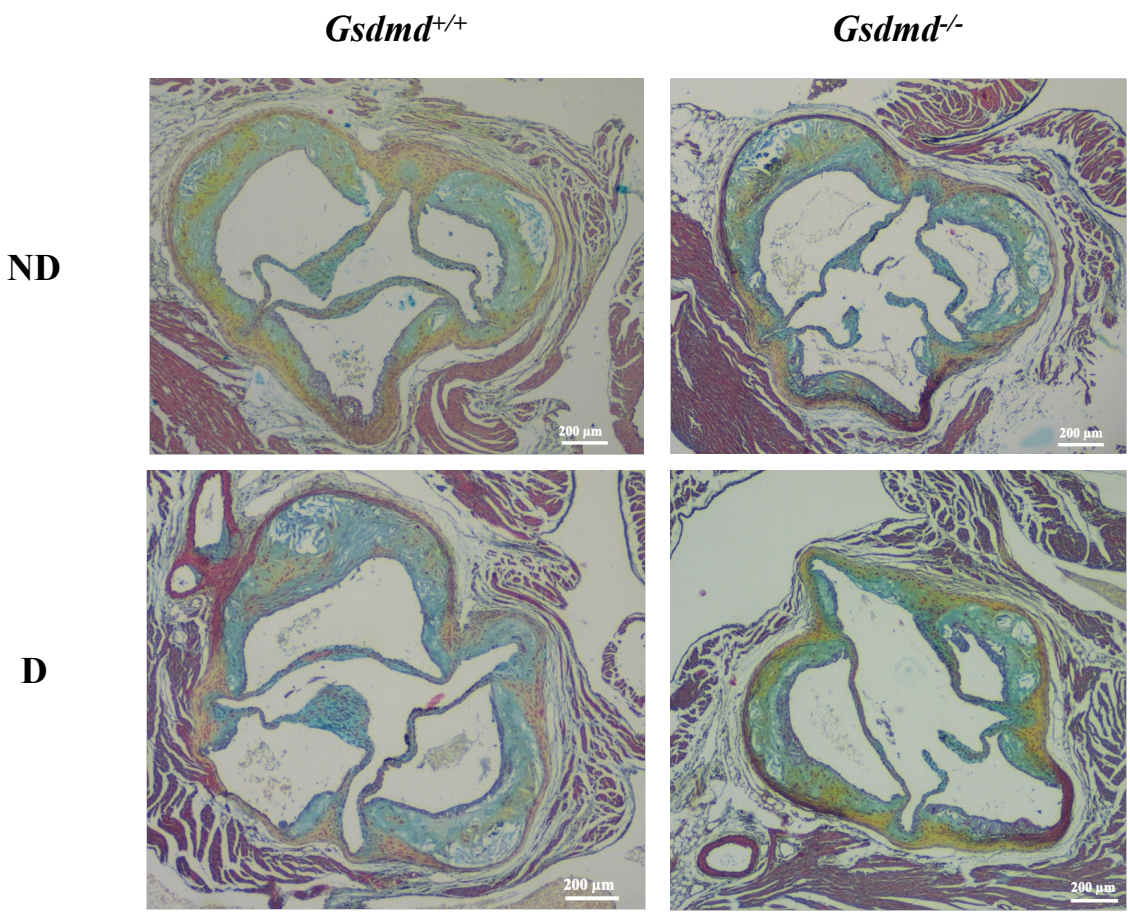

Figure 19: Unmarked aortic lesion images used in figure 5J.

Chapter 3 : Apolipoprotein C3 Induces Inflammasome Activation Only In Its Delipidated Form

Portions of this chapter were published as a manuscript in *Nature Immunology (72)* and *Arteriosclerosis, Thrombosis, and Vascular Biology (101)*.

3.1 Background

Apolipoprotein C3 (APOC3) is the most well-studied apolipoprotein in the APOC family. Like the other APOCs, the lipoprotein distribution of APOC3 depends on an individual's metabolic state; with elevated levels in individuals with diabetes and elevated levels of TRLs. Moreover, APOC3 can be glycosylated and sialylated in humans, modulating its hepatic clearance (102), adding another layer of complexity. As with all apolipoproteins, plasma levels are a reflection of both production and clearance rates. Lipoprotein-bound APOC3 is associated with TRLs when they are produced by the intestine and liver. As lipoproteins are cleared from circulation via receptor-mediated hepatic uptake, lipoprotein-bound APOC3 is cleared simultaneously and non-lipidated APOC3 is cleared via renal filtration (40; 103). Kinetic studies have shown that individuals with T2D have an increased APOC3 secretion rate that is associated with increased TRL levels (104). Diabetes also likely reduces the clearance rate of APOC3 by dampening LPL activity and, presumably, hepatic clearance of TRLs (84; 105).

The seminal study by Pollin and colleagues first demonstrated that individuals with *APOC3* loss-of-function mutations have reduced levels of plasma triglycerides and an apparent protection against CVD (36). Three separate studies on distinct cohorts of people with T1D in the US and Europe have now shown that serum levels of APOC3 predict cardiovascular events independent of traditional CVD risk factors (15; 33; 34). The mechanisms whereby APOC3 promotes atherosclerotic cardiovascular disease risk have been the topic of intense studies. We have previously demonstrated that silencing APOC3 protects against diabetes-accelerated atherosclerosis, both measured as early lesion initiation and the expansion of the necrotic cores associated with more advanced atherosclerosis (15). Importantly, the beneficial effect of APOC3 lowering was observed despite the lack of effects of APOC3 silencing on hyperglycemia. The

lesion-stabilizing effect of APOC3 reduction was also reported in mice without diabetes, but only in mice in which APOC3 also regulated TRLs (106), suggesting that the pro-atherogenic effects of APOC3 are likely mediated by its effects on TRLs and their remnants. However, individuals with type 1 diabetes (T1D) often have normal plasma lipid profiles, suggesting that APOC3 contributes to CVD events in individuals with T1D via other mechanisms.

As CVD is accompanied by heightened inflammation, and the recent Canakinumab Anti-inflammatory Thrombosis Outcome Study (CANTOS) highlighted a causal role for the cytokine interleukin-1β (IL-1β) in incident cardiovascular disease (53), a possible pro-inflammatory role for APOC3 has generated much interest. A previous study has demonstrated that de-lipidated APOC3 induces IL-1β release from human monocytes without requiring priming by lipopolysaccharide (LPS) (35). The mechanism involved APOC3-induced dimerization of toll-like receptor (TLR) 2 and TLR4, Ca^{2+}-dependent superoxide production and activation of caspase 8 via an alternative NLRP3 inflammasome activation pathway. Although NLRP3 inflammasome activation has been shown to contribute to the diabetes-associated atherosclerosis (16; 66), whether APOC3 is the underlying mediator of NLRP3 inflammasome activation under diabetes conditions remained elusive.

To address whether APOC3 contributes to diabetes-associated atherosclerosis via NLRP3 inflammasome activation, we investigated the ability of lipidated and de-lipidated APOC3 to induce NLRP3 inflammasome activation. We demonstrate that the ability of APOC3 to induce IL-1β release from human and mouse monocytes depends on the lipidation state of APOC3, and that only de-lipidated APOC3 can induce IL-1β release. Furthermore, lowering circulating APOC3 levels did not suppress the release of inflammasome-associated proinflammatory cytokine in a mouse model of T1D. Suggests that the atherogenic effects of APOC3 are

principally mediated by its effects on TRL or remnant lipoprotein (RLP) metabolism rather than by increased inflammasome activation.

3.2 Materials and Methods

3.2.1 APOC3 and other reagents

Ultrapure LPS from *Escherichia coli* was purchased from List Lab (catalog#421). Human VLDL was purchased from Kalen Biomedical, LLC (catalog#770100-7). The VLDL preparations used for this study contained endotoxin levels less than 0.1 EU/mL, as measured by the amebocyte lysate assay (Pierce™ Chromogenic Endotoxin Quant Kit, ThermoFisher Scientific, catelog#A39552). De-lipidated human APOC3 was purchased from Academy Bio-medical Company, Inc. (catalog#33P-102). We used the same source and range of concentrations of de-lipidated APOC3 as Zewinger et al.(35) Endotoxin levels in the batches of de-lipidated APOC3 available from the company for our study were higher than those reported by Zewinger et al (<0.03 EU/mL). Endotoxin levels in several batches of purchased de-lipidated APOC3, measured in the linear range (dilution in endotoxin-free water) by the amebocyte lysate assay (Pierce™ Chromogenic Endotoxin Quant Kit, ThermoFisher Scientific, catalog#A39552) ranged between <0.01 to 1.7 EU/mL in the concentrations of APOC3 used (0.0004 – 4 mg/dL) as shown by **Figure 20a-b**. These findings suggest that de-lipidated APOC3 is capable of inducing IL-1b release even when endotoxin levels are very low or undetectable. Human APOC3 ELISA and mouse APOC3 ELISA were purchased from Abcam (Human, catalog#ab154131; mouse, catalog#ab217777).

Mice. All animal procedures were reviewed and approved by the Institutional Animal Care and Use Committee of the University of Washington (protocol 3154-01) or by the Ionis Institutional Animal Care and Use Committee, and were conducted in conformity with the Public Health

Service Policy on Humane Care and Use of Laboratory Animals. Adult (8-12 weeks old) female and male LDL receptor-deficient (*Ldlr*$^{-/-}$) mice with or without a lymphocytic choriomeningitis virus (LCMV) glycoprotein transgene (*GP*^{Tg}) under control of the rat insulin promoter on a C57BL/J6 background were used for part of this study(81). All mice were housed in a specific pathogen-free facility and kept in a temperature-controlled room set to a light and dark cycle of 12 hours each. The mice had *ad libitum* access to standard mouse chow (LabDiet, catalog#5053), or a low-fat diet(81), and water during the study. *Ldlr*$^{-/-}$ mice without the *GP*^{Tg} were used for monocyte experiments *in vitro*. Females with the *GP*^{Tg} were used for the type 1 diabetes study. Female mice were injected with LCMV to induce diabetes. After the onset of diabetes, diabetic and non-diabetic mice were injected i.p. with 10 mg/kg/week GalNac control or APOC3 ASOs. Mice carrying a human *APOC3* transgene were purchased from The Jackson Laboratory (B6;CBA-Tg(APOC3)3707Bres/J; JAX stock #006907). Chow-fed male hAPOC3 mice with plasma triglycerides greater than ~4,000 mg/dL were selected for this study.

3.2.2 Mouse monocyte experiments

Mouse bone marrow cells were harvested from the femur and tibia with 8 seconds centrifugation at 11,000xg in the presence of sterile ACK lysing buffer (0.15 M NH_4Cl, 1 mM $KHCO_3$, and 0.1 mM Na_2EDTA). Bone marrow cells were further enriched for monocytes using an immunomagnetic negative selection kit from STEMCELL Technologies (catalog#19861) as per manufacturer's instructions. $0.2x10^6$ freshly isolated monocytes per well were cultured in 96-well tissue-culture-treated flat-bottom plates (Corning, catalog#353072) with 0.22 μm filtered (Millipore, catalog#S2GPU05RE) complete medium (RPMI with 10% fetal bovine serum and 1% penicillin/streptomycin) in a water-jacket incubator for 1 hour at 37°C with 5% CO_2. Non-adhered cells were removed by aspiration and cultured with serum-free medium (RPMI with 1%

penicillin/streptomycin) with or without treatments for 16 hours at 37ºC with 5% CO_2. Conditioned media were harvested for IL-1β release measurements via ELISA (ThermoFisher Scientific, catalog# 88701388). Cells were lysed with RIPA lysis buffer (ThermoFisher Scientific, catalog#89901) with protease and phosphatase inhibitor cocktail (ThermoFisher Scientific, catalog#78430). Total protein concentration was measured with the BCA protein assay (ThermoFisher Scientific, catalog#23227). Measurements were taken from distinct samples.

3.2.3 Mouse bone-marrow-derived macrophage experiments

Mouse bone marrow cells were harvested as described above in the murine monocyte experiments. The bone marrow cells were cultured in complete medium (RPMI, 30% L-conditioned medium, 7% fetal bovine serum, 1% penicillin/streptomycin) in a water-jacket incubator for 7 days at 37ºC with 5% CO_2. Cultured macrophages were incubated with or without treatments for 16 hours at 37ºC with 5% CO_2. For LPS priming, cells were stimulated with 10 ng/mL ultrapure LPS for 4 hours before treatments. Conditioned media were harvested for IL-1β measurements via ELISA (ThermoFisher Scientific, catalog# 88701388). Cells were lysed with RIPA lysis buffer (ThermoFisher Scientific, catalog#89901) with a protease and phosphatase inhibitor cocktail (ThermoFisher Scientific, catalog#78430). Total protein concentration was measured with the BCA protein assay (ThermoFisher Scientific, catalog#23227). Measurements were taken from distinct samples.

3.2.4 Mouse models with APOC3 ASO treatment

Type 1 diabetes mouse model: 8- to 12-weeks old female *Ldlr*$^{-/-}$*;GP*^{Tg} mice were injected with saline or LCMV. Diabetic (defined by blood glucose levels > 250 mg/dl) and non-diabetic mice were fed a low-fat, semi-purified diet without added cholesterol, as previously described(81). The diabetic mice received insulin pellets (LinShin Canada Inc.) to provide baseline insulin and

were treated with liquid insulin (Lantus; Sanofi) as needed to prevent ketonuria and extensive weight loss. Blood glucose was measured via a glucose meter. Values above 600 mg/dL are shown as 600 mg/dL due to the maximal range of the glucometer. After the onset of diabetes, diabetic and non-diabetic mice were injected i.p. with 10 mg/kg/week liver-targeted GalNAC control or APOC3 ASOs. Liver-specific delivery was achieved by targeting the hepatocyte-specific asialoglycoprotein receptor via triantennary GalNAc conjugation to the 5' end of the sense strand(107). The APOC3 ASO (CCAGCTTTATTAGGGACAGC) and control ASO (CCTTCCCTGAAGGTTCCTCC) were produced by Ionis Pharmaceuticals. The animals were maintained for 4 weeks before the termination of the study.

Human APOC3 transgenic mouse model: Chow-fed 8- to 12-weeks old male hAPOC3 mice (JAX stock #006907)(108) were injected with saline or 1 mg/kg of a siRNA targeting hAPOC3. The siRNAs consisted of a chemically modified antisense strand with sequence TCACTGAGAATACTGTCCCTTTT (hAPOC3 siRNA 1) or TCACTGAGAATACTGTCCCTT (hAPOC3 siRNA 2), hybridized with a chemically modified sense strand of sequence AAGGGACAGTATTCTCAGTGA (hAPOC3 siRNA 1) or AAGGGACAGTATTCTCAGTGA (hAPOC3 siRNA 2). Liver-specific delivery was achieved by targeting the hepatocyte-specific asialoglycoprotein receptor via triantennary GalNAc conjugation to the 5' end of the sense strand(107).

Plasma IL-18 and IL-1β levels were measured by ELISA (ThermoFisher Scientific, catalog#BMS618-3; BD Biosciences, catalog# 562278). Plasma human APOC3 levels were measured by an immunoturbidimetric automated assay using the Olympus/Beckman Coulter AU400 Chemistry Analyzer and ApoC3 K-Assay (Kamiya Biomedical). Measurements were

taken from distinct samples but different analytes were measured in the same samples for different figure panels.

3.2.5 Human monocyte isolation

Experiments were approved by the Institutional Review Board at the University of Washington (IRB# STUDY00008441) and were performed according to local ethics regulations and NIH guidelines. Informed consent was obtained from each participant and they received donuts or similar snacks and juice or water and $15 for participating in the study. Human peripheral blood mononuclear cells were isolated from the peripheral blood of healthy subjects (4 male and 3 female participants between the ages of 21 and 55) and enriched for monocytes with an immunodensity negative selection cocktail from STEMCELL Technologies (catalog#15068) as per the manufacturer's instructions. $1x10^6$ enriched freshly isolated human monocytes per well were cultured in 96-well tissue-culture-treated flat-bottom plates (Corning, catalog#353072) with 0.22 μm filtered (Millipore, catalog#S2GPU05RE) complete medium (RPMI, 1xGlutaMax, 1% penicillin/streptomycin, 10% fetal bovine serum, and 10 mM HEPES pH 7.4) in a water-jacket incubator for 1 hour at 37°C with 5% CO_2. Non-adherent cells were removed by aspiration and were then incubated in serum-free medium (RPMI, 1xGlutaMax, 1% penicillin/streptomycin, and 10 mM HEPES pH 7.4) with or without treatments for 16 hours at 37°C with 5% CO_2. Conditioned media were harvested for IL-1β measurements via ELISA (ThermoFisher Scientific, catalog# BMS224-2). Cells were lysed with RIPA lysis buffer (ThermoFisher Scientific, catalog#89901) with protease and phosphatase inhibitor cocktail (ThermoFisher Scientific, catalog#78430). Total protein concentration was measured with the BCA protein assay (ThermoFisher Scientific, catalog#23227). Measurements were taken from distinct samples.

3.2.6 Small unilamellar vesicles and lipidated APOC3 synthesis

1-palmitoyl-2-oleoyl-glycerol-3-phosphocholine (POPC) was purchased from Avanti Polar Lipids (catalog#850457). The chloroform from the POPC stock was completely removed by evaporation under nitrogen gas for 24 hours on ice. 3 mL of sterile PBS (pH 7.4, ThermoFisher Scientific, catalog#10010023) was added and the samples were vortexed until the lipid was in suspension. The samples were pulse-sonicated on ice for 1 hour with a 1-second on and 1-second off-duty cycle at 75% of the probe's maximum setting (Fisher Biosciences probe). The vesicles were centrifuged at 300xg for 20 minutes at 4°C to remove unreacted lipids and titanium residues. Reacted vesicles were applied to a Superose 6 gel filtration column (Amersham Biosciences) and SUV fractions 16-17, corresponding to an average SUV size of 27 nm were collected (**Figure 20**). The SUV fractions were concentrated with a 3 kDa molecular cutoff filter (Millipore, catalog#UFC5003) and the phospholipid content was quantified (Sigma-Aldrich, catalog#MAK122). Purified and concentrated SUVs were analyzed with ion mobility analysis on differential mobility for size distribution as previously described(109). Homogenized samples were used for the lipidation of APOC3. De-lipidated APOC3 was incubated with SUVs at a 1:10 molecular ratio for 24 hours at 4°C. Samples were filtered and concentrated with a 100 kDa molecular cutoff filter (Millipore, catalog#UFC5100) to remove free APOC3. SUVs and lipidated APOC3 were sterile filtered with a 0.45 μm filter (Corning, catalog#8162) before applying to monocytes. The SUV preparations contained no detectable endotoxin (Pierce™ Chromogenic Endotoxin Quant Kit, ThermoFisher Scientific, catelog#A39552).

3.2.7 Isolation of HDL, LDL, VLDL + IDL, and lipoprotein-free serum from subjects with type 1 diabetes

HDL (density 1.063-1.21 g/mL), LDL (1.019-1.063 g/mL), VLDL + IDL (<1.019 g/mL), and lipoprotein-free serum (>1.21 g/mL) were isolated by density gradient ultracentrifugation from

rapidly thawed previously collected serum from 10 subjects with T1D in the Coronary Artery Calcification in Type 1 Diabetes (CACTI)(15) study cohort as previously reported(110). For HDL: 50 µL serum was adjusted to a density of 1.21 g/mL using potassium bromide solution (KBr) in a 230 µL centrifuge tube. The samples were spun in a TLA 100 rotor (Beckman Coulter) at 436,000×g for 5.5 hours at 5°C. The top 57.5 µL was collected with a pipette for HDL isolation and the bottom fraction was used for the isolation of the lipoprotein-free fraction. The top fraction was adjusted to a density of 1.063 g/mL and the samples were spun in a TLA 100 rotor at 436,000×g for 5.5 hours at 5°C. The bottom 58 µL was collected with a Hamilton syringe as the HDL fraction. For LDL: 100 µL serum was adjusted to a density of 1.063 g/mL using KBr in a 230 µL centrifuge tube. The samples were spun in a TLA 100 rotor at 436,000×g for 5.5 hours at 5°C. The top 57.5 µL was collected with a pipette and was adjusted to a density of 1.019 g/mL using KBr. Then the samples were spun in a TLA 100 rotor at 436,000×g for 5.5 hours at 5°C. The bottom 58 µL was collected with a Hamilton syringe as the LDL fraction. For VLDL and IDL: 300 µL serum was adjusted to a density of 1.019 g/mL using KBr in a 500 µL centrifuge tube and the samples were spun in a TLA 120 rotor (Beckman Coulter) at 627,000×g for 12 hours at 5°C. The top 125 µL was collected with a pipette as the VLDL and IDL fraction. For the lipoprotein-free fraction: the remaining bottom fraction from the HDL isolation spin (above) was adjusted to a density of 1.21 g/mL using KBr and spun in a TLA 100 rotor at 436,000×g for 5.5 hours at 5°C. The bottom 58 µL was collected with a Hamilton syringe as the lipid-free fraction. All fractions were dialyzed against 20 mM potassium phosphate (pH 7.0) with 100 µM DTPA before digestion and mass spectrometry analysis of APOC3.

3.2.8 Digestion of HDL, LDL, VLDL + IDL, and lipoprotein-free serum

Following the addition of freshly prepared methionine (5 mM), 10 µg of HDL, LDL, VLDL + IDL, or lipid-free serum was reduced with dithiothreitol and then alkylated with iodoacetamide in 3% sodium deoxycholate (SDC) and 100 mM ammonium bicarbonate (NH_4HCO_3). The HDL, LDL, VLDL+IDL, or lipoprotein free serum proteins were then incubated overnight (18 hours) at 37°C with 20:1 (w/w, protein/enzyme) of sequencing grade modified trypsin. An appropriate amount of 20% trifluoroacetic acid was added to the reaction mixture (to pH 2–3) to stop the digestion and precipitate the SDC. The SDC precipitation was spun down in a microcentrifuge (Eppendorf® 5424R) at 19,745×g for 20 minutes. The supernatant of the digested samples was desalted and cleaned up by solid-phase extraction using Waters HLB 1cc (30 mg) extraction cartridges. The digested peptides were eluted from the cartridges with 60% of acetonitrile containing 0.3% of trifluoroacetic acid, and the eluted samples were dried and stored at −80°C until mass spectrometry analysis.

3.2.9 Liquid chromatography-electrospray ionization tandem mass spectrometric (LC-ESI-MS/MS) analysis of APOC3 in HDL, LDL, VLDL +IDL, and lipoprotein-free serum by parallel reaction monitoring (PRM)

We used targeted proteomics with PRM to quantify APOC3 in HDL, LDL, VLDL+IDL, and lipoprotein-free serum(110). Briefly, LC-ESI-MS/MS analyses were performed in the positive ion mode with an ultrahigh-resolution accurate mass Orbitrap Fusion Lumos Tribrid Mass Spectrometer (Thermo Fisher Scientific, San Jose, CA) coupled to a nano-flow UHPLC system (EASY-nLC™ 1200 System, Thermo Fisher Scientific). Peptide digests (equivalent to 0.3 µg of protein) were loaded onto a C-18 trap column (0.1 × 40 mm) at a flow rate of 2.5 µL/min for 4 minutes and desalted for 10 minutes using 0.1% formic acid in water (solvent A). They were then

separated at a flow rate of 0.3 µL/min, using a C-18 analytical column (0.1 × 200 mm). A multistep gradient of solvent A and 0.1% formic acid in 90% acetonitrile (solvent B) was used for the separation. The trap and analytical columns were packed in-house with Magic C-18 reverse-phase resin (5 µm; 100 Å; Michrom Bioresources). The columns were kept at room temperature, and the peptides were separated using a multistep gradient as follows: 1% to 8% solvent B for 1 min; 8% to 28% solvent B for 24 min; 28% to 40% solvent B for 6 min; and 40% to 90% solvent B for 5 min. The column was subsequently washed for 3 min in 90% B and re-equilibrated in 1% B for 12 min. The mass spectrometer was operated in the data-independent acquisition PRM mode.

3.2.10 Quantifying APOC3 in HDL, LDL, VLDL + IDL, and lipoprotein-free serum

The PRM data were analyzed with Skyline (version 21.1.0.278), an open-source program(111). The peptide DALSSVQESQVAQQAR from APOC3 was monitored for quantifying APOC3. To get the total peak area for the peptide, the peak areas of all the transitions of the peptide detected by PRM analysis were summed but the transitions with interferences were deleted. Because the intensity of the doubly charged and triply charged peptides was comparable, we measured the peak areas of the peptide at both charge states and their areas were added. In order to compare the relative intensity of APOC3 in different fractions, the sum peak area of that peptide from each sample was normalized to the average peak area of that peptide in HDL in the control group. Thus, the average level of APOC3 in HDL in the control group was defined as an arbitrary unit of 1 and the relative levels of APOC3 in other lipoprotein fractions and lipoprotein-free serum were expressed as the percentage of HDL levels. Measurements were taken from distinct samples.

3.2.11 Analysis of association between an APOC3 loss-of-function variant, triglycerides, high sensitivity C-reactive protein and myocardial infarction in the UK Biobank

The UK Biobank is a prospective cohort of approximately 500,000 individuals in the UK aged 40-69 at the time of recruitment between 2006 and 2010(112). Genotyping was performed on one of two genotyping arrays: the UK BiLEVE Axiom Array (49,950 participants) or the UK Biobank Axiom Array (438,427 participants). To obtain a more comprehensive set of genetic variants that were not directly genotyped on the arrays, we performed imputation utilizing the TOPMed reference panel via the TOPMed imputation server(113; 114). We focused our analyses on 452,401 individuals of broadly European ancestry and on rs138326449 (IVS2 + 1G-A), a rare (MAF = 0.002) *APOC3* splice donor variant that results in APOC3 loss-of-function and for which carriers exhibit ~50% reduced circulating APOC3(115). rs138326449 was well imputed using the TOPMed reference panel (R2~0.9). We identified 1,928 carriers of the rs138326449 alternative (A) allele, of which 1,926 are heterozygotes and 2 are homozygotes.

We performed association analyses under an additive model using GloWGR, a distributed version of the REGENIE whole-genome regression method(116). Analyses were adjusted for participant age, genetic sex, genotyping batch, assessment center, and the first ten principal components of genetic ancestry. We evaluated associations between rs138326449 and three phenotypes: serum triglycerides, serum high sensitivity C-reactive protein (hsCRP) and myocardial infarction (MI). Serum triglyceride (n=430,833) and hsCRP (n=426,774) measures were derived from the blood biochemistry assays (https://biobank.ctsu.ox.ac.uk/ukb/ukb/docs/serum_biochemistry.pdf) generated by UK Biobank by first removing outlier values ± 5 standard deviations from the mean and then log10

transforming remaining values prior to analysis. MI cases (n=20,851) and controls (n=318,164) were defined using composite criteria from linked longitudinal health records, death registry data and self-reported information from the UK Biobank in-person evaluations. Briefly, cases were defined as individuals with codes that capture incident or prevalent MI (ICD-10 codes: I21*, I22*, I23*; UK Biobank fields: 20002_1075, 6150_1) and controls were defined as individuals without any codes that capture incident or prevalent ischemic heart disease more broadly (ICD-10 codes: I20*, I21*, I22*, I23*, I24*, I25*, Z95.1, Z95.5; OPCS-4 Codes: K40*, K45*, K49*, K50*, K75*; UK Biobank fields: 20002_1074, 20002_1075, 6150_1, 6150_2, 20004_1070, 20004_1095, 20004_1523).

In order to evaluate whether the observed association between rs138326449 and elevated hsCRP was robust to adjustment for potential confounders present at the time of serum sample ascertainment, these analyses were repeated with the addition of relevant covariates, including use of lipid-lowering medications (captured by UK Biobank fields (limited to Instance '0'): 20003_1140861958, 20003_1141146234, 20003_1141146138, 20003_1141192410, 20003_1141192736, 20003_1140888648, 20003_1141192740, 20003_1140861954, 20003_1141188146, 20003_1140861924, 20003_1141192414, 20003_1140888594, 20003_1141162544, 20003_1140862026, 20003_1140861928, 20003_1141172214, 20003_1140881748, 20003_1140861926, 20003_1140861970, 20003_1141201306, 20003_1140862028, 20003_1141157260, 20003_1140861856, 20003_1140864592, 20003_1141171548, 6177_1, 6153_1) and diabetes (captured by UK Biobank fields (limited to Instance '0'): 20002_1220, 20002_1222, 20002_1223, 2443_1, 20003_1140884600, 20003_1140883066, 20003_1140874744, 20003_1141171646, 20003_1141177600, 20003_1141152590, 20003_1140874686, 20003_1141189090, 20003_1141189094,

20003_1140874718, 20003_1140874646, 20003_1141171652, 20003_1141168660, 20003_1140910566, 20003_1141177606, 20003_1140874746, 20003_1140874674, 20003_1140868902, 20003_1141156984, 20003_1141173882).

3.2.12 Statistical Analysis

Power analyses were performed to determine the number of mice needed for experiments when sufficient preliminary information on response variables was available. For example, one critical parameter was the plasma IL-18 in mice. Preliminary studies indicated a mean value of 124 pg/mL in non-diabetic mice and a mean value of 257 pg/mL in diabetic mice with a standard deviation of 93 pg/mL. Power analysis showed that n=11 or n= 13 was needed to reject the null hypothesis with 90% or 95% probability and 5% type 1 error in a two-sided test. Statistical analyses were performed using GraphPad Prism 9.4.0 (GraphPad Software). Samples were assigned to various groups by block randomization with a block size of 2-4 (depending on the experiment). Data collection and analysis were performed blind to the conditions of the experiments. Normality tests were performed by the D'Agostino & Pearson test and outliers were removed based on the robust regression and outlier removal (ROUT) method with Q=0.1%. Data are displayed as mean ± SEM. Based on the normality of the data, they were analyzed with two-sided Mann-Whitney test, one-way ANOVA followed by Holm-Šídák's multiple comparisons test, Kruskal-Wallis test and Dunn's multiple comparisons tests, or two-way ANOVA followed by Tukey multiple comparisons test. A p-value of less than 0.05 was considered statistically significant.

3.2.13 Data Availability

All original data are available from the corresponding author upon request.

3.3 Results

3.3.1 APOC3-associated IL-1β release is dependent on APOC3 lipidation state and cell type

We show that both de-lipidated APOC3 (4 mg/dL) and ultrapure LPS induce a striking increase in IL-1β release from human blood monocytes without prior priming of the NLRP3 inflammasome (**Fig. 21a**), consistent with the study by Zewinger and colleagues (35). However, this effect was not mimicked by human VLDL, which contained sufficient APOC3 (0.35 mg/dL) to induce IL-1β release (**Fig. 20a**). To investigate whether the APOC3-induced alternative inflammasome pathway is unique to human monocytes, we isolated mouse bone marrow monocytes, using an immunomagnetic negative selection method. Like in the human monocytes, de-lipidated APOC3 (0.004 – 4 mg/dL) induced significant increases in IL-1β release from mouse monocytes (**Fig. 21b** and **Fig. 20a-b**). Again, VLDL was unable to induce IL-1β release from these cells.

APOC3 is an amphipathic lipid-binding apolipoprotein (117). We therefore investigated whether the IL-1β stimulating effect of de-lipidated APOC3 is also observed when APOC3 is lipid-bound. We generated lipidated APOC3 by synthesizing small unilamellar vesicles (SUVs), approximately 27 nm in size (**Fig. 20c-e**), with 1-palmitoyl-2-oleoyl-glycerol-3-phosphocholine (POPC)(118) and bound de-lipidated APOC3 to these vesicles. Lipidated APOC3 was co-incubated with isolated human and mouse monocytes as above. Strikingly, lipidated APOC3 at the same concentration as the de-lipidated APOC3 failed to induce IL-1β release from either human or mouse monocytes (**Fig.21a-b**). These results are consistent with the interpretation that the ability of APOC3 to induce IL-1β release in monocytes is dependent on the lipidation state of APOC3. The lack of IL-1β-inducing effect of lipidated APOC3 is consistent with the lack of VLDL-induced IL-1β release from monocytes observed in our study. The discrepancy in the

ability of VLDL to induce IL-1β release in our study and that of Zewinger et al. (35) could be due to differences in VLDL preparations or endotoxin levels.

De-lipidated APOC3 failed to induce significant IL-1β release from differentiated mouse bone marrow-derived macrophages (vehicle = 0.50±0.50 pg/mL; APOC3 = 2.39±1.27 pg/mL; mean±SEM; n=3; p=0.4 by Mann-Whitney test), consistent with the findings of Zewinger et. al. (35) and with the ability of TLR activation alone to induce release IL-1b in monocytes, but not in macrophages (119), suggesting that the ability of de-lipidated APOC3 to induce inflammasome activation is lost with monocyte to macrophage maturation.

3.3.2 Delipidated APOC3 does not exist in the circulation

APOC3 predicts incident coronary artery events in individuals with T1D (15; 33; 34). The lack of VLDL-induced IL-1β release from monocytes prompted us to question whether free APOC3 exists at sufficiently high levels to activate the inflammasome under physiological conditions in diabetes. We collected serum samples from individuals with T1D and measured the amount of APOC3 within each lipoprotein fraction (VLDL + intermediate-density lipoprotein [IDL], LDL, and HDL) and in the lipoprotein-free fraction by targeted mass spectrometry. We observed APOC3 in all the lipoprotein fractions, but the lipid-free fraction contained little APOC3 (0.00024 ±0.000007 mg/dL, mean±SEM, n=10, **Fig. 21c-d**). These results show that APOC3 exists primarily in a lipid-bound state in circulation. Concentrations of APOC3 mimicking those free in circulation were unable to induce IL-1β release (**Fig. 20a**).

3.3.3 Reduced plasma APOC3 fails to suppress elevated plasma IL-18 under diabetes conditions

To investigate the *in vivo* effects of APOC3 reductions on diabetes-associated inflammasome activity, we used an antisense oligonucleotide (ASO) approach to reduce APOC3 in animals with T1D. We silenced hepatic APOC3 production using a liver-targeted APOC3 GalNAc-conjugated

ASO in non-diabetic and diabetic mice (**Fig. 22a**). Controls were treated with a control GalNAc ASO. After four weeks, diabetic mice exhibited elevated blood glucose, plasma triglycerides, APOC3, and IL-18 levels (**Fig. 22b-e**). IL-18, like IL-1 β, is released through the inflammasome pathway. It should be noted that IL-18 is bound to IL-18 binding proteins in plasma, and therefore the total concentrations of IL-18 do not reflect its biological activity (95). Silencing of hepatic APOC3 markedly reduced plasma APOC3 levels in diabetic mice, however, the elevated plasma IL-18 remained unaffected. Similarly, although plasma IL-1β levels were approximately 100 times lower than those of IL-18, APOC3 ASO treatment did not significantly reduce plasma IL-1β levels in diabetic mice (control ASO = 3.8 ± 1.2 pg/mL, APOC3 ASO = 1.7 ± 0.8 pg/mL, mean±SEM; n=12-14; p=0.17 by Mann-Whitney test). These results indicate that endogenous APOC3 does not contribute significantly to inflammasome activation in diabetic mice *in vivo*.

3.3.4 Humanized APOC3 transgenic mice fail to elevate plasma IL-18

Since endogenous APOC3 is not responsible for inflammasome activation in diabetic mice, we questioned the association between APOC3 and inflammasome activation *in vivo.* To investigate the *in vivo* effects of APOC3 reductions on inflammasome activity, we use small interfering RNAs (siRNA) approach to reduce APOC3. We evaluated mice with transgenic expression of human APOC3 to strengthen the conclusion that plasma APOC3 does not impact inflammasome activity. We measured plasma levels of IL-1β and IL-18 from human APOC3 transgenic mice treated with saline or two different human APOC3 GalNAc-conjugated siRNAs. Despite the highly elevated plasma APOC3 and triglycerides, which were markedly reduced by the APOC3 siRNA treatment, levels of IL-18 were unchanged (**Fig. 22f-h**). It should be noted that these mice exhibited 62-times higher plasma APOC3 concentrations versus the free APOC3 used in our *in vitro* assay and 22-times higher plasma APOC3 levels versus that observed in

individuals with diabetes (33; 120). Human APOC3 transgenic mice had plasma IL-1β levels below the lowest standard (<0.3 pg/mL, n=4-7). These results strongly support the finding that APOC3 does not lead to elevated levels of circulating IL-1β and IL-18 *in vivo* in mice.

3.3.5 Carriers of APOC3 loss-of-function variants are associated with decrease TG but not high-sensitivity C-reactive protein

Zewinger and colleagues demonstrated that subjects with elevated plasma levels of APOC3 also had elevated levels of high sensitivity C-reactive protein (hsCRP; a marker of systemic inflammation) when adjusted for age and sex (35). If this observed positive correlation is reflective of a causal relationship between APOC3 and systemic inflammation, a reasonable expectation might be that genetically-mediated reductions in APOC3 would result in reduced levels of hsCRP. We utilized data from the UK Biobank to explore whether this hypothesis can be supported by analyses in carriers of *APOC3* loss-of-function variants (**Fig. 23** and **Table 9**). We identified 1,928 individuals carrying rs138326449 (IVS2 + 1G-A), a rare (MAF = 0.002) *APOC3* loss-of-function variant that results in ~50% reduced circulating APOC3 in heterozygotes(115). We confirmed that *APOC3* loss-of-function is significantly associated with decreased serum triglycerides and nominally associated with decreased risk of myocardial infarction. However, paradoxically, *APOC3* loss-of-function is associated with modestly increased levels of serum hsCRP, rather than reduced levels as would be expected if APOC3 promoted inflammatory processes. The association between rs138326449 and elevated hsCRP was robust to adjustment for potential confounders present at the time of serum sample ascertainment, including the use of lipid-lowering medications and diabetes (**Table 10)**. Overall, the data from the UK Biobank support the hypothesis that the atherosclerotic cardiovascular

disease protection conferred by APOC3 loss-of-function is mediated by triglyceride lowering rather than by reduced inflammation.

3.4 Discussion

APOC3 has been identified as a CVD risk factor in three different cohorts of people with T1D (15; 33; 34). The association between APOC3 and CVD is independent of traditional lipid risk factors and has generated much interest. Although the mechanism whereby suppression of APOC3 prevents atherosclerosis in the setting of diabetes is still an enigma, it is most likely due to its inhibition of clearance of TRLs and RLPs. Immunoreactive APOC3 accumulates at a greater extent in lesions in diabetic mice and co-localizes with APOB and APOE, suggesting accumulation of TRLs and/or RLPs, and this accumulation is prevented by silencing of APOC3 or by increasing hepatic clearance of TRLs (15; 84; 121). However, some studies have suggested a role for APOC3 beyond that of TRL lipolysis and clearance. For example, non-lipidated APOC3 can induce alternative NLRP3 (NOD-, LRR- and pyrin domain-containing protein 3) inflammasome activation in isolated human monocytes (35). Although it is tempting to speculate that elevated levels of inflammatory markers in humans or mice with diabetes may be due to elevated plasma APOC3, we demonstrated that the inflammasome-activating effect of non-lipidated APOC3 is lost when APOC3 is bound to lipid particles, as it is in circulation in people with and without diabetes.

Furthermore, diabetic mice in which APOC3 was silenced did not have reduced plasma levels of IL-18 or IL-1β, pro-inflammatory cytokines released through inflammasome pathways, and APOC3 transgenic mice did not exhibit increased plasma levels of IL-1β or IL-18 despite the high levels of APOC3. Although we cannot exclude the possibility that sufficient free APOC3 exists physiologically in tissues at concentrations high enough to induce inflammasome

activation *in vivo* (122), our findings provided strong evidence suggesting that endogenous APOC3 does not act upstream of NLRP3 activation in diabetes. Investigation of whether APOC3 exists free of lipoproteins in tissues from humans or animal models will be challenging, although novel approaches, such as single-cell transcriptomics and spatial proteomics and metabolomics in conjunction with artificial intelligence technology provide strides in the right direction (123; 124).

The recent human study also shows an intriguing interaction between an NLRP3 intron variant associated with increased NLRP3 activation and APOC3 plasma concentrations (100). Such a connection might be explained by a mechanism in which plasma APOC3 levels are regulated downstream of NLRP3 because recent mouse studies demonstrated reduced serum APOC3 levels in diabetic mice with hematopoietic NLRP3 deficiency (66). These results highlight the importance of considering the function of APOC3 in its physiological lipidated state and support the notion that APOC3 acts to promote atherosclerosis primarily by its effects on TRLs and RLPs.

In summary, de-lipidated APOC3 stimulates IL-1β release from human and mouse monocytes, consistent with the results by Zewinger and colleagues (35), but we provide strong evidence from an array of different analyses – including *in vitro*, *in vivo*, and genomic data - demonstrating that this effect is lost when APOC3 is bound to a lipid particle. The very low levels of free APOC3 in serum samples from individuals with T1D, the inability of APOC3 silencing or overexpression to alter plasma levels of IL-18 and IL-1 β in mice and the analyses of *APOC3* loss-of-function variant carriers in the UK Biobank also support the conclusion that endogenous lipid-bound APOC3 does not induce inflammasome activation *in vivo*. Overall, our data suggest that the atherogenic effects of APOC3 are principally mediated by its effects on

TRL/RLP metabolism rather than by increased inflammasome activation. Future studies should determine whether lipid-free APOC3 exists in vascular tissue at sufficient levels to elicit atherogenic inflammatory responses.

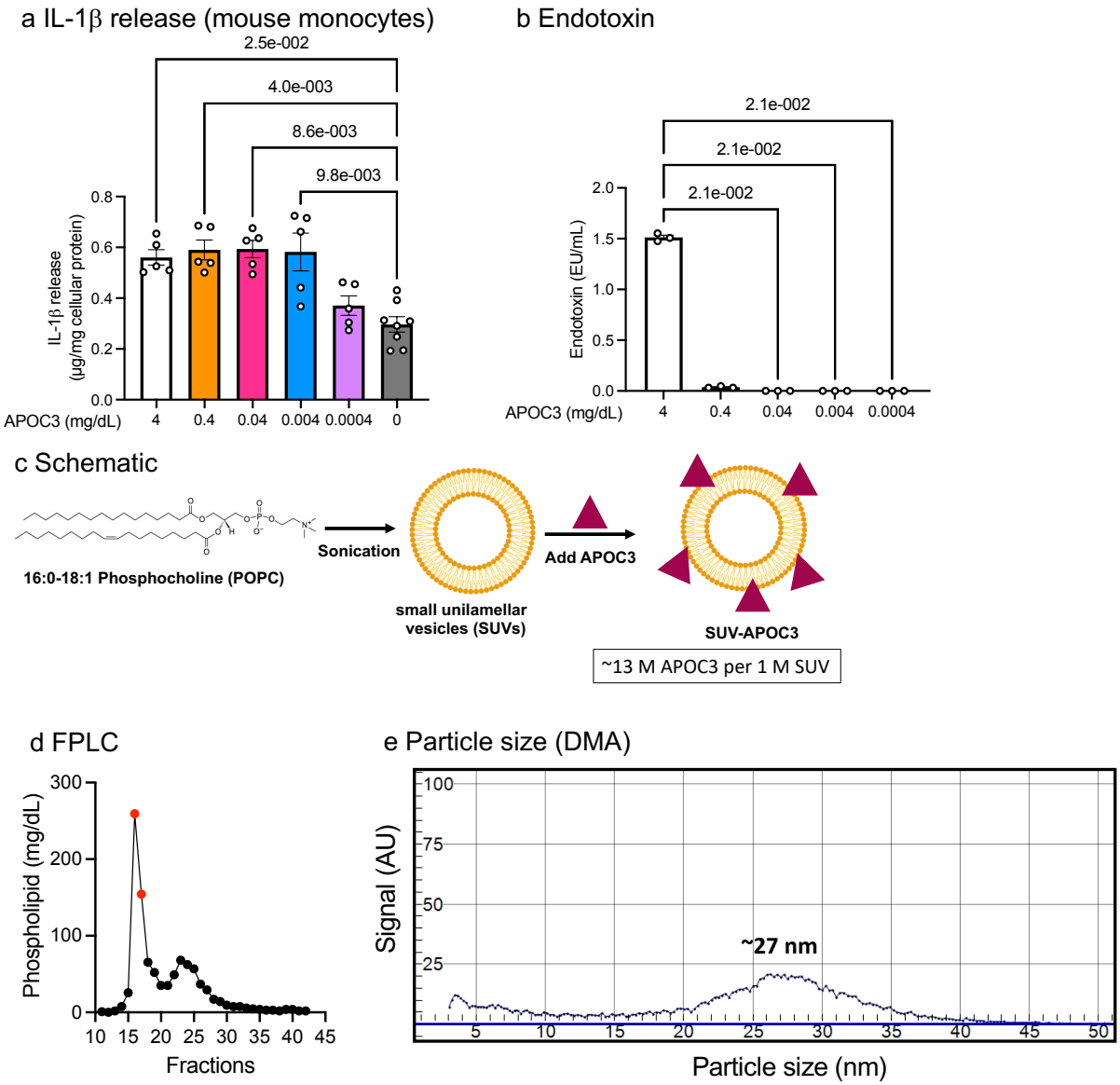

Figure 20: Characterization of small unilamellar vesicles (SUVs) and APOC3.

a, IL-1b release from mouse bone marrow-derived monocytes incubated in indicated APOC3 concentrations. IL-1b measurements were conducted by ELISA and the data were normalized to total cellular protein determined by a BCA protein assay. Data show means ± SEM (n=5, 5, 5, 5, 5, 8 replicates/group, respectively). **b,** Endotoxin levels in the final concentrations of APOC3 used in panel a, measured by the amebocyte lysate assay (Pierce™ Chromogenic Endotoxin Quant Kit). Data show means ± SEM (n=3 replicates/group). In a and b, statistical analyses were performed by Kruskal-Wallis tests and Dunn's multiple comparisons tests. **c,** 1-palmitoyl-2-oleoyl-glycerol-3-phosphocholine (POPC) in PBS was sonicated on ice to allow the formation of small unilamellar vesicles (SUVs). The SUVs were purified on a Superose 6 column before the incorporation of APOC3**.** SUV-APOC3 was isolated with various centrifugation columns and was sterile filtered. The molar concentrations of APOC3 and SUVs were measured by ELISA,

BCA protein assay, and phospholipid assay. **d,** FPLC profile of synthesized SUVs and fractions 16 and 17 (shown in red) were purified and used for the lipidation of APOC3. **e,** Ion mobility analysis on differential mobility analyzer (DMA) of SUVs from fractions 16 and 17, demonstrating a homogenized particle population around 27 nm. Extended Data Figure 1c was created with BioRender.com.

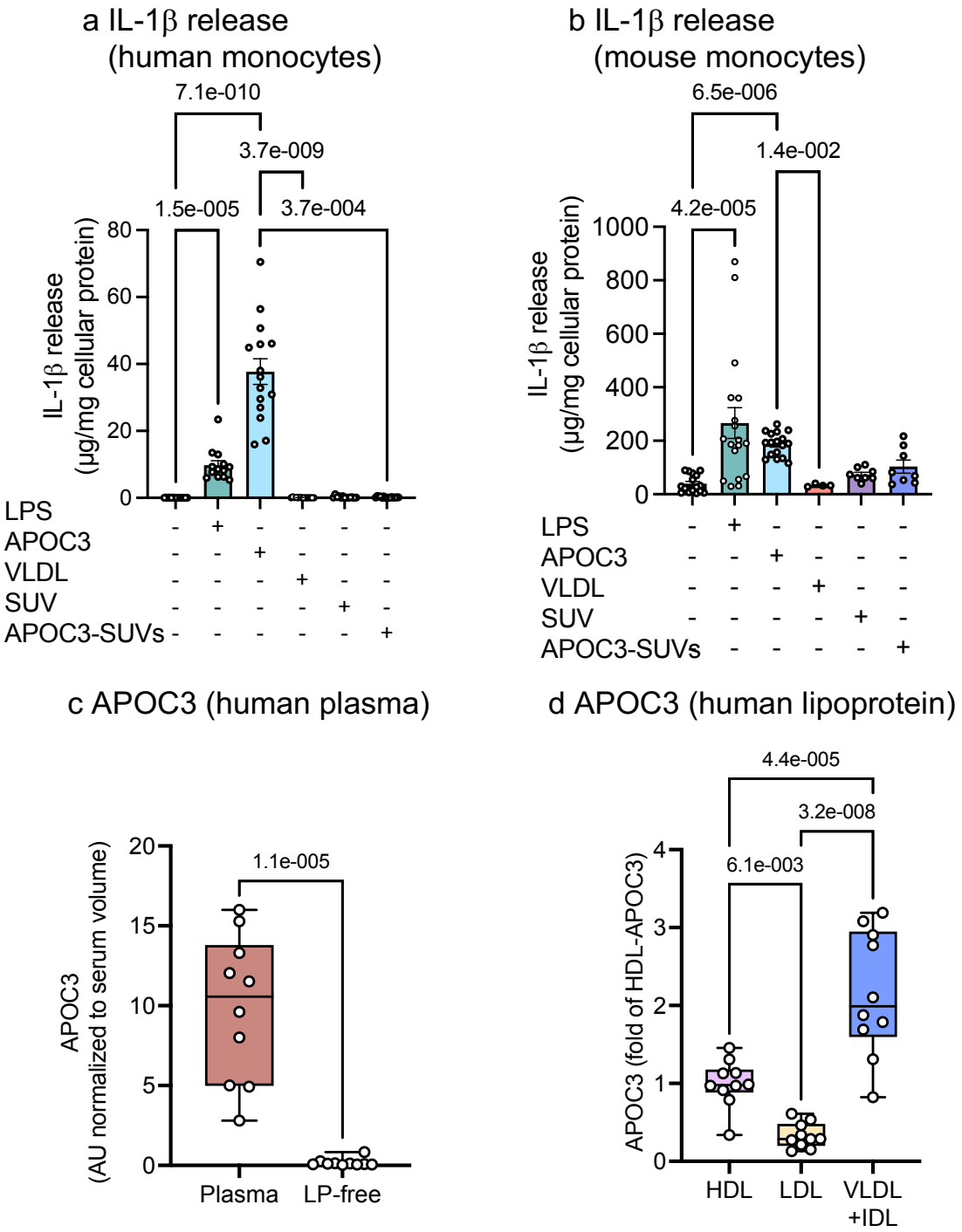

Figure 21: De-lipidated APOC3, but not lipid-bound APOC3, induces IL-1β release from human and mouse monocytes.

a, IL-1b release from human blood monocytes incubated with or without ultrapure LPS (10 ng/mL), small unilamellar vesicles (SUVs) with an average diameter of 27 nm (70.5 mg/dL), de-lipidated human APOC3 (4 mg/dL), APOC3-SUVs complex (4 mg/dL APOC3 and 70.5 mg/dL SUVs), or human VLDL (4 mg/dL) for 16 hr. **b,** IL-1b release from mouse bone marrow-derived monocytes incubated as in a. IL-1b measurements were conducted by ELISA and the data were

normalized to total cellular protein determined by a BCA protein assay. Data show means ± SEM (n=14, 13, 15, 13, 10, 15 replicates/group, respectively, of pooled samples isolated from 7 subjects in A and n=16, 18, 17, 8, 8, 4 individual mice/group in b). **c-d,** Serum samples from 10 individuals with T1D were used to investigate total serum levels and relative levels of APOC3 in different lipoprotein fractions and the lipoprotein-free (LP-free) fraction. Lipoprotein fractions were isolated by density ultracentrifugation and APOC3 levels were measured by targeted mass spectrometry (DALS peptide). **c,** APOC3 levels in whole serum versus the LP-free fraction (d>1.021 g/mL). **d,** APOC3 levels in HDL, LDL and VLDL+IDL. The data are shown in box-and-whisker plots (the bound of the box extends from the 25^{th} to 75^{th} percentiles and the whisker covers the minima and maxima) with the median marked by a center line. Statistical analyses were performed by Kruskal-Wallis test and Dunn's multiple comparisons tests in a and b, two-sided, Mann-Whitney test in c, and one-way ANOVA followed by Holm-Šídák's multiple comparisons test in d. Normality test was performed by D'Agostino & Pearson test. Outliers were removed based on robust regression and outlier removal method with Q=0.1%. (0, 0, 1, 2, 0, 0) datapoints were removed in a; no datapoint was removed in b, c, or d.

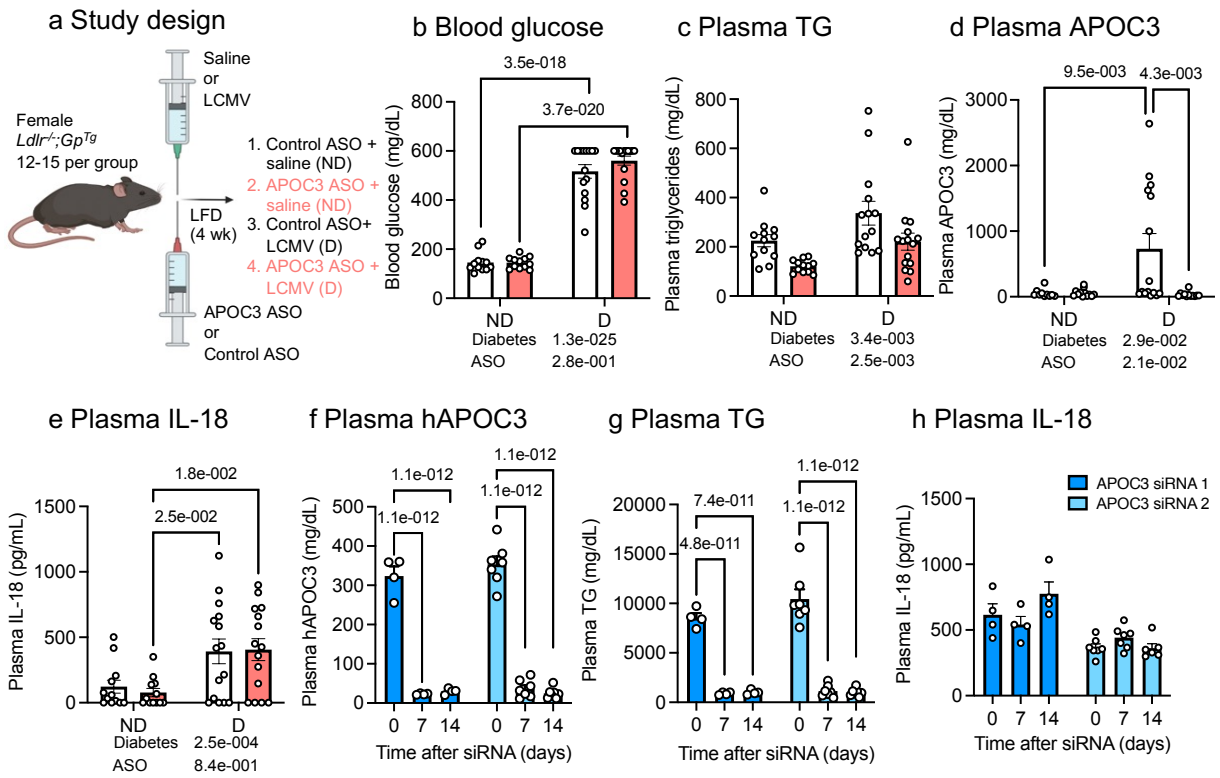

Figure 22: APOC3-deficiency does not reduce plasma IL-18.

Female low-density lipoprotein receptor-deficient mice with a virus glycoprotein transgene (*Ldlr*$^{-/-}$*;GP*^{Tg}) were rendered diabetic (D) with lymphocytic choriomeningitis virus (LCMV). Saline was used as a control (non-diabetic, ND). At the onset of diabetes, the animals were switched to a low-fat, semipurified diet (LFD) and maintained for 4 weeks**.** Animals received weekly i.p. injections of 10 mg/kg control or APOC3 GalNAc ASOs. **a,** Schematic of study design for panel b-e. **b,** Blood glucose levels**. c,** Plasma triglyceride (TG) levels. **d,** Plasma APOC3. **e,** Plasma IL-18. Blood glucose was measured via a glucose meter. Plasma triglyceride levels were measured via colorimetric assay. Plasma APOC3 and IL-18 levels were measured via ELISA. **f-h,** Plasma samples collected from hAPOC3 transgenic mice treated with two different human APOC3 siRNAs were measured via ELISA. **f,** Plasma hAPOC3. **g,** Plasma TGs. **h,** Plasma IL-18**.** Control GalNAc ASO did not affect plasma TG, APOC3, or IL-18 levels. Data show means ± SEM (n=12, 12, 15, 15 individual mice in b and e; n=12, 12, 14, 15 in c; n=10, 15, 12, 12 in d) and (n=4 and n=7 individual mice for APOC3 siRNA 1 and siRNA 2 in f-h, except n=6 for t=14 for siRNA 2 in h); two-way ANOVA followed by Tukey multiple comparisons tests vs day 0. Outliers were removed based on robust regression and outlier removal method with Q=0.1%; (0, 0; 1, 0) datapoint was removed in c; (2, 0; 0, 3) datapoints in d; and (0,0,0; 0,0,1) datapoints in h. Panel a was created by BioRender.com

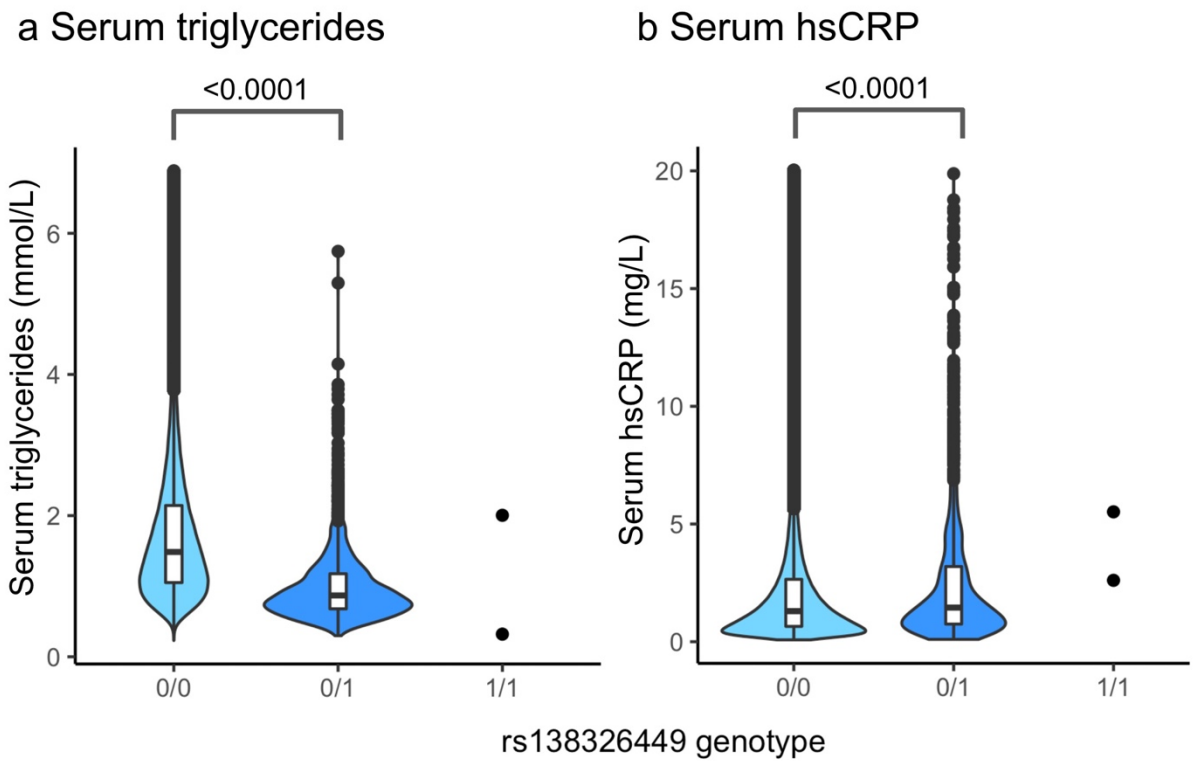

Figure 23: Distribution and density of serum triglyceride and high sensitivity C-reactive protein (hsCRP) values by *APOC3* rs138326449 genotype in the UK Biobank.

Unadjusted serum levels of **a**, triglycerides (n=430,833) and **b**, hsCRP (n=426,774) among UK Biobank carriers of 0, 1 or 2 alternative (A) alleles of the *APOC3* loss-of-function variant rs138326449 (IVS2 + 1G-A). Specifically, 0/0 indicates homozygosity of the reference (G) allele, 0/1 indicates heterozygosity and 1/1 indicates homozygosity of the alternative (A) allele. The data are shown in box-and-whisker plots (the bound of the box extends from the 25th to 75th percentiles and the whisker covers the minima and maxima) with the median marked by a center line, remaining distribution and kernel density estimations of each trait (outlier values ± 5 standard deviations from the mean were removed). Compared with rs138326449-G homozygotes, rs138326449-A heterozygotes demonstrate a 0.62 mmol/L decrease in median triglycerides ($p = <2.00 \times 10^{-16}$ by one-way ANOVA) and a 0.16 mg/L increase in median hsCRP ($p = 1.54 \times 10^{-5}$ by one-way ANOVA).

Table 9: Associations between *APOC3* rs138326449 and serum triglycerides, high-sensitivity C-reactive protein, and myocardial infarction were evaluated in UK Biobank participants.

Analyses were performed under an additive model in GloWGR and adjusted for participant age, genetic sex, genotyping batch, assessment center, and the first ten principal components of genetic ancestry. A linear regression model was used to test associations between rs138326449 and quantitative traits (serum triglycerides and serum high-sensitivity C-reactive protein) and a logistic regression model was used to test the association between rs138326449 and the binary trait (myocardial infarction). The p value for triglycerides (<4.90E-324) represents the system minimum floating-point value, indicating that the true p value is lower than this value. The p values presented in the table have not been adjusted for multiple comparisons.

rsID	Consequence	MAF	Serum Triglycerides (n=430,833)		Serum High-Sensitivity C-Reactive Protein (n=426,774)		Myocardial Infarction (n=20,851)	
			p value	beta (95% CI)	p value	beta (95% CI)	p value	OR (95% CI)
rs138326449	APOC3 Splice Donor Variant (IVS2 + 1G-A)	0.002	<4.90E-324	-0.224 (-0.234, -0.215)	1.75E-07	0.051 (0.032, 0.070)	0.025	0.765 (0.602, 0.971)

Table 10: Conditioned *APOC3* rs138326449 high-sensitivity C-reactive protein (hsCRP) associations in the UK Biobank.

Associations between rs138326449 and hsCRP with and without adjustment for potential confounders present at the time of serum sample ascertainment. All analyses were performed under an additive linear regression model in GloWGR and adjusted for participant age, genetic sex, genotyping batch, assessment center, and the first ten principal components of genetic ancestry (Standard Covariates), with the addition of a covariate indicating either the use of lipid-lowering medication (Lipid Rx) or diabetes (D). The p-values presented in the table have not been adjusted for multiple comparisons.

rsID	Consequence	MAF	Serum hsCRP [Standard Covariates] (n=426,774)		Serum hsCRP [Standard Covariates + Lipid Rx] (n=426,774)		Serum hsCRP [Standard Covariates + D] (n=426,774)	
			p value	beta (95% CI)	p value	beta (95% CI)	p value	beta (95% CI)
rs138326449	APOC3 Splice Donor Variant (IVS2 + 1G-A)	0.002	1.75E-07	0.051 (0.032, 0.070)	8.29E-08	0.052 (0.033, 0.071)	1.25E-07	0.051 (0.032, 0.070)

Chapter 4 : Summary, Study Strengths and Weaknesses, and Future Directions

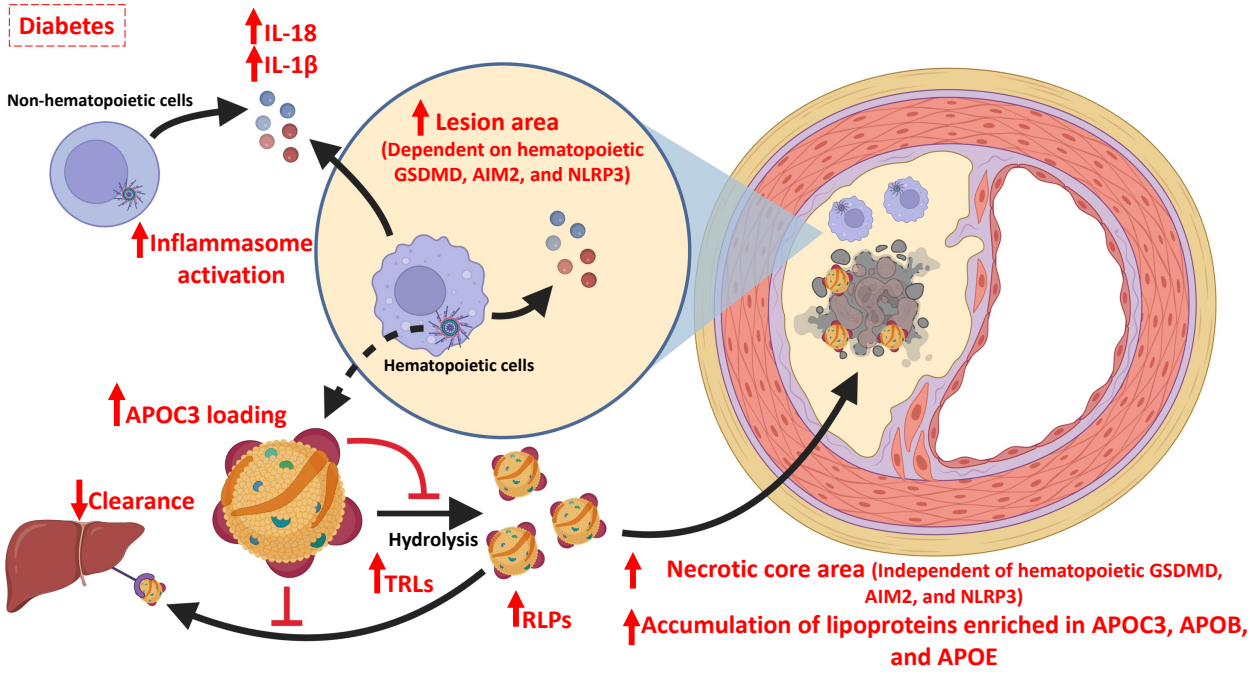

Figure 24: Graphical summary of the dissertation

4.1 Diabetes exacerbates atherosclerosis via inflammasome- and APOC3-dependent pathways.

The current work has provided strong evidence that diabetes can accelerate atherosclerosis progression through inflammasome- and APOC3-dependent pathways, where the two pathways affect atherosclerotic lesion morphology differently (**Fig. 24**). The inflammasome-dependent pathways affect lesion area progression, and the APOC3-dependent pathway affects the necrotic core expansion under diabetes conditions. Although the mediator of inflammasome activation under diabetes conditions remains largely unknown, Chapter 2 provided evidence that hematopoietic inflammasome activation is, at least in part, responsible for lesion area progression under diabetic conditions. Interestingly, hematopoietic deletion of NLRP3, AIM2, or GSDMD caused smaller atherosclerotic lesions in diabetic mice without reducing circulating levels of IL-18 and IL-1β. These findings suggest that hematopoietic inflammasome activation has the ability to promote atherogenesis via pathways independent of circulating levels of IL-18 and IL-1β. However, the proatherogenic effect of hematopoietic inflammasome activation is limited to lesion area progression; suggesting diabetes promotes necrotic core expansion via an alternative pathway.

The association between increased necrotic core area and lesional accumulation of lipoproteins enriched in APOC3 suggests that diabetes likely accelerates necrotic core expansion via the APOC3-associated pathway. APOC3 has been shown to promote necrotic core expansion in a mouse model of T1D (15), but the underlying mechanism remained largely unknown. The work described in Chapter 3 provided evidence that APOC3 induces inflammasome activation only in its delipidated form, suggesting that APOC3 exacerbates the necrotic core expansion via reduced clearance of circulating TRLs and RLPs and not via inflammasome activation. This is

consistent with an increased lesional accumulation of lipoproteins enriched in APOB and APOE in diabetic mice.

Interestingly, the current work also provides evidence suggesting that the hematopoietic NLRP3 inflammasome might contribute to the regulation of circulating APOC3 levels because diabetic mice with hematopoietic NLRP3-deficiency exhibited lower plasma APOC3 levels. Although the exact mechanism remains unexplored, it is possible that hematopoietic inflammasome activation in the liver regulates APOC3 secretion and/or clearance; highlighting the many points of crosstalk between inflammation and lipid metabolism. Furthermore, the current work also emphasizes the importance of the lesional environment in promoting atherogenesis under diabetes conditions. Although hematopoietic NLRP3 deficiency modestly reduced circulating levels of APOC3 in diabetic mice, neither lesional APOC3 accumulation nor necrotic core expansion were suppressed. It is possible that delipidated APOC3 can induce lesional inflammasome activation and promote atherogenesis via a feedforward loop, however, the methods used in the current work do not have enough resolution to differentiate between lipidated and delipidated APOC3 in the lesion.

Together, the thesis work provided valuable insights into the roles of hematopoietic inflammasome activation and APOC3 in diabetes-associated atherosclerosis. Despite the current work being largely conducted in mouse models of T1D, the findings suggest that inhibiting both inflammasome and APOC3 pathways may provide novel therapeutics for reducing CVD risk in individuals with diabetes.

4.2 Study Strengths and Weaknesses

The major strength of the current work is the use of multiple genetically modified mouse models for the investigation of the role of different diabetes-associated CVD risk factors. Our

studies used mice with hematopoietic GSDMD-, NLRP3-, and AIM2-deficiencies to provide strong evidence that the hematopoietic compartment contributes to diabetes-associated atherosclerotic lesion progression via NLRP3 and AIM2 inflammasome pathways. Importantly, the findings were consistent among mice with different components of the inflammasome pathway deleted, either GSDMD- or upstream NLRP3- and AIM2-deficiency. Our work also suggests that diabetes increases plasma levels of IL-18 and IL-1β largely independent of these hematopoietic inflammasome components. Not only did our experiments provide mechanistic insights into the role of inflammasome in diabetes-associated atherosclerosis, but they also included critical control studies that facilitated data interpretation. For example, considering that one of our models of diabetes is a virus-induced model of T1D, the inclusion of a virus control group demonstrated that the phenotypes we observed were due to diabetes and were not replicated by the virus in the absence of diabetes.

Besides providing novel mechanistic insights based on mouse models, the work included in this dissertation includes studies that provide human relevance. Thus, our experiments incorporated studies that utilized lipid particle mimics, or SUVs, to simulate the effects of APOC3 at different lipidation states. Since circulating APOC3 is mostly lipid-bound in humans with T1D, studies on the role of lipidated APOC3 will better mimic the role of APOC3 in humans in future research. In addition, this work further provides human relevance by including studies with human plasma, monocytes, and genomic data.

Nevertheless, despite current work providing strong evidence that diabetes promotes atherogenesis via inflammasome- and APOC3-dependent pathways, the in vivo mechanistic studies were conducted only in mouse models of T1D. T2D accounts for 90-95% of the total diabetes cases in humans. Future studies on mouse models of T2D will therefore be important.

Furthermore, the projects described in this dissertation focus heavily on the use of knockout mouse models in investigating the roles of hematopoietic inflammasome compartment in diabetes-associated atherosclerosis. Providing evidence that activation of hematopoietic inflammasomes (e.g., in overexpression models) promotes diabetes-associated atherosclerosis progression would further strengthen the findings of the current work. We also provided evidence that the hematopoietic inflammasome compartment does not contribute significantly to plasma levels of IL-18 and IL-1β; however, this conclusion was based on knockout experiments as well. A reciprocal experiment, in which GSDMD-deficient mice receive wildtype bone marrow cells, would provide more insights into the relationship between the hematopoietic inflammasome compartment and circulating levels of IL-18 and IL-1β. The human relevance of our findings related to inflammasome activation in diabetes would be strengthened by including studies that involve human plasma or cells from humans with diabetes.

Although the research described includes studies that support human relevance of our APOC3 findings, the APOC3 study would benefit from more mechanistic studies. Our work shows delipidated APOC3 does not lead to inflammasome activation in isolated human monocytes, but how lipidation affects other potential effects of APOC3 in monocytes or other cell types, such as cells in lesions of atherosclerosis, remains unknown. Although challenging, studies that can provide insights into whether de-lipidated APOC3 exists in human atherosclerotic lesions would begin to address this question.

4.3 How does diabetes alter the cellular landscape in lesions?

Although the current work provided strong evidence that diabetes promotes atherogenesis via inflammasome- and APOC3-dependent pathways, we have yet to understand how diabetes alters lesional immune cells. Diabetes has been shown to promote necrotic core expansion and

macrophage death in humans (44), but how macrophages or other immune cells contribute to necrotic core expansion remains largely unknown. To investigate how diabetes alters lesional immune cells, we aim to perform single-cell RNA sequencing on lesional immune cells ($CD45^+$, a pan-leukocyte marker) from our mouse model of T1D-accelerated atherosclerosis (**Fig. 25**). This mouse model has increased necrotic core area without changes in the lesion area (15; 66), which mimics the lesion morphology reported in humans with diabetes (44). The findings from the single-cell RNA sequencing analysis will help identify potential mechanistic pathways involved in the promotion of necrotic core expansion under diabetes conditions.

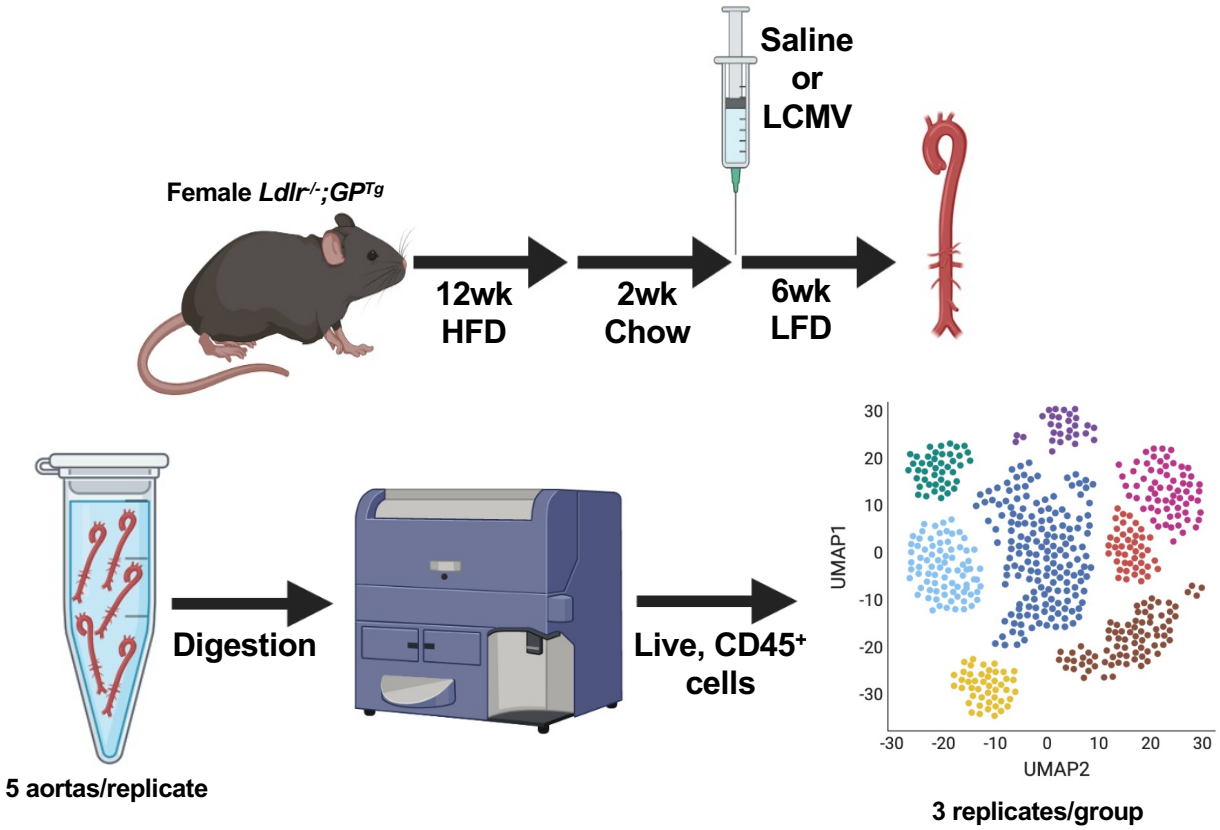

Figure 25: Schematic of the proposed research plan

Female *Ldlr*$^{-/-}$*;GP*^{Tg} mice will be maintained on a high-fat diet (HFD) for 12 weeks to allow the formation of pre-existing lesions. The mice will be switched to chow for 2 weeks before being rendered diabetic with lymphocytic choriomeningitis virus (LCMV). Saline will be used as a control (non-diabetic, ND). After the onset of diabetes, the animals will be switched to a low-fat, semipurified diet with no added cholesterol (LFD) and maintained for 6 weeks. The aorta will be collected after termination and digested before sorting. Live, CD45^{+}cells will be sorted for single-cell RNA sequencing analysis.

Bibliography

1. Ross R: Atherosclerosis--an inflammatory disease. N Engl J Med 1999;340:115-126

2. Tsao CW, Aday AW, Almarzooq ZI, Alonso A, Beaton AZ, Bittencourt MS, Boehme AK, Buxton AE, Carson AP, Commodore-Mensah Y, Elkind MSV, Evenson KR, Eze-Nliam C, Ferguson JF, Generoso G, Ho JE, Kalani R, Khan SS, Kissela BM, Knutson KL, Levine DA, Lewis TT, Liu J, Loop MS, Ma J, Mussolino ME, Navaneethan SD, Perak AM, Poudel R, Rezk-Hanna M, Roth GA, Schroeder EB, Shah SH, Thacker EL, VanWagner LB, Virani SS, Voecks JH, Wang NY, Yaffe K, Martin SS: Heart Disease and Stroke Statistics-2022 Update: A Report From the American Heart Association. Circulation 2022;145:e153-e639

3. Moore KJ, Tabas I: Macrophages in the pathogenesis of atherosclerosis. Cell 2011;145:341-355

4. Skalen K, Gustafsson M, Rydberg EK, Hulten LM, Wiklund O, Innerarity TL, Boren J: Subendothelial retention of atherogenic lipoproteins in early atherosclerosis. Nature 2002;417:750-754

5. Libby P, Buring JE, Badimon L, Hansson GK, Deanfield J, Bittencourt MS, Tokgozoglu L, Lewis EF: Atherosclerosis. Nat Rev Dis Primers 2019;5:56

6. Yurdagul A, Jr., Subramanian M, Wang X, Crown SB, Ilkayeva OR, Darville L, Kolluru GK, Rymond CC, Gerlach BD, Zheng Z, Kuriakose G, Kevil CG, Koomen JM, Cleveland JL, Muoio DM, Tabas I: Macrophage Metabolism of Apoptotic Cell-Derived Arginine Promotes Continual Efferocytosis and Resolution of Injury. Cell Metab 2020;31:518-533 e510

7. Yurdagul A, Jr., Doran AC, Cai B, Fredman G, Tabas IA: Mechanisms and Consequences of Defective Efferocytosis in Atherosclerosis. Front Cardiovasc Med 2017;4:86

8. Laakso M, Kuusisto J: Insulin resistance and hyperglycaemia in cardiovascular disease development. Nat Rev Endocrinol 2014;10:293-302

9. Rawshani A, Rawshani A, Franzen S, Eliasson B, Svensson AM, Miftaraj M, McGuire DK, Sattar N, Rosengren A, Gudbjornsdottir S: Mortality and Cardiovascular Disease in Type 1 and Type 2 Diabetes. N Engl J Med 2017;376:1407-1418

10. Mills EJ, Rachlis B, Wu P, Devereaux PJ, Arora P, Perri D: Primary prevention of cardiovascular mortality and events with statin treatments: a network meta-analysis involving more than 65,000 patients. J Am Coll Cardiol 2008;52:1769-1781

11. Matsuura Y, Kanter JE, Bornfeldt KE: Highlighting Residual Atherosclerotic Cardiovascular Disease Risk. Arterioscler Thromb Vasc Biol 2019;39:e1-e9

12. Zhao Y, Xiang P, Coll B, Lopez JAG, Wong ND: Diabetes associated residual atherosclerotic cardiovascular risk in statin-treated patients with prior atherosclerotic cardiovascular disease. J Diabetes Complications 2021;35:107767

13. Chait A, Ginsberg HN, Vaisar T, Heinecke JW, Goldberg IJ, Bornfeldt KE: Remnants of the Triglyceride-Rich Lipoproteins, Diabetes, and Cardiovascular Disease. Diabetes 2020;69:508-516

14. Nishikawa T, Edelstein D, Du XL, Yamagishi S, Matsumura T, Kaneda Y, Yorek MA, Beebe D, Oates PJ, Hammes HP, Giardino I, Brownlee M: Normalizing mitochondrial superoxide production blocks three pathways of hyperglycaemic damage. Nature 2000;404:787-790

15. Kanter JE, Shao B, Kramer F, Barnhart S, Shimizu-Albergine M, Vaisar T, Graham MJ, Crooke RM, Manuel CR, Haeusler RA, Mar D, Bomsztyk K, Hokanson JE, Kinney GL, Snell-Bergeon JK, Heinecke JW, Bornfeldt KE: Increased apolipoprotein C3 drives cardiovascular risk in type 1 diabetes. J Clin Invest 2019;129:4165-4179

16. Sharma A, Choi JSY, Stefanovic N, Al-Sharea A, Simpson DS, Mukhamedova N, Jandeleit-Dahm K, Murphy AJ, Sviridov D, Vince JE, Ritchie RH, de Haan JB: Specific NLRP3 Inhibition Protects Against Diabetes-Associated Atherosclerosis. Diabetes 2021;70:772-787

17. Kanter JE, Hsu CC, Bornfeldt KE: Monocytes and Macrophages as Protagonists in Vascular Complications of Diabetes. Front Cardiovasc Med 2020;7:10

18. American Diabetes A: 2. Classification and Diagnosis of Diabetes: Standards of Medical Care in Diabetes-2021. Diabetes Care 2021;44:S15-S33

19. Hirano T: Pathophysiology of Diabetic Dyslipidemia. J Atheroscler Thromb 2018;25:771-782

20. Verges B: Pathophysiology of diabetic dyslipidaemia: where are we? Diabetologia 2015;58:886-899

21. Eckel RH, Bornfeldt KE, Goldberg IJ: Cardiovascular disease in diabetes, beyond glucose. Cell Metab 2021;33:1519-1545

22. Nathan DM, Cleary PA, Backlund JY, Genuth SM, Lachin JM, Orchard TJ, Raskin P, Zinman B, Diabetes C, Complications Trial/Epidemiology of Diabetes I, Complications Study Research G: Intensive diabetes treatment and cardiovascular disease in patients with type 1 diabetes. N Engl J Med 2005;353:2643-2653

23. Diabetes Control and Complications Trial (DCCT)/Epidemiology of Diabetes Interventions and Complications (EDIC) Study Research Group: Mortality in Type 1 Diabetes in the DCCT/EDIC Versus the General Population. Diabetes Care 2016;39:1378-1383

24. Nathan DM, Group DER: The diabetes control and complications trial/epidemiology of diabetes interventions and complications study at 30 years: overview. Diabetes Care 2014;37:9-16

25. Ninomiya T, Perkovic V, de Galan BE, Zoungas S, Pillai A, Jardine M, Patel A, Cass A, Neal B, Poulter N, Mogensen CE, Cooper M, Marre M, Williams B, Hamet P, Mancia G, Woodward

M, Macmahon S, Chalmers J, Group AC: Albuminuria and kidney function independently predict cardiovascular and renal outcomes in diabetes. J Am Soc Nephrol 2009;20:1813-1821

26. Zoungas S, Chalmers J, Neal B, Billot L, Li Q, Hirakawa Y, Arima H, Monaghan H, Joshi R, Colagiuri S, Cooper ME, Glasziou P, Grobbee D, Hamet P, Harrap S, Heller S, Lisheng L, Mancia G, Marre M, Matthews DR, Mogensen CE, Perkovic V, Poulter N, Rodgers A, Williams B, MacMahon S, Patel A, Woodward M, Group A-OC: Follow-up of blood-pressure lowering and glucose control in type 2 diabetes. N Engl J Med 2014;371:1392-1406

27. Parhofer KG, Laufs U: The Diagnosis and Treatment of Hypertriglyceridemia. Dtsch Arztebl Int 2019;116:825-832

28. Ference BA, Kastelein JJP, Ray KK, Ginsberg HN, Chapman MJ, Packard CJ, Laufs U, Oliver-Williams C, Wood AM, Butterworth AS, Di Angelantonio E, Danesh J, Nicholls SJ, Bhatt DL, Sabatine MS, Catapano AL: Association of Triglyceride-Lowering LPL Variants and LDL-C-Lowering LDLR Variants With Risk of Coronary Heart Disease. JAMA 2019;321:364-373

29. Group AS, Ginsberg HN, Elam MB, Lovato LC, Crouse JR, 3rd, Leiter LA, Linz P, Friedewald WT, Buse JB, Gerstein HC, Probstfield J, Grimm RH, Ismail-Beigi F, Bigger JT, Goff DC, Jr., Cushman WC, Simons-Morton DG, Byington RP: Effects of combination lipid therapy in type 2 diabetes mellitus. N Engl J Med 2010;362:1563-1574

30. Elam MB, Ginsberg HN, Lovato LC, Corson M, Largay J, Leiter LA, Lopez C, O'Connor PJ, Sweeney ME, Weiss D, Friedewald WT, Buse JB, Gerstein HC, Probstfield J, Grimm R, Ismail-Beigi F, Goff DC, Jr., Fleg JL, Rosenberg Y, Byington RP, Investigators AS: Association of Fenofibrate Therapy With Long-term Cardiovascular Risk in Statin-Treated Patients With Type 2 Diabetes. JAMA Cardiol 2017;2:370-380

31. Das Pradhan A, Glynn RJ, Fruchart JC, MacFadyen JG, Zaharris ES, Everett BM, Campbell SE, Oshima R, Amarenco P, Blom DJ, Brinton EA, Eckel RH, Elam MB, Felicio JS, Ginsberg HN, Goudev A, Ishibashi S, Joseph J, Kodama T, Koenig W, Leiter LA, Lorenzatti AJ, Mankovsky B, Marx N, Nordestgaard BG, Pall D, Ray KK, Santos RD, Soran H, Susekov A, Tendera M, Yokote K, Paynter NP, Buring JE, Libby P, Ridker PM, Investigators P: Triglyceride Lowering with Pemafibrate to Reduce Cardiovascular Risk. N Engl J Med 2022;

32. Ginsberg HN, Packard CJ, Chapman MJ, Boren J, Aguilar-Salinas CA, Averna M, Ference BA, Gaudet D, Hegele RA, Kersten S, Lewis GF, Lichtenstein AH, Moulin P, Nordestgaard BG, Remaley AT, Staels B, Stroes ESG, Taskinen MR, Tokgozoglu LS, Tybjaerg-Hansen A, Stock JK, Catapano AL: Triglyceride-rich lipoproteins and their remnants: metabolic insights, role in atherosclerotic cardiovascular disease, and emerging therapeutic strategies-a consensus statement from the European Atherosclerosis Society. Eur Heart J 2021;42:4791-4806

33. Basu A, Bebu I, Jenkins AJ, Stoner JA, Zhang Y, Klein RL, Lopes-Virella MF, Garvey WT, Budoff MJ, Alaupovic P, Lyons TJ, Diabetes Control Complications Trial/Epidemiology of Diabetes Interventions Complications Research G: Serum apolipoproteins and apolipoprotein-defined lipoprotein subclasses: a hypothesis-generating prospective study of cardiovascular events in T1D. J Lipid Res 2019;60:1432-1439

34. Jansson Sigfrids F, Stechemesser L, Dahlstrom EH, Forsblom CM, Harjutsalo V, Weitgasser R, Taskinen MR, Groop PH, FinnDiane Study G: Apolipoprotein C-III predicts cardiovascular events and mortality in individuals with type 1 diabetes and albuminuria. J Intern Med 2022;291:338-349

35. Zewinger S, Reiser J, Jankowski V, Alansary D, Hahm E, Triem S, Klug M, Schunk SJ, Schmit D, Kramann R, Korbel C, Ampofo E, Laschke MW, Selejan SR, Paschen A, Herter T, Schuster S, Silbernagel G, Sester M, Sester U, Assmann G, Bals R, Kostner G, Jahnen-Dechent W, Menger MD, Rohrer L, Marz W, Bohm M, Jankowski J, Kopf M, Latz E, Niemeyer BA, Fliser D, Laufs U, Speer T: Apolipoprotein C3 induces inflammation and organ damage by alternative inflammasome activation. Nat Immunol 2020;21:30-41

36. Pollin TI, Damcott CM, Shen H, Ott SH, Shelton J, Horenstein RB, Post W, McLenithan JC, Bielak LF, Peyser PA, Mitchell BD, Miller M, O'Connell JR, Shuldiner AR: A null mutation in human APOC3 confers a favorable plasma lipid profile and apparent cardioprotection. Science 2008;322:1702-1705

37. Aalto-Setala K, Fisher EA, Chen X, Chajek-Shaul T, Hayek T, Zechner R, Walsh A, Ramakrishnan R, Ginsberg HN, Breslow JL: Mechanism of hypertriglyceridemia in human apolipoprotein (apo) CIII transgenic mice. Diminished very low density lipoprotein fractional catabolic rate associated with increased apo CIII and reduced apo E on the particles. J Clin Invest 1992;90:1889-1900

38. Larsson M, Allan CM, Jung RS, Heizer PJ, Beigneux AP, Young SG, Fong LG: Apolipoprotein C-III inhibits triglyceride hydrolysis by GPIHBP1-bound LPL. J Lipid Res 2017;58:1893-1902

39. Boren J, Packard CJ, Taskinen MR: The Roles of ApoC-III on the Metabolism of Triglyceride-Rich Lipoproteins in Humans. Front Endocrinol (Lausanne) 2020;11:474

40. Gordts PL, Nock R, Son NH, Ramms B, Lew I, Gonzales JC, Thacker BE, Basu D, Lee RG, Mullick AE, Graham MJ, Goldberg IJ, Crooke RM, Witztum JL, Esko JD: ApoC-III inhibits clearance of triglyceride-rich lipoproteins through LDL family receptors. J Clin Invest 2016;126:2855-2866

41. Reyes-Soffer G, Sztalryd C, Horenstein RB, Holleran S, Matveyenko A, Thomas T, Nandakumar R, Ngai C, Karmally W, Ginsberg HN, Ramakrishnan R, Pollin TI: Effects of APOC3 Heterozygous Deficiency on Plasma Lipid and Lipoprotein Metabolism. Arterioscler Thromb Vasc Biol 2019;39:63-72

42. Gaudet D, Brisson D, Tremblay K, Alexander VJ, Singleton W, Hughes SG, Geary RS, Baker BF, Graham MJ, Crooke RM, Witztum JL: Targeting APOC3 in the familial chylomicronemia syndrome. N Engl J Med 2014;371:2200-2206

43. Breyer ED, Le NA, Li X, Martinson D, Brown WV: Apolipoprotein C-III displacement of apolipoprotein E from VLDL: effect of particle size. J Lipid Res 1999;40:1875-1882

44. Burke AP, Kolodgie FD, Zieske A, Fowler DR, Weber DK, Varghese PJ, Farb A, Virmani R: Morphologic findings of coronary atherosclerotic plaques in diabetics: a postmortem study. Arterioscler Thromb Vasc Biol 2004;24:1266-1271

45. Lee HM, Kim JJ, Kim HJ, Shong M, Ku BJ, Jo EK: Upregulated NLRP3 inflammasome activation in patients with type 2 diabetes. Diabetes 2013;62:194-204

46. Bradshaw EM, Raddassi K, Elyaman W, Orban T, Gottlieb PA, Kent SC, Hafler DA: Monocytes from patients with type 1 diabetes spontaneously secrete proinflammatory cytokines inducing Th17 cells. J Immunol 2009;183:4432-4439

47. Yeboah J, McClelland RL, Polonsky TS, Burke GL, Sibley CT, O'Leary D, Carr JJ, Goff DC, Greenland P, Herrington DM: Comparison of novel risk markers for improvement in cardiovascular risk assessment in intermediate-risk individuals. JAMA 2012;308:788-795

48. King DE, Mainous AG, 3rd, Buchanan TA, Pearson WS: C-reactive protein and glycemic control in adults with diabetes. Diabetes Care 2003;26:1535-1539

49. Svensson E, Mor A, Rungby J, Berencsi K, Nielsen JS, Stidsen JV, Friborg S, Brandslund I, Christiansen JS, Beck-Nielsen H, Sorensen HT, Thomsen RW: Lifestyle and clinical factors associated with elevated C-reactive protein among newly diagnosed Type 2 diabetes mellitus patients: a cross-sectional study from the nationwide DD2 cohort. BMC Endocr Disord 2014;14:74

50. Soinio M, Marniemi J, Laakso M, Lehto S, Ronnemaa T: High-sensitivity C-reactive protein and coronary heart disease mortality in patients with type 2 diabetes: a 7-year follow-up study. Diabetes Care 2006;29:329-333

51. Berkley A, Ferro A: Changes in C-reactive protein in response to anti-inflammatory therapy as a predictor of cardiovascular outcomes: A systematic review and meta-analysis. JRSM Cardiovasc Dis 2020;9:2048004020929235

52. Ridker PM, Everett BM, Pradhan A, MacFadyen JG, Solomon DH, Zaharris E, Mam V, Hasan A, Rosenberg Y, Iturriaga E, Gupta M, Tsigoulis M, Verma S, Clearfield M, Libby P, Goldhaber SZ, Seagle R, Ofori C, Saklayen M, Butman S, Singh N, Le May M, Bertrand O, Johnston J, Paynter NP, Glynn RJ, Investigators C: Low-Dose Methotrexate for the Prevention of Atherosclerotic Events. N Engl J Med 2019;380:752-762

53. Ridker PM, Everett BM, Thuren T, MacFadyen JG, Chang WH, Ballantyne C, Fonseca F, Nicolau J, Koenig W, Anker SD, Kastelein JJP, Cornel JH, Pais P, Pella D, Genest J, Cifkova R, Lorenzatti A, Forster T, Kobalava Z, Vida-Simiti L, Flather M, Shimokawa H, Ogawa H, Dellborg M, Rossi PRF, Troquay RPT, Libby P, Glynn RJ, Group CT: Antiinflammatory Therapy with Canakinumab for Atherosclerotic Disease. N Engl J Med 2017;377:1119-1131

54. Everett BM, Donath MY, Pradhan AD, Thuren T, Pais P, Nicolau JC, Glynn RJ, Libby P, Ridker PM: Anti-Inflammatory Therapy With Canakinumab for the Prevention and Management of Diabetes. J Am Coll Cardiol 2018;71:2392-2401

55. Ridker PM, MacFadyen JG, Everett BM, Libby P, Thuren T, Glynn RJ, Group CT: Relationship of C-reactive protein reduction to cardiovascular event reduction following treatment with canakinumab: a secondary analysis from the CANTOS randomised controlled trial. Lancet 2018;391:319-328

56. Nidorf SM, Fiolet ATL, Mosterd A, Eikelboom JW, Schut A, Opstal TSJ, The SHK, Xu XF, Ireland MA, Lenderink T, Latchem D, Hoogslag P, Jerzewski A, Nierop P, Whelan A, Hendriks R, Swart H, Schaap J, Kuijper AFM, van Hessen MWJ, Saklani P, Tan I, Thompson AG, Morton A, Judkins C, Bax WA, Dirksen M, Alings M, Hankey GJ, Budgeon CA, Tijssen JGP, Cornel JH, Thompson PL, LoDoCo2 Trial I: Colchicine in Patients with Chronic Coronary Disease. N Engl J Med 2020;383:1838-1847

57. Mohammadnia N, Los J, Opstal TSJ, Fiolet ATL, Eikelboom JW, Mosterd A, Nidorf SM, Budgeon CA, Tijssen JGP, Thompson PL, Tack CJ, Simsek S, Bax WA, Cornel JH, El Messaoudi S: The effects of colchicine in patients with diabetes mellitus and chronic coronary artery disease: a post-hoc analysis of the LoDoCo2-trial. European Heart Journal 2022;43

58. LaRock CN, Cookson BT: Burning down the house: cellular actions during pyroptosis. PLoS Pathog 2013;9:e1003793

59. Karasawa T, Takahashi M: Role of NLRP3 Inflammasomes in Atherosclerosis. J Atheroscler Thromb 2017;24:443-451

60. Zhu J, Wu S, Hu S, Li H, Li M, Geng X, Wang H: NLRP3 inflammasome expression in peripheral blood monocytes of coronary heart disease patients and its modulation by rosuvastatin. Mol Med Rep 2019;20:1826-1836

61. Duewell P, Kono H, Rayner KJ, Sirois CM, Vladimer G, Bauernfeind FG, Abela GS, Franchi L, Nunez G, Schnurr M, Espevik T, Lien E, Fitzgerald KA, Rock KL, Moore KJ, Wright SD, Hornung V, Latz E: NLRP3 inflammasomes are required for atherogenesis and activated by cholesterol crystals. Nature 2010;464:1357-1361

62. Hendrikx T, Jeurissen ML, van Gorp PJ, Gijbels MJ, Walenbergh SM, Houben T, van Gorp R, Pottgens CC, Stienstra R, Netea MG, Hofker MH, Donners MM, Shiri-Sverdlov R: Bone marrow-specific caspase-1/11 deficiency inhibits atherosclerosis development in Ldlr(-/-) mice. FEBS J 2015;282:2327-2338

63. Janoudi A, Shamoun FE, Kalavakunta JK, Abela GS: Cholesterol crystal induced arterial inflammation and destabilization of atherosclerotic plaque. Eur Heart J 2016;37:1959-1967

64. Liu W, Yin Y, Zhou Z, He M, Dai Y: OxLDL-induced IL-1 beta secretion promoting foam cells formation was mainly via CD36 mediated ROS production leading to NLRP3 inflammasome activation. Inflamm Res 2014;63:33-43

65. Sheedy FJ, Grebe A, Rayner KJ, Kalantari P, Ramkhelawon B, Carpenter SB, Becker CE, Ediriweera HN, Mullick AE, Golenbock DT, Stuart LM, Latz E, Fitzgerald KA, Moore KJ: CD36 coordinates NLRP3 inflammasome activation by facilitating intracellular nucleation of soluble ligands into particulate ligands in sterile inflammation. Nat Immunol 2013;14:812-820

66. Hsu CC, Fidler TP, Kanter JE, Kothari V, Kramer F, Tang J, Tall AR, Bornfeldt KE: Hematopoietic NLRP3 and AIM2 Inflammasomes Promote Diabetes-Accelerated Atherosclerosis, but Increased Necrosis Is Independent of Pyroptosis. Diabetes 2023;72:999-1011

67. Virani SS, Alonso A, Aparicio HJ, Benjamin EJ, Bittencourt MS, Callaway CW, Carson AP, Chamberlain AM, Cheng S, Delling FN, Elkind MSV, Evenson KR, Ferguson JF, Gupta DK, Khan SS, Kissela BM, Knutson KL, Lee CD, Lewis TT, Liu J, Loop MS, Lutsey PL, Ma J, Mackey J, Martin SS, Matchar DB, Mussolino ME, Navaneethan SD, Perak AM, Roth GA, Samad Z, Satou GM, Schroeder EB, Shah SH, Shay CM, Stokes A, VanWagner LB, Wang NY, Tsao CW, American Heart Association Council on E, Prevention Statistics C, Stroke Statistics S: Heart Disease and Stroke Statistics-2021 Update: A Report From the American Heart Association. Circulation 2021;143:e254-e743

68. CDC: National Diabetes Statistics Report, 2020. Atlanta, GA: Centers for Disease Control and Prevention, US Dept of Health and Human Services 2020;

69. Bornfeldt KE: The Remnant Lipoprotein Hypothesis of Diabetes-Associated Cardiovascular Disease. Arterioscler Thromb Vasc Biol 2022;42:819-830

70. Tall AR, Thomas DG, Gonzalez-Cabodevilla AG, Goldberg IJ: Addressing dyslipidemic risk beyond LDL-cholesterol. J Clin Invest 2022;132

71. Bentzon JF, Otsuka F, Virmani R, Falk E: Mechanisms of plaque formation and rupture. Circ Res 2014;114:1852-1866

72. Hsu CC, Shao B, Kanter JE, He Y, Vaisar T, Witztum JL, Snell-Bergeon J, McInnes G, Bruse S, Gottesman O, Mullick AE, Bornfeldt KE: Apolipoprotein C3 induces inflammasome activation only in its delipidated form. Nat Immunol 2023;24:408-411

73. Henriksbo BD, Lau TC, Cavallari JF, Denou E, Chi W, Lally JS, Crane JD, Duggan BM, Foley KP, Fullerton MD, Tarnopolsky MA, Steinberg GR, Schertzer JD: Fluvastatin causes NLRP3 inflammasome-mediated adipose insulin resistance. Diabetes 2014;63:3742-3747

74. Henriksbo BD, Tamrakar AK, Xu J, Duggan BM, Cavallari JF, Phulka J, Stampfli MR, Ashkar AA, Schertzer JD: Statins Promote Interleukin-1beta-Dependent Adipocyte Insulin Resistance Through Lower Prenylation, Not Cholesterol. Diabetes 2019;68:1441-1448

75. Westerterp M, Fotakis P, Ouimet M, Bochem AE, Zhang H, Molusky MM, Wang W, Abramowicz S, la Bastide-van Gemert S, Wang N, Welch CL, Reilly MP, Stroes ES, Moore KJ, Tall AR: Cholesterol Efflux Pathways Suppress Inflammasome Activation, NETosis, and Atherogenesis. Circulation 2018;138:898-912

76. Tumurkhuu G, Shimada K, Dagvadorj J, Crother TR, Zhang W, Luthringer D, Gottlieb RA, Chen S, Arditi M: Ogg1-Dependent DNA Repair Regulates NLRP3 Inflammasome and Prevents Atherosclerosis. Circ Res 2016;119:e76-90

77. Zhang X, McDonald JG, Aryal B, Canfran-Duque A, Goldberg EL, Araldi E, Ding W, Fan Y, Thompson BM, Singh AK, Li Q, Tellides G, Ordovas-Montanes J, Garcia Milian R, Dixit VD, Ikonen E, Suarez Y, Fernandez-Hernando C: Desmosterol suppresses macrophage inflammasome activation and protects against vascular inflammation and atherosclerosis. Proc Natl Acad Sci U S A 2021;118

78. Fidler TP, Xue C, Yalcinkaya M, Hardaway B, Abramowicz S, Xiao T, Liu W, Thomas DG, Hajebrahimi MA, Pircher J, Silvestre-Roig C, Kotini AG, Luchsinger LL, Wei Y, Westerterp M, Snoeck HW, Papapetrou EP, Schulz C, Massberg S, Soehnlein O, Ebert B, Levine RL, Reilly MP, Libby P, Wang N, Tall AR: The AIM2 inflammasome exacerbates atherosclerosis in clonal haematopoiesis. Nature 2021;592:296-301

79. Puylaert P, Zurek M, Rayner KJ, De Meyer GRY, Martinet W: Regulated Necrosis in Atherosclerosis. Arterioscler Thromb Vasc Biol 2022;42:1283-1306

80. Opoku E, Traughber CA, Zhang D, Iacano AJ, Khan M, Han J, Smith JD, Gulshan K: Gasdermin D Mediates Inflammation-Induced Defects in Reverse Cholesterol Transport and Promotes Atherosclerosis. Front Cell Dev Biol 2021;9:715211

81. Renard CB, Kramer F, Johansson F, Lamharzi N, Tannock LR, von Herrath MG, Chait A, Bornfeldt KE: Diabetes and diabetes-associated lipid abnormalities have distinct effects on initiation and progression of atherosclerotic lesions. J Clin Invest 2004;114:659-668

82. Chen S, Markman JL, Shimada K, Crother TR, Lane M, Abolhesn A, Shah PK, Arditi M: Sex-Specific Effects of the Nlrp3 Inflammasome on Atherogenesis in LDL Receptor-Deficient Mice. JACC Basic Transl Sci 2020;5:582-598

83. Kayagaki N, Stowe IB, Lee BL, O'Rourke K, Anderson K, Warming S, Cuellar T, Haley B, Roose-Girma M, Phung QT, Liu PS, Lill JR, Li H, Wu J, Kummerfeld S, Zhang J, Lee WP, Snipas SJ, Salvesen GS, Morris LX, Fitzgerald L, Zhang Y, Bertram EM, Goodnow CC, Dixit VM: Caspase-11 cleaves gasdermin D for non-canonical inflammasome signalling. Nature 2015;526:666-671

84. Shimizu-Albergine M, Basu D, Kanter JE, Kramer F, Kothari V, Barnhart S, Thornock C, Mullick AE, Clouet-Foraison N, Vaisar T, Heinecke JW, Hegele RA, Goldberg IJ, Bornfeldt KE: CREBH normalizes dyslipidemia and halts atherosclerosis in diabetes by decreasing circulating remnant lipoproteins. J Clin Invest 2021;131

85. Subramanian S, Han CY, Chiba T, McMillen TS, Wang SA, Haw A, 3rd, Kirk EA, O'Brien KD, Chait A: Dietary cholesterol worsens adipose tissue macrophage accumulation and atherosclerosis in obese LDL receptor-deficient mice. Arterioscler Thromb Vasc Biol 2008;28:685-691

86. Stary HC, Chandler AB, Dinsmore RE, Fuster V, Glagov S, Insull W, Jr., Rosenfeld ME, Schwartz CJ, Wagner WD, Wissler RW: A definition of advanced types of atherosclerotic lesions and a histological classification of atherosclerosis. A report from the Committee on Vascular Lesions of the Council on Arteriosclerosis, American Heart Association. Circulation 1995;92:1355-1374

87. Nagareddy PR, Murphy AJ, Stirzaker RA, Hu Y, Yu S, Miller RG, Ramkhelawon B, Distel E, Westerterp M, Huang LS, Schmidt AM, Orchard TJ, Fisher EA, Tall AR, Goldberg IJ: Hyperglycemia promotes myelopoiesis and impairs the resolution of atherosclerosis. Cell Metab 2013;17:695-708

88. Swirski FK, Libby P, Aikawa E, Alcaide P, Luscinskas FW, Weissleder R, Pittet MJ: Ly-6Chi monocytes dominate hypercholesterolemia-associated monocytosis and give rise to macrophages in atheromata. J Clin Invest 2007;117:195-205

89. Tonnus W, Maremonti F, Belavgeni A, Latk M, Kusunoki Y, Brucker A, von Massenhausen A, Meyer C, Locke S, Gembardt F, Beer K, Hoppenz P, Becker JU, Hugo C, Anders HJ, Bornstein SR, Shao F, Linkermann A: Gasdermin D-deficient mice are hypersensitive to acute kidney injury. Cell Death Dis 2022;13:792

90. Hu Y, Jiang Y, Li S, Ma X, Chen M, Yang R, Wen S, Moynagh PN, Wang B, Hu G, Yang S: The Gasdermin D N-terminal fragment acts as a negative feedback system to inhibit inflammasome-mediated activation of Caspase-1/11. Proc Natl Acad Sci U S A 2022;119:e2210809119

91. Tang C, Kanter JE, Bornfeldt KE, Leboeuf RC, Oram JF: Diabetes reduces the cholesterol exporter ABCA1 in mouse macrophages and kidneys. J Lipid Res 2010;51:1719-1728

92. Mauldin JP, Nagelin MH, Wojcik AJ, Srinivasan S, Skaflen MD, Ayers CR, McNamara CA, Hedrick CC: Reduced expression of ATP-binding cassette transporter G1 increases cholesterol accumulation in macrophages of patients with type 2 diabetes mellitus. Circulation 2008;117:2785-2792

93. Soehnlein O, Tall AR: AIMing 2 treat atherosclerosis. Nat Rev Cardiol 2022;19:567-568

94. Matsuura Y, Shimizu-Albergine M, Barnhart S, Kramer F, Hsu CC, Kothari V, Tang J, Gharib SA, Kanter JE, Abel ED, Tian R, Shao B, Bornfeldt KE: Diabetes Suppresses Glucose Uptake and Glycolysis in Macrophages. Circ Res 2022;130:779-781

95. Dinarello CA, Novick D, Kim S, Kaplanski G: Interleukin-18 and IL-18 binding protein. Front Immunol 2013;4:289

96. Shi J, Zhao Y, Wang K, Shi X, Wang Y, Huang H, Zhuang Y, Cai T, Wang F, Shao F: Cleavage of GSDMD by inflammatory caspases determines pyroptotic cell death. Nature 2015;526:660-665

97. Ohwada T, Sakamoto T, Suzuki S, Sugawara Y, Sakamoto K, Ikeda A, Haga F, Sato T, Nakazato K, Takeishi Y, Watanabe K: Apolipoprotein C3 and necrotic core volume are correlated but also associated with future cardiovascular events. Sci Rep 2022;12:14554

98. Van Lenten BJ, Fogelman AM, Jackson RL, Shapiro S, Haberland ME, Edwards PA: Receptor-mediated uptake of remnant lipoproteins by cholesterol-loaded human monocyte-macrophages. J Biol Chem 1985;260:8783-8788

99. Cabodevilla AG, Tang S, Lee S, Mullick AE, Aleman JO, Hussain MM, Sessa WC, Abumrad NA, Goldberg IJ: Eruptive xanthoma model reveals endothelial cells internalize and metabolize chylomicrons, leading to extravascular triglyceride accumulation. J Clin Invest 2021;131

100. Zewinger S, Reiser J, Jankowski V, Alansary D, Hahm E, Triem S, Klug M, Schunk SJ, Schmit D, Kramann R, Korbel C, Ampofo E, Laschke MW, Selejan SR, Paschen A, Herter T, Gaul S, Silbernagel G, Sester M, Sester U, Assmann G, Bals R, Kostner G, Jahnen-Dechent W, Menger MD, Rohrer L, Marz W, Bohm M, Jankowski J, Kopf M, Latz E, Niemeyer BA, Fliser D, Laufs U, Speer T: Reply to: Apolipoprotein C3 induces inflammasome activation only in its delipidated form. Nat Immunol 2023;24:412-413

101. Hsu CC, Kanter JE, Kothari V, Bornfeldt KE: Quartet of APOCs and the Different Roles They Play in Diabetes. Arterioscler Thromb Vasc Biol 2023;43:1124-1133

102. Kegulian NC, Ramms B, Horton S, Trenchevska O, Nedelkov D, Graham MJ, Lee RG, Esko JD, Yassine HN, Gordts P: ApoC-III Glycoforms Are Differentially Cleared by Hepatic TRL (Triglyceride-Rich Lipoprotein) Receptors. Arterioscler Thromb Vasc Biol 2019;39:2145-2156

103. Ooi EM, Chan DT, Watts GF, Chan DC, Ng TW, Dogra GK, Irish AB, Barrett PH: Plasma apolipoprotein C-III metabolism in patients with chronic kidney disease. J Lipid Res 2011;52:794-800

104. Adiels M, Taskinen MR, Bjornson E, Andersson L, Matikainen N, Soderlund S, Kahri J, Hakkarainen A, Lundbom N, Sihlbom C, Thorsell A, Zhou H, Pietilainen KH, Packard C, Boren J: Role of apolipoprotein C-III overproduction in diabetic dyslipidaemia. Diabetes Obes Metab 2019;21:1861-1870

105. Willecke F, Scerbo D, Nagareddy P, Obunike JC, Barrett TJ, Abdillahi ML, Trent CM, Huggins LA, Fisher EA, Drosatos K, Goldberg IJ: Lipolysis, and not hepatic lipogenesis, is the primary modulator of triglyceride levels in streptozotocin-induced diabetic mice. Arterioscler Thromb Vasc Biol 2015;35:102-110

106. Ramms B, Patel S, Sun X, Pessentheiner AR, Ducasa GM, Mullick AE, Lee RG, Crooke RM, Tsimikas S, Witztum JL, Gordts PL: Interventional hepatic apoC-III knockdown improves atherosclerotic plaque stability and remodeling by triglyceride lowering. JCI Insight 2022;7

107. Prakash TP, Yu J, Migawa MT, Kinberger GA, Wan WB, Ostergaard ME, Carty RL, Vasquez G, Low A, Chappell A, Schmidt K, Aghajan M, Crosby J, Murray HM, Booten SL, Hsiao J, Soriano A, Machemer T, Cauntay P, Burel SA, Murray SF, Gaus H, Graham MJ, Swayze EE, Seth PP: Comprehensive Structure-Activity Relationship of Triantennary N-Acetylgalactosamine Conjugated Antisense Oligonucleotides for Targeted Delivery to Hepatocytes. J Med Chem 2016;59:2718-2733

108. Reaven GM, Mondon CE, Chen YD, Breslow JL: Hypertriglyceridemic mice transgenic for the human apolipoprotein C-III gene are neither insulin resistant nor hyperinsulinemic. J Lipid Res 1994;35:820-824

109. Vaisar T, Kanter JE, Wimberger J, Irwin AD, Gauthier J, Wolfson E, Bahnam V, Wu IH, Shah H, Keenan HA, Greenbaum CJ, King GL, Heinecke JW, Bornfeldt KE: High Concentration of Medium-Sized HDL Particles and Enrichment in HDL Paraoxonase 1 Associate With Protection From Vascular Complications in People With Long-standing Type 1 Diabetes. Diabetes Care 2020;43:178-186

110. Shao B, Snell-Bergeon JK, Pyle LL, Thomas KE, de Boer IH, Kothari V, Segrest J, Davidson WS, Bornfeldt KE, Heinecke JW: Pulmonary surfactant protein B carried by HDL predicts incident CVD in patients with type 1 diabetes. J Lipid Res 2022;63:100196

111. MacLean B, Tomazela DM, Shulman N, Chambers M, Finney GL, Frewen B, Kern R, Tabb DL, Liebler DC, MacCoss MJ: Skyline: an open source document editor for creating and analyzing targeted proteomics experiments. Bioinformatics 2010;26:966-968

112. Sudlow C, Gallacher J, Allen N, Beral V, Burton P, Danesh J, Downey P, Elliott P, Green J, Landray M, Liu B, Matthews P, Ong G, Pell J, Silman A, Young A, Sprosen T, Peakman T, Collins R: UK biobank: an open access resource for identifying the causes of a wide range of complex diseases of middle and old age. PLoS Med 2015;12:e1001779

113. Das S, Forer L, Schonherr S, Sidore C, Locke AE, Kwong A, Vrieze SI, Chew EY, Levy S, McGue M, Schlessinger D, Stambolian D, Loh PR, Iacono WG, Swaroop A, Scott LJ, Cucca F, Kronenberg F, Boehnke M, Abecasis GR, Fuchsberger C: Next-generation genotype imputation service and methods. Nat Genet 2016;48:1284-1287

114. Taliun D, Harris DN, Kessler MD, Carlson J, Szpiech ZA, Torres R, Taliun SAG, Corvelo A, Gogarten SM, Kang HM, Pitsillides AN, LeFaive J, Lee SB, Tian X, Browning BL, Das S, Emde AK, Clarke WE, Loesch DP, Shetty AC, Blackwell TW, Smith AV, Wong Q, Liu X, Conomos MP, Bobo DM, Aguet F, Albert C, Alonso A, Ardlie KG, Arking DE, Aslibekyan S, Auer PL, Barnard J, Barr RG, Barwick L, Becker LC, Beer RL, Benjamin EJ, Bielak LF, Blangero J, Boehnke M, Bowden DW, Brody JA, Burchard EG, Cade BE, Casella JF, Chalazan B, Chasman DI, Chen YI, Cho MH, Choi SH, Chung MK, Clish CB, Correa A, Curran JE, Custer B, Darbar D, Daya M, de Andrade M, DeMeo DL, Dutcher SK, Ellinor PT, Emery LS, Eng C, Fatkin D, Fingerlin T, Forer L, Fornage M, Franceschini N, Fuchsberger C, Fullerton SM, Germer S, Gladwin MT, Gottlieb DJ, Guo X, Hall ME, He J, Heard-Costa NL, Heckbert SR, Irvin MR, Johnsen JM, Johnson AD, Kaplan R, Kardia SLR, Kelly T, Kelly S, Kenny EE, Kiel DP, Klemmer R, Konkle BA, Kooperberg C, Kottgen A, Lange LA, Lasky-Su J, Levy D, Lin X, Lin KH, Liu C, Loos RJF, Garman L, Gerszten R, Lubitz SA, Lunetta KL, Mak ACY, Manichaikul A, Manning AK, Mathias RA, McManus DD, McGarvey ST, Meigs JB, Meyers DA, Mikulla JL, Minear MA, Mitchell BD, Mohanty S, Montasser ME, Montgomery C, Morrison AC, Murabito JM, Natale A, Natarajan P, Nelson SC, North KE, O'Connell JR, Palmer ND, Pankratz N, Peloso GM, Peyser PA, Pleiness J, Post WS, Psaty BM, Rao DC, Redline S, Reiner AP, Roden D, Rotter JI, Ruczinski I, Sarnowski C, Schoenherr S, Schwartz DA, Seo JS, Seshadri S, Sheehan VA, Sheu WH, Shoemaker MB, Smith NL, Smith JA, Sotoodehnia N, Stilp AM, Tang W, Taylor KD, Telen M, Thornton TA, Tracy RP, Van Den Berg DJ, Vasan RS, Viaud-Martinez KA, Vrieze S, Weeks DE, Weir BS, Weiss ST, Weng LC, Willer CJ, Zhang Y, Zhao X, Arnett DK, Ashley-Koch AE, Barnes KC, Boerwinkle E, Gabriel S, Gibbs R, Rice KM, Rich SS, Silverman EK, Qasba P, Gan W, Consortium NT-OfPM, Papanicolaou GJ, Nickerson DA,

Browning SR, Zody MC, Zollner S, Wilson JG, Cupples LA, Laurie CC, Jaquish CE, Hernandez RD, O'Connor TD, Abecasis GR: Sequencing of 53,831 diverse genomes from the NHLBI TOPMed Program. Nature 2021;590:290-299

115. Tg, Hdl Working Group of the Exome Sequencing Project NHL, Blood I, Crosby J, Peloso GM, Auer PL, Crosslin DR, Stitziel NO, Lange LA, Lu Y, Tang ZZ, Zhang H, Hindy G, Masca N, Stirrups K, Kanoni S, Do R, Jun G, Hu Y, Kang HM, Xue C, Goel A, Farrall M, Duga S, Merlini PA, Asselta R, Girelli D, Olivieri O, Martinelli N, Yin W, Reilly D, Speliotes E, Fox CS, Hveem K, Holmen OL, Nikpay M, Farlow DN, Assimes TL, Franceschini N, Robinson J, North KE, Martin LW, DePristo M, Gupta N, Escher SA, Jansson JH, Van Zuydam N, Palmer CN, Wareham N, Koch W, Meitinger T, Peters A, Lieb W, Erbel R, Konig IR, Kruppa J, Degenhardt F, Gottesman O, Bottinger EP, O'Donnell CJ, Psaty BM, Ballantyne CM, Abecasis G, Ordovas JM, Melander O, Watkins H, Orho-Melander M, Ardissino D, Loos RJ, McPherson R, Willer CJ, Erdmann J, Hall AS, Samani NJ, Deloukas P, Schunkert H, Wilson JG, Kooperberg C, Rich SS, Tracy RP, Lin DY, Altshuler D, Gabriel S, Nickerson DA, Jarvik GP, Cupples LA, Reiner AP, Boerwinkle E, Kathiresan S: Loss-of-function mutations in APOC3, triglycerides, and coronary disease. N Engl J Med 2014;371:22-31

116. Mbatchou J, Barnard L, Backman J, Marcketta A, Kosmicki JA, Ziyatdinov A, Benner C, O'Dushlaine C, Barber M, Boutkov B, Habegger L, Ferreira M, Baras A, Reid J, Abecasis G, Maxwell E, Marchini J: Computationally efficient whole-genome regression for quantitative and binary traits. Nat Genet 2021;53:1097-1103

117. Segrest JP, Jones MK, De Loof H, Brouillette CG, Venkatachalapathi YV, Anantharamaiah GM: The amphipathic helix in the exchangeable apolipoproteins: a review of secondary structure and function. J Lipid Res 1992;33:141-166

118. Davidson WS, Ghering AB, Beish L, Tubb MR, Hui DY, Pearson K: The biotin-capture lipid affinity assay: a rapid method for determining lipid binding parameters for apolipoproteins. J Lipid Res 2006;47:440-449

119. Netea MG, Nold-Petry CA, Nold MF, Joosten LA, Opitz B, van der Meer JH, van de Veerdonk FL, Ferwerda G, Heinhuis B, Devesa I, Funk CJ, Mason RJ, Kullberg BJ, Rubartelli A, van der Meer JW, Dinarello CA: Differential requirement for the activation of the inflammasome for processing and release of IL-1beta in monocytes and macrophages. Blood 2009;113:2324-2335

120. Qamar A, Khetarpal SA, Khera AV, Qasim A, Rader DJ, Reilly MP: Plasma apolipoprotein C-III levels, triglycerides, and coronary artery calcification in type 2 diabetics. Arterioscler Thromb Vasc Biol 2015;35:1880-1888

121. Kanter JE, Bornfeldt KE: Apolipoprotein C3 and apolipoprotein B colocalize in proximity to macrophages in atherosclerotic lesions in diabetes. J Lipid Res 2021;62:100010

122. Schlotter F, de Freitas RCC, Rogers MA, Blaser MC, Wu PJ, Higashi H, Halu A, Iqbal F, Andraski AB, Rodia CN, Kuraoka S, Wen JR, Creager M, Pham T, Hutcheson JD, Body SC, Kohan AB, Sacks FM, Aikawa M, Singh SA, Aikawa E: ApoC-III is a novel inducer of calcification in human aortic valves. J Biol Chem 2021;296:100193

123. Liu Z, Zhang Z: Mapping cell types across human tissues. Science 2022;376:695-696

124. Mund A, Brunner AD, Mann M: Unbiased spatial proteomics with single-cell resolution in tissues. Mol Cell 2022;82:2335-2349